

2-P

**AMERICAN  
SCIENCE**   
AND ENGINEERING

15 MAY 1972

ASE-2978  
VOL II OF 2

955 MASSACHUSETTS AVENUE, CAMBRIDGE,  
MASSACHUSETTS 02139 (617) (868-1600)

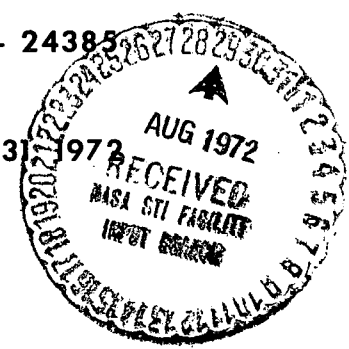
123816  
(NASA-CR-~~127608~~) RESEARCH STUDY ON STELLAR  
X-RAY IMAGING EXPERIMENT, VOLUME 2 Final  
Report, 12 Jun. 1969 - H.H. Wilson, et al  
(American Science and Engineering, Inc.)  
15 May 1972 131 p  
N72-29466  
Unclas  
CSCL 14B G3/14 15859

FINAL REPORT:  
**RESEARCH STUDY  
ON STELLAR X-RAY  
IMAGING EXPERIMENT**

HENRY H. WILSON  
LEON P. VANSPEYBROECK

CONTRACT NO. NAS8 - 24385

PERIOD COVERED:  
JUNE 12, 1969 - MARCH 31, 1972



Reproduced by  
**NATIONAL TECHNICAL  
INFORMATION SERVICE**  
U S Department of Commerce  
Springfield VA 22151

PREPARED FOR:  
**NATIONAL AERONAUTICS  
AND SPACE ADMINISTRATION  
GEORGE C. MARSHALL  
SPACE FLIGHT CENTER  
MARSHALL SPACE FLIGHT CENTER, ALABAMA 35812**

Final Report

RESEARCH STUDY ON STELLAR X-RAY  
IMAGING EXPERIMENT

Period Covered:

June 12, 1969 - March 31, 1972

Contract No. NAS8-24385

Henry H. Wilson  
Leon P. VanSpeybroeck

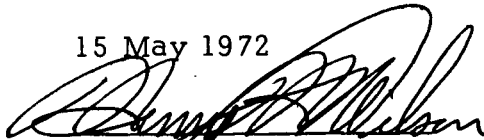
Prepared for:

National Aeronautics and Space Administration  
George C. Marshall Space Flight Center  
Marshall Space Flight Center, Alabama 35812

Prepared by:

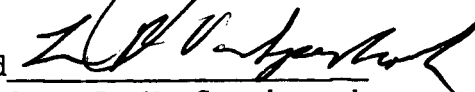
American Science & Engineering, Inc.  
955 Massachusetts Avenue  
Cambridge, Massachusetts 02139

15 May 1972



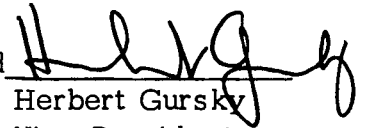
Henry H. Wilson  
Senior Scientist

Approved



Leon P. VanSpeybroeck  
Project Scientist

Approved



Herbert Gursky  
Vice President  
Space Research  
Division

CONTENTS (Cont'd from ASE-2978 - Volume I)

<u>Section</u>	<u>Page</u>
APPENDIX D Telescopes and Scientific Subsystems for a High-Energy Astronomy Observatory	iii
APPENDIX E Effect of Varying Microchannel Plate and Phosphor Voltage on X-Ray Image Quality	E-1

APPENDIX D  
from ASE-2266A

Telescopes and Scientific Subsystems  
for a High-Energy Astronomy Observatory

## FOREWORD

This document is the result of a series of meetings between selected X-ray astronomers and NASA personnel who convened for the purpose of defining the design parameters for a national X-ray orbiting observatory which utilizes focusing X-ray telescopes. The participants in these meetings have been:

### NASA Headquarters

Richard Halpern  
Nancy G. Roman

### NASA/Huntsville

Jean Oliver  
James Downey  
Ernst Stuhlinger

### Experimenters

1. American Science and Engineering, Inc.  
Riccardo Giacconi  
Herbert Gursky  
Edwin Kellogg  
Guiseppe Vaiana  
Leon Van Speybroeck  
Theodore Zehnpfennig
2. Columbia University  
J. Roger Angel  
Robert Novick  
Martin Weisskopf  
L. Woltjer
3. Goddard Space Flight Center  
Elihu Boldt  
Stephen Holt  
Peter Serlemitsos
4. Massachusetts Institute of Technology  
George Clark  
Kenneth Kalata  
Herbert Schnopper

The idea for such a facility originated with the recognition that X-ray astronomy has come to the point that instruments making use of focusing optics will be required for further advances. It was recognized that several users might occupy the focal plane of a single telescope and that one should consider a "facility" approach whereby a group of interested scientists define the requirements of the optics which could ultimately be shared among even a larger group.

At the onset of the discussion, the approach was, therefore, to assume that a single X-ray reflecting telescope would be used at the focus of which several experiments could be performed. The task was to set the design specifications of this single telescope in sufficient detail for engineering studies on feasibility to be undertaken.

Early in the discussion, however, it became clear that a "standard" X-ray telescope design did not exist and could not be defined without taking into consideration the scientific aim and the detailed experimental techniques of the several experiments to be carried out at the focus. The group, therefore, undertook to review the scientific objectives of an integrated X-ray orbiting telescope facility, to define a set of observations which could be carried out to achieve these objectives, to consider what techniques (both with and without focusing optics) could be used to perform these observations and, finally, what telescope or telescopes would be required.

The discussion was confined to state-of-the-art techniques with a view to a possible launch date of 1974-1975. Thus, we did not attempt to design the ultimate set of telescopes and payloads, but rather the logical next step which we believe feasible and necessary for the advance of X-ray astronomy. An observatory

of the type here described is susceptible to refinements and improvements in later versions and additional flights.

Since several large scientific groups were involved, a free, creative and imaginative approach was taken by the participants in suggesting possible technical solutions to each observational problem. A large number of ancillary instruments, techniques, and approaches were considered, and the most promising are included in this report. This effort resulted in some major conclusions:

1. A national X-ray telescope observatory mission can be accomplished within the present capabilities of launch vehicles, spacecraft systems and techniques. If the program could be initiated by July 1970, launch could occur in 1974 or 1975.

2. No single X-ray telescope can satisfy the broad range of observational requirements. We have, however, found it possible to divide the major observational requirements in two broad classes each of which could be satisfied by use of a proper telescope. We have then studied in detail the characteristics of these two telescopes and we conclude that their construction is within the state of the art.

3. We have identified a set of observations requiring pointed capabilities for which at the present time there is no advantage in using focusing optics. These observations should be carried out as part of this mission, but not at the focus of the telescope.

4. We have identified other activities which must be carried out in conjunction with and in support of the primary X-ray telescope mission. These include X-ray and UV observations from space and visible light observations from the ground which should be performed simultaneously with the primary mission.

5. We believe it essential to the success of a project of this magnitude that adequate support for a program of rocket flights to test instruments and components and X-ray ground test facilities be planned as part of the program.

6. The characteristics of the telescopes and experiments are so intimately related that we conclude that the specifications for the optics must ultimately be set by the users. In addition, the users must retain technical control of the implementation and testing of the devices.

We have attempted to consider these several points in the report in some detail. In particular, several different technical approaches to each observational problem were worked out in sufficient detail to evaluate their impact on telescope design specifications and spacecraft requirements. It should be pointed out, however, that these are not proposed experiments or instruments, but rather typical or representative experiments. Thus, certain imprecisions or inadequate scientific justifications for specific experiments may be contained in the report. This is in part due to our approach which has been of continuous iteration between the scientific objectives, the instruments and the telescopes. However, the group which contributed to this report is sufficiently representative that we feel quite confident about the soundness of our overall conclusions. The combination of telescopes here discussed will provide focused X-rays to a variety of focal plane instruments and, when used in conjunction with other instruments, will satisfy the requirement of a large group of potential investigators and provide for qualitative advances in X-ray astronomy. What has evolved and is described in this report is an integrated facility incorporating two X-ray telescopes, focal plane instruments,



pointed instruments, and support sub-systems designed to perform sophisticated observations in X-ray astronomy. The payload should fall within the lifting capability of the Titan III-C launch vehicle and thus is suitable for inclusion within NASA's Super-Explorer series; however, no consideration was given for the non-scientific sub-systems except for specifying the requirements such as weight, power, and telemetry. It may be that some of these requirements cannot be met; however, it should be possible to scale down the size of the instruments and the telescopes to fit within the constraints of a properly engineered spacecraft without sacrificing the major scientific objectives.

A great deal of work has gone into the evolution and preparation of this report. The authors have been motivated mainly by their desire to see this mission undertaken and by the hope that they will be allowed to play a significant role in it. We strongly urge NASA to implement this program which would provide a quality of X-ray observations comparable to the one now attainable only in visible light by ground-based observatory.

## TABLE OF CONTENTS

INTRODUCTION	xii
1.0 EXPERIMENTAL OBJECTIVES AND TECHNIQUES	1-1
1.1 Source Characteristics	1-1
1.2 Experimental Techniques	1-4
1.3 Summary of Support Programs	1-8
2.0 X-RAY TELESCOPE	2-1
2.1 High Resolution Mirror	2-3
2.2 Large Area Mirror	2-20
3.0 PRIMARY EXPERIMENT	3-1
3.1 High Resolution Imagery	3-1
3.2 High Resolution Spectrometer	3-6
3.3 Polarimeters	3-16
3.4 Non-Dispersive Spectroscopy and Stellar Identification	3-23
4.0 SUPPORT AND SUBSIDIARY EXPERIMENTS	4-1
4.1 Proportional Counter	4-1
4.2 Flat Crystal Spectrometer	4-5
4.3 Large Area Telescope Imaging System	4-10
4.4 Large Area Telescope Mosaic Crystal Spectrometer	4-15
4.5 Scintillation Counter Assembly	4-19
4.6 An All-Sky Detector for Transient X-ray Phenomena	4-22
5.0 ESSENTIAL SCIENTIFIC SUPPORT SYSTEMS	5-1
5.1 Aspect System	5-1
5.2 Vehicle Pointing System	5-5
5.3 Detector Interchange System	5-5
5.4 Telemetry Buffer and Storage	5-5
5.5 Command System	5-6
5.6 Common Electronics	5-6
5.7 Thermal Control System	5-6
6.0 SUMMARY OF VEHICLE REQUIREMENT	6-1
6.1 Vehicle Experiment Package Dimensions	6-1
6.2 Pointing Requirements	6-1
6.3 Thermal Control	6-1

6.4	Experiment Telemetry Requirements	6-1
6.5	Experiment Command Bits	6-2
6.6	Experiment Power Requirements	6-3
6.7	Experiment Weights	6-5
7.0	SUPPORTING PROGRAMS	7-1
7.1	350-Sounding Rockets	7-1
7.2	One-mile X-ray Test Facility	7-2
7.3	Orbital Operations and Data Retrieval	7-3
7.4	Coordinated Ground-based Observations	7-3

## LIST OF ILLUSTRATIONS

<u>Figures</u>		<u>Page</u>
1-1	Possible High Energy Astronomy Satellite Payload	1-10
2-1	Schematic cross section of the high resolution X-ray telescope	2-4
2-2	Total blur circle diameter versus angular distance from the optical axis, from a ray tracing done on a telescope system with the characteristics $F = 20y_0$ and $L = 2y_0$	2-5
2-3	High resolution telescope effective area	2-18
2-4	Baez geometry for large area telescope	2-21
2-5	Large area telescope modular construction	2-22
2-6	Large area telescope effective area	2-24
3-1	Block diagram, AS&E high resolution imaging experiment	3-2
3-2	Focusing circle geometry	3-8
3-3	Flat crystal spectrometer	3-10
3-4	Spiraltron organization	3-12
3-5	LiH polarimeter concept	3-17
3-6	LiH polarimeter	3-19
3-7	Composite Si(Li) detector	3-29
3-8	GSFC optical correlator	3-30
3-9	Block diagram for GSFC Experiment	3-31
4-1	Proportional counter	4-3
4-2	Crystal spectrograph 500 cm	4-6
4-3	Spectrograph	4-9
4-4	Multi-celled proportional counter array	4-12
4-5	X-ray transient detector element	4-26
4-6	X-Y transient detection system	4-27
5-1	Aspect sensor	5-2
6-1	Weight distribution (boom extended)	6-6
 <u>Drawings</u>		
SK-614-304	X-ray high resolution mirror (1000 cm <sup>2</sup> ) (AS&E and MIT)	
SK-614-305	X-ray proportional counter array (2500 cm <sup>2</sup> )	
SK-614-306	Baez X-ray mirror segment	
SK-614-307	Crystal spectrograph (500 cm <sup>2</sup> )	
SK-614-308	X-ray slit mirror system (5000 cm <sup>2</sup> ) (AS&E, Columbia and GSFC)	
SK-614-315	Titan IIIC Satellite Experimental Payload	
SK-614-318	Aerobee 350 Payload	

## INTRODUCTION

A decade of development in space science and technology has given the United States the capability to accomplish new and challenging goals in space astronomy. The exploration of the astronomical universe has always inspired the best work of scientists and engineers, and the active interest of a large and influential portion of the general public. It is now clear that a major effort in the specific area of X-ray astronomy, aimed at the launching of a national orbiting X-ray observatory in 1975 could achieve an ideal match between opportunities for profound scientific advances and our present technical capabilities. A strong case can therefore be made for the establishment of such an observatory as one of the nation's new goals in space.

The unexpected discovery in 1962 of powerful X-ray sources outside the solar system is the most important scientific breakthrough of space astronomy to date. In seven years, this breakthrough has been exploited in scores of rocket and balloon experiments that have opened up the new field of X-ray astronomy with many surprising discoveries and profound new insights into cosmic processes. Scientists around the world have focused their attention on the interpretation of the new discoveries, and many scientific groups both here and abroad have joined the observational work. In no other area during the past decade has there been a more fruitful interplay between technical innovation and scientific discovery.

X-ray astronomy is now an established discipline which can be broadly defined as the study of cosmic electromagnetic radiation in the broad range of energies from the effective interstellar absorption cutoff near 0.20 Kev ( $\sim 70\overset{\circ}{\text{A}}$ ) to the gamma ray region

above several hundred Mev. Since atmospheric absorption limits all direct cosmic X-ray observations to altitudes near the top or above the atmosphere, the exploration of this wide and important window in the cosmic electromagnetic spectrum waited on the availability of appropriate vehicles. Once the breakthrough was made, important and surprising discoveries followed one another in rapid succession.

NASA, with the broad approval of the scientific community, has supported a logical and steady growth of United States' capabilities in X-ray astronomy. Now, after seven years of extraordinarily productive exploratory work the NASA program is on the threshold of a period of explosive growth in our knowledge of cosmic X-ray sources with the planned launchings during 1970 of the first two major satellite experiments in X-ray astronomy -- the X-ray Explorer on the first Small Astronomy Satellite (SAS-A), and the Multicolor X-Ray Survey on the Orbiting Solar Observatory (OSO-H).

The 1970 satellite experiments however, are based on straightforward extensions of tested rocket instrumentation. Their main advantage over previous rocket experiments is that they will provide a much greater observing time and therefore, a much greater sensitivity. Specifically, these first-generation satellite experiments will employ mechanical collimators to define the region of sky under examination, and conventional gas proportional counters with only modest energy analyzing capabilities.

At the present time however, theoretical and experimental studies, together with several highly successful exploratory rocket investigations have demonstrated the feasibility of constructing an orbiting X-ray observatory which would greatly

exceed the capabilities of the 1970 satellites. This observatory would employ precision image-forming X-ray telescopes equipped with high-resolution image analyzers, Bragg crystal spectrographs, and sensitive polarimeters. These instruments would achieve a degree of refinement in astronomical X-ray observations which has theretofore been achieved only in ground-based optical astronomy. Thus, an orbiting high-resolution X-ray observatory which is a technically sound next step in the NASA astronomy program could well produce a "quantum-jump" in the science of astronomy with a resulting impact on the whole of science comparable to that which was caused by the introduction of modern methods in optical astronomy. The certain prospect of fundamental astronomical discovery implicit in the construction of such a facility gives good assurance of sustained public support, provided the public and the scientific community are thoroughly informed. As for the key issue of stimulating technological growth, an X-ray observatory would represent the very cutting edge of the new observational space astronomy, and as such would demand a high but attainable performance by the supporting systems with regard to stability, control, radiation sensing, information handling, and space-maintenance. This is the kind of challenge to which creative scientists and engineers and their supporting organizations respond most effectively.

The remaining sections of this report describe an integrated, X-ray observational facility that should fit within the capability of a Titan III-C launch. We discuss the scientific objectives such a mission could accomplish, the telescopes that are required, the experimental hardware, certain essential subsystems, and a summary of vehicle requirements. In addition, we have identified supporting programs that are required.

It is useful to discuss the general approach taken in configuring this facility. The essential ground rules were:

1. The facility should point with high precision to selected targets. This requirement allows for the long observing times needed to record very faint objects.
2. X-ray optics shall be utilized. This allows attaining high spatial resolution and for achieving very favorable signal to noise in certain instruments.
3. The facility shall be able to accommodate a wide variety of users. Provision is made for inclusion of more than one instrument in the focal plane of the telescopes and for the incorporation of instruments that do not make use of the optics but do need to be pointed at the target.

The principal design problems that have arisen involve the questions: what are the characteristics of the X-ray optics? what are the requirements of the scientific instruments? which instruments go with which optics and which instruments require no optics at all? The essential characteristics of the telescope which are involved are: firstly, the grazing angle determines the high-energy cutoff of the telescope. The smaller this angle, the higher the energy X-rays which will reflect from the surfaces. There is no intrinsic low-energy cutoff. However, the maximum aperture is constrained by the maximum allowable focal length, and smaller grazing angles make for smaller apertures. Secondly, the requirement for the highest attainable angular resolution results in utilization of less than the maximum available aperture because of the necessarily closer tolerances.



Based on these considerations, we identified two classes of instruments; those requiring the maximum angular resolution for which we were willing to sacrifice aperture, and those requiring the maximum aperture for which we were willing to sacrifice angular resolution. Also we set the high-energy cut-offs at around several Kev. Above these energies, it is difficult to achieve a significant aperture using X-ray optics and observations can be made using conventional mechanical collimators. The characteristics of the corresponding two telescopes are as follows:

High Resolution Mirror - (nested paraboloid-hyperboloid)  
1000 cm<sup>2</sup> net area, 1 arc second resolution.

Large Area Mirror - (Baez reflector) 5000 cm<sup>2</sup> net area,  
10 arc second resolution.

We have incorporated what seemed to us the largest sensible telescopes into the Titan envelope. The net system requirements have been arrived at by summing individual requirements in the simplest way without attempting weight or telemetry reduction. These requirements can be scaled down somewhat if need be without seriously affecting performance.

It should also be emphasized that the instruments, including the telescopes, are essentially state-of-the-art. Virtually every element of hardware has flown in one form or another in sounding rocket or satellite experiments.

## 1.0 EXPERIMENTAL OBJECTIVES AND TECHNIQUES

### 1.1 Source Characteristics

A brief summary of some characteristics of x-ray sources and the experimental objectives is included here to enable a better understanding of the various instruments; the individual experiment proposals should be consulted for a more complete discussion.

The importance of the soft x-ray portion of the electromagnetic spectrum is in part due to the properties of the interstellar media, which strongly absorbs between the near ultraviolet and ultra-soft x-ray region; thus, the first opportunity to observe objects at photon energies appreciably higher than the visible occurs in the soft x-ray region. Empirically, however, the spectrum of all objects yet observed are rapidly decreasing with increasing energy in this wavelength interval, and consequently precise observations become much more difficult with increasing energy. The soft x-ray window is thus of natural importance.

The principal feature of x-ray astronomy is the presence of discrete sources in which the x-ray emission equals or exceeds all other forms of radiation output. About 30 sources are reported at the present time; the variety and number of sources indicate that x-ray production on this scale is not some minor astrophysical phenomenon but is dominant in many instances. Some examples of sources will illustrate the variety of emitting objects.

Sco X-1, the strongest extra solar x-ray source and the first to be discovered, has been identified with a peculiar but previously undistinguished starlike optical object which has also been recently detected as a faint radio and infra-red source.

The x-ray emission region is less than 15 arc-seconds in extent, and the spectrum appears to be falling exponentially with increasing energy. Optically, Sco X-1 exhibits apparently erratic variability and spectroscopically shows the characteristics of high excitation phenomena. The x-ray emission was observed to vary by a factor of four at energies between 20 and 130 Kev during a single balloon flight, and comparisons of measurements by different experimenters indicate variations at longer wavelengths, although less convincingly. The source is thought to be about 350 pc away; the observed x-ray flux then implies an emission above 1 Kev of  $6 \times 10^{36}$  ergs, or more than 1,000 times the emission of the sun at all wavelengths. The x-ray emission is consistent with thermal emission from a hot thin plasma; if this model is correct, the spectrum may be expected to include emission lines.

The Crab Nebula, which is the 900 year old remnant of a supernova explosion and one of the most luminous objects in the Galaxy in the optical, infra-red and radio wavelengths, is also the most intense of several x-ray sources associated with supernova remnants. The x-ray emission is centered with respect to the visible nebula with a precision of about 20 arc-seconds, and extends over a diameter of at least 1.5 arc-minutes. The spectrum of the x-ray emission follows a power law distribution over a wide energy interval extending at least from 1 to 100 Kev. The greater part of the optical radio, and x-ray emission are consistent with synchrotron radiation from a single electron distribution. If this model is correct, the x-rays will be polarized, as observed at optical and radio wavelengths.

Recently a starlike object embedded in the Crab Nebula was found to be a pulsar which emits two somewhat differently shaped

pulses of a few milliseconds duration during a 33 ms. period. These pulses have been observed in radio, optical, and x-ray wavelengths; the ratio of x-ray to optical flux in the pulsar is about 50 times the x-ray to optical flux ratio for the total emission from the Nebula, and the pulsar x-ray spectrum is somewhat harder than that of the rest of the Nebula. The period is gradually increasing, and calculations indicate that the loss of kinetic energy corresponding to the slowing down of a rotating neutron star is approximately equal to the total emission from the entire Nebula.

The source Centaurus X-2 is the most dramatic example of source intensity variations; this source was undetected in 1965; by 1967 its flux had increased by a factor of at least 100, and it was the brightest x-ray object in the sky. The flux decreased by a factor of six within about a month, and the source was again unobservable by September, 1967. The source was observed at higher energies ( $> 20$  Kev) during October, 1967, and the flux at these energies declined by 35% during a nine day interval. This source clearly demonstrates the necessity of constantly monitoring the intensity, both for its intrinsic interest and to evaluate the interpretation of measurements which require the comparison of data taken at different times.

In addition to the discrete sources there is a diffuse x-ray background which appears to be largely of extragalactic origin. The spectral shape and spatial intensity distribution of the background is affected by interstellar absorption and can be used to infer the distribution of interstellar matter in this and possibly other galaxies. The x-ray absorption is sensitive to elements of intermediate atomic number but is reasonably insensitive to their ionization state, and therefore provides a useful method for

determining the distribution of these elements. The absorption may occur largely in interstellar clouds with typical diameters of a few arc-minutes, and therefore measurements should be made with this angular resolution.

There are, of course, many additional interesting objects to be observed in x-ray wavelengths, but the above examples illustrate the fact that there is useful astronomical information in almost all measurable parameters of the x-ray radiation field. Positional accuracy and high angular resolution are necessary for studying the structure of extended objects, for separating point-like objects in dense source regions such as nearby galaxies, and for enabling a correspondence between a source x-ray emission and emission at other wavelengths. The x-ray emission may be polarized if the emission is synchrotron radiation or has a nonsymmetric environment such as would result from a binary star association. The spectrum may include emission lines, absorption edges, and continuum. For stronger sources it will be possible to study emission line profiles to obtain knowledge of the temperature, turbulence, and velocity distribution in the source. For weaker sources it will only be possible to determine the existence of the lines, or perhaps only the general spectral shape.

The source intensity may vary periodically, as in a pulsar, or erratically, as in Centaurus X-2. Finally, it is necessary to study comparatively weak sources as unusual objects are usually at great distances and correspondingly faint.

## 1.2 Experimental Techniques

The four basic experiments that have been studied for the proposed Large Orbiting X-Ray Telescope satellite are of the type which were originally proposed by the four groups participating in this

study and which were reviewed and recommended by the Astronomy Subcommittee as potential experiments for an advanced x-ray astronomy mission with focusing optics. These experiments would constitute the first attempt to observe x-ray sources with instruments having quality and flexibility comparable to a ground-based optical observatory.

In addition to the four basic experiments several experiments were suggested in the course of the meetings by various of the participants with the aim of utilizing fully the scientific opportunities offered by the proposed mission. Although these latter experiments have not been formally proposed to NASA, several of them have been included in this study in order to insure that the basic design of the satellite will accommodate all the variety of experiments necessary for a comprehensive advanced mission.

The principal instrument is the x-ray telescope which utilizes the efficient reflection of x-rays at grazing incidence to form high resolution images of the x-ray sky. The grazing incidence requirement for efficient reflection unfortunately results in surfaces which are approximately parallel to the incident radiation, and therefore it becomes difficult to utilize efficiently the telescope aperture because the mirror wall materials must consume part of the available area. For reasons to be discussed further the potential principal investigators concluded that the requirement of maximum collecting area and highest angular resolution are not compatible and that two mirrors would be required. Fortunately, the experiments to be performed can be divided into those more sensitive to area and those more sensitive to angular resolution.

The following telescopes, associated focal plane instruments, and the experiments were selected for the design study:

- A. A high resolution ( $\sim 2$  arc-seconds) telescope of

approximately  $1,000 \text{ cm}^2$  effective area with the following focal plane instruments:

1. An (AS&E) image intensifier for accurate position and spatial structure measurements with an accompanying high-resolution optical aspect system. This may be used in conjunction with a transmission grating to provide moderate quality spectral data of sources too weak to be studied with the higher resolution crystal spectrometers.

2. A (MIT) Focusing Circle type crystal spectrometer for the highest possible spectral resolution including line profile measurements.

B. A large area ( $\sim 5,000 \text{ cm}^2$ ) telescope of moderate ( $\sim 10$  arc-seconds) angular resolution with the following associated instruments:

1. Two (Columbia University) polarimeters to measure the polarization at approximately 1.3, 2.6 and 4.3 Kev. This experiment consists of a set of polarimeters utilizing the polarization dependence of Bragg reflection. Mosaic crystals of lithium hydride, graphite and (possibly) tungsten disulphide are to be employed to cover the energy range.

2. A (Goddard Space Flight Center) solid state detector designed to achieve the maximum sensitivity at the highest energy available in the focal plane, energy resolution, sufficient for line, identification, and optical correlation sufficient for unambiguous identification of x-ray sources with their optical counterparts. These objectives are to be met by using a cooled Si(Li) detector, in conjunction with a modulator in the focal plane which interrupts both the x-ray and optical beams focused by the telescope.

The following experiments were identified during the course of this work as being potential candidates for inclusion in the facility:

1. A position sensitive proportional counter to be used at the focus of the B telescope for moderate resolution studies of low intensity diffuse objects and of structure in the diffuse background.

2. A mosaic crystal spectrometer to be used in conjunction with the B telescope. This type crystal can disperse a range of wavelengths and may be more sensitive than the MIT instrument. It can be used only at the higher photon energies. Several different crystal arrangements are possible.

3. A flat crystal spectrometer for obtaining spectra in the energy region beyond the telescope high energy cutoff; this region includes the important iron lines. This experiment would be limited to strong isolated sources because of the poorer angular resolution and low fluxes expected.

4. A proportional counter array to provide a time history of the intensity of the stronger sources during their observation by the crystal spectrometer and polarimeters which must compare data taken at different times.

5. A Scintillation Counter to extend the range to much higher energies.

6. An omnidirectional x-ray source detector, to be used to detect nova-like outbursts of x-ray sources.

7. High-Energy Polarimeters. In addition to polarimetry being performed at the low energies accessible in the focal plane of the telescopes, several efficient polarimeters are possible at high energies.

8. Vacuum ultraviolet measurements. Extensive correlated ground measurements are a requirement for many of the scientific observations. These are limited by the atmosphere to wavelengths longward of  $3000\text{\AA}$ ; the shorter wavelength observations can be accomplished as part of the facility; perhaps even sharing the



mirror used for the aspect measurement.

The system requirements (weight, power, telemetry, etc.) of these experiments is presented and summarized. A possible experimental configuration is shown in Drawing B-SK-614-315.

### 1.3 Summary of Support Programs

In addition to flight hardware requirements, we also identify unique supporting programs which are essential to the ultimate success of the mission. In particular,

1. 350-Sounding Rocket Program. Many of the experimental techniques and certain observations can be carried out using sounding rockets. The existing Aerobee 350, with a stellar pointing control and payload recovery, would provide an economical capability for doing this.

2. X-ray Test Facility. The only practical means for testing large x-ray optics requires very long distances to produce almost-parallel beams of x-rays. A facility of the order of one mile in overall length is required for these purposes.

3. Orbital Operations and Data Retrieval. Plans must be made to provide adequate support for the ground facilities necessary to control the vehicle in orbit, for the retrieval of data, and for the rapid analysis and interpretation of data. The essential element that distinguishes this mission from others is that the observational capability will exceed previous ones both qualitatively and quantitatively in their variety and sensitivity. In order that maximum benefit accrues from the mission, it is essential that data be retrieved, processed and analyzed without delay.

4. Coordinated Ground Based Observations. It is expected that correlated and supplementary observations will be conducted using ground facilities; namely, optical and radio observatories.

It is important that such facilities be provided for the exclusive use of astronomers collaborating with those individuals participating in the orbital observations.

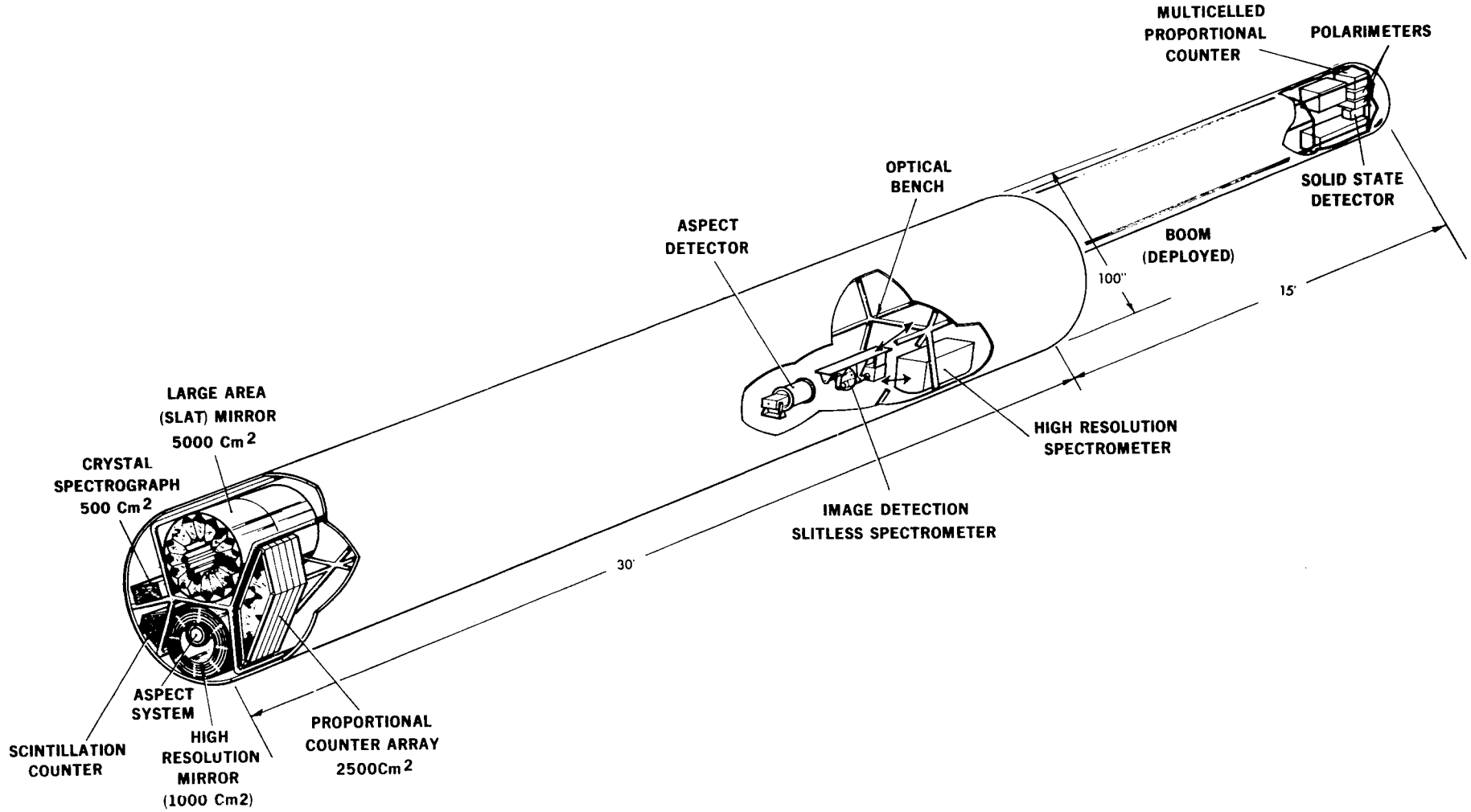


Figure 1-1  
Possible High Energy Astronomy Satellite Payload

## 2.0 X-RAY TELESCOPES

The history of the proposal for a large orbiting x-ray telescope facility involves a very early proposal by the AS&E group for a large area ( $1000 \text{ cm}^2$ ), very high resolution telescope of the paraboloid, hyperboloid type. Without question such an instrument could be constructed and will certainly yield very high angular definition. The uncertainty in the design and construction of this instrument relates to the question of its efficiency. This is an area that is extremely difficult to predict, an area in which insufficient research has been done. In spite of this limitation there is absolutely no question at all but that this is the most important instrument to be placed in a major orbiting x-ray observatory. This is true because the first problem in x-ray astronomy is to determine the location of point sources with sufficient precision so that they can be studied with ground-based instruments in the optical, infrared, and radio frequency regions of the spectrum. The progress made in our understanding of Sco X-1 dramatically increased when its location was determined with high enough precision so that such refined instruments as the 200" telescope at Mt. Palomar could be used effectively to study it. Even if one makes a very pessimistic assumption about the reflection efficiency of the high resolution telescope, i. e., if we assume that it is no greater than 10%, the instrument could still be used for the precise location of many hundreds of x-ray objects and would doubtlessly lead to a very revolutionary advancement in the field of x-ray astronomy.

In view of the uncertainty of the efficiency of the high resolution instrument, it is absolutely essential that the orbiting x-ray observatory contain another focusing instrument which is almost

certainly guaranteed to have a high effective collecting area even if the angular resolution is somewhat sacrificed. It appears that the Baez-type x-ray telescope might be a suitable candidate for consideration. The reason for this is that the individual focusing elements can probably be made in the form of flat sheets of glass which can be fabricated and polished with the best possible optical techniques. Also since this instrument employs modular construction, each glass plate can be separately tested for reflectivity before it is installed in the telescope. This belief is based on the hope that the curvature required in these elements can be obtained by elastically deforming the glass plates in a suitable holder.

The question of whether or not the above can be achieved depends in part upon the focal length of the instrument. The longer the focal length the less curvature is required, and the more likely it becomes that one can in fact use optical flats as the basic element. In view of this it is extremely important that the spacecraft be large enough to accommodate an instrument of at least 50-ft focal length. Many laboratories have succeeded in obtaining the theoretically predicted x-ray reflection coefficient for suitably coated optical glass plates, and there seems to be no question whatsoever but that the Baez telescope would in fact have a very high x-ray reflection coefficient. According to the estimates by the AS&E group it appears that it is reasonable to assume that the geometrical aberrations of this lens will correspond to an angular size of  $1/22$  of the angle that the starlight makes with the axis of the telescope, and in addition it appears that it is realistic to think in terms of a 10 to 20 arc sec resolution for objects on the axis of the telescope. This is more than adequate for purposes of polarimetry and spectroscopy,

and in fact can also be used with efficiency for the study of the distribution of extended objects, especially the Crab Nebula. It also could obviously be used very effectively to search for new weak sources and to locate them with sufficient precision so that the high resolution telescope could be brought to bear on these objects and their position determined with an accuracy of about 1 to 2 arc seconds.

The remainder of this section will be devoted to a description of the individual instruments.

### 2.1 High Resolution Mirror

This mirror is a paraboloid-hyperboloid type device as shown in Figure 2-1 in which x-rays are first focused at the common paraboloid-hyperboloid focal plane but with severe comatic distortion; the x-rays are then focused from the common focal plane to the near focal plane of the hyperboloid and most of the distortion is compensated.

The tentative optical design includes 5 concentric nested surfaces to increase the effective area of the telescope. Each mirror is essentially a scaled-up copy of the present S-054 experiment mirrors, and therefore can be expected to have the same limiting theoretical resolution. These results are shown in Figure 2-2. The actual resolution will depend upon the surface finish and contour accuracies obtained. The mirror parameters are summarized in Table II-1.

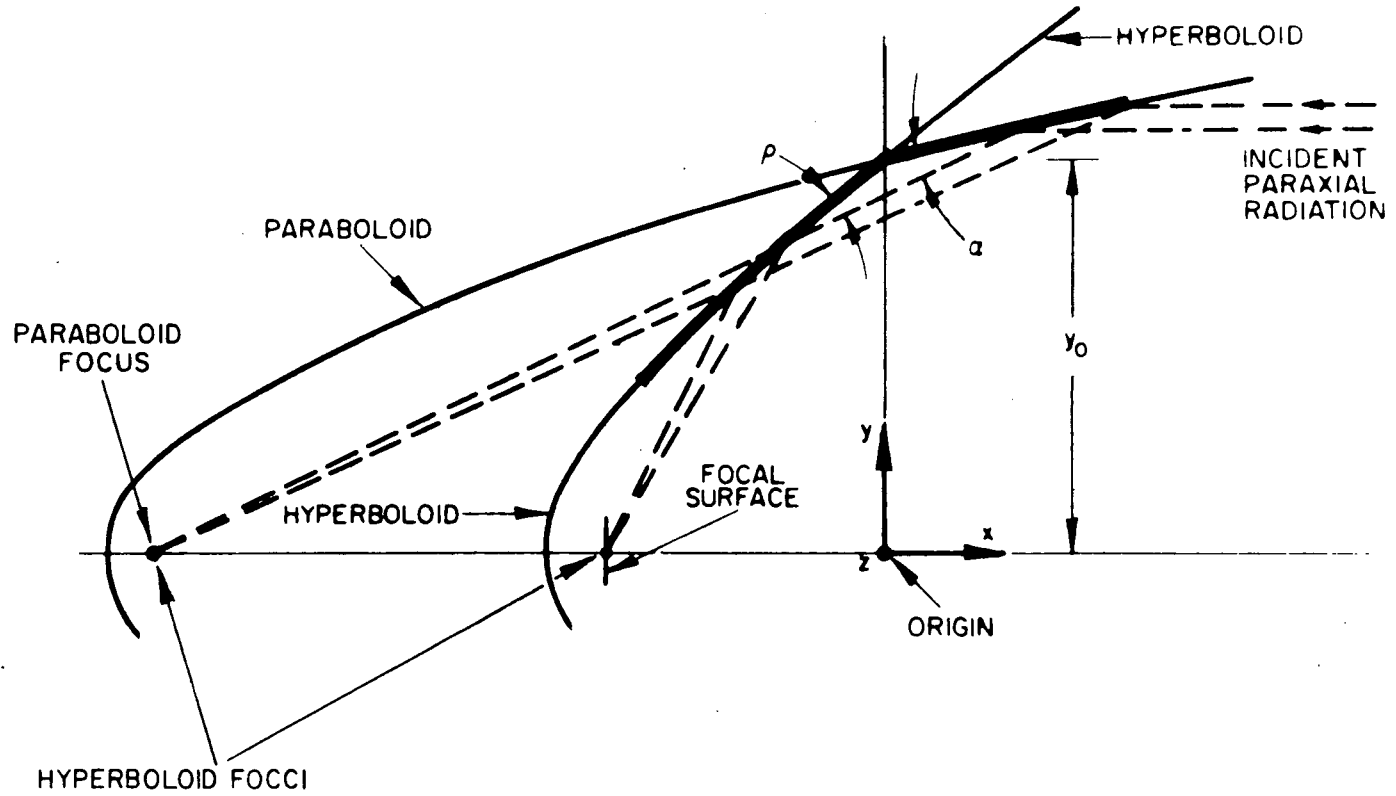


Figure 2-1. Schematic Cross Section of the High Resolution X-Ray Telescope

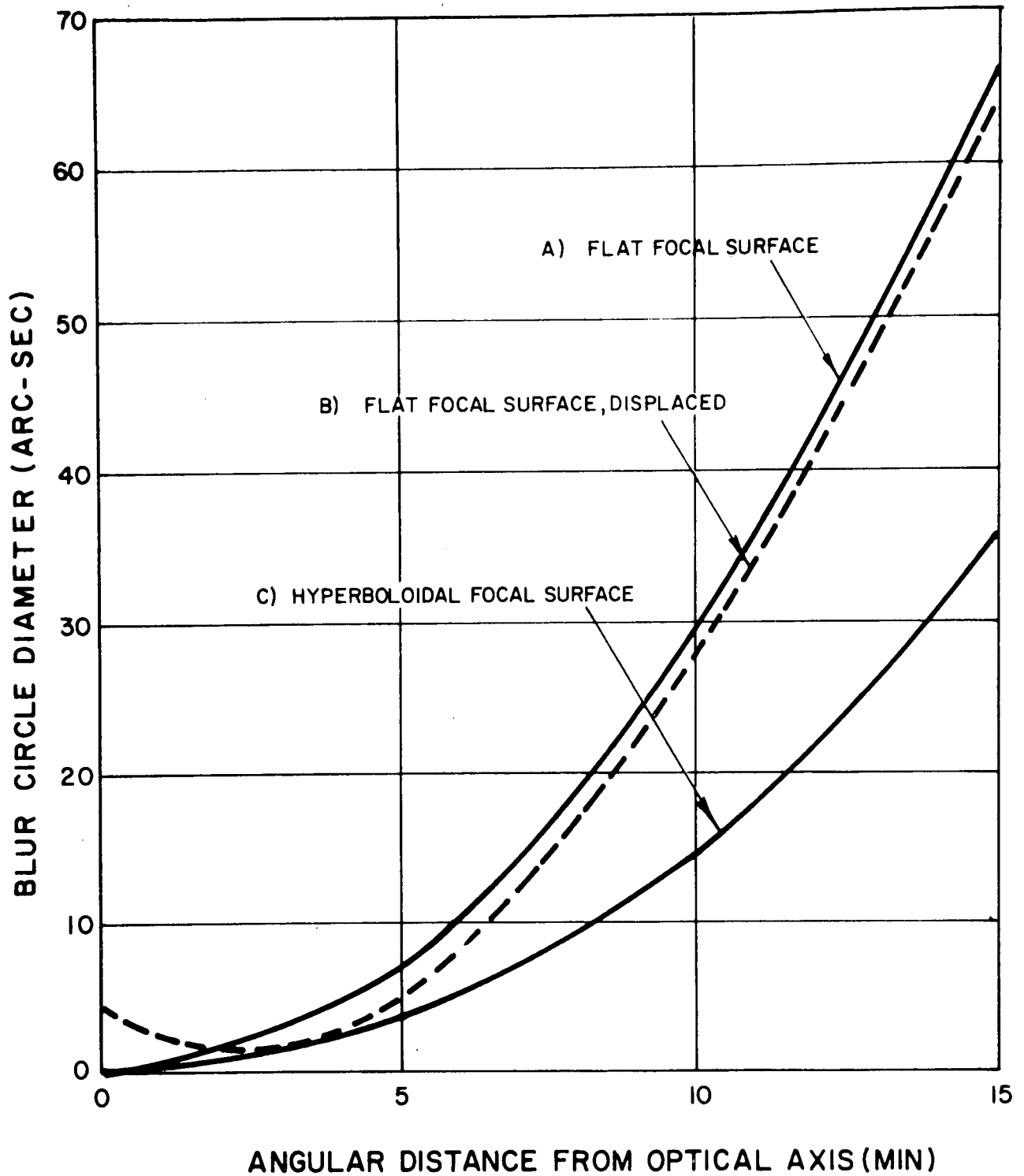


Figure 2-2 Total blur circle diameter versus angular distance from the optical axis, from a ray tracing done on a telescope system with the characteristics  $F = 20y_0$  and  $L = 2y_0$ .



TABLE II-1

Mirror Diameter (H-P Intersection, Inches)	Grazing Angle for on Axis Rays (mr)	Geometrical Effec- tive area (cm <sup>2</sup> ) for Axial Rays
35.24	18.32	287.9
33.29	17.31	257.0
31.33	16.29	227.7
29.37	15.28	200.1
27.41	14.28	<u>174.5</u>
Total		1147.2

All mirrors have an axial length of 44 inches (22 inches/segment), and a focal length of 240 inches. The final optical design of the mirrors should include slight modifications of the paraboloid-hyperboloid geometry to improve the off axis resolution, but the case described here is adequate for experiment planning purposes and to allow a discussion of the various tolerances.

The equations for the hyperboloid and paraboloid which are con-focal and coaxial can be written:

Paraboloid:

$$y^2 + z^2 = d [ 2 (x + F + 2ae) + d ] \quad (1)$$

Hyperboloid:

$$\frac{(x + F + ae)^2}{a^2} - \frac{(y^2 + z^2)}{a^2(e^2 - 1)} = 1 \quad (2)$$

In these equations F is the focal length, and d, e, and a are parameters which describe the surfaces and obey the constraint:

$$F = \frac{d}{e-1} - a(e-1) \quad (3)$$

and the common focus of the hyperboloid and paraboloid is at  $x = -F-2ea$ .

The reflection efficiency at short wavelengths with a given aperture and focal length is maximized by choosing the grazing angles at both surfaces to be the same. This condition results in the constraint:

$$\left(\frac{a}{d}\right) = \frac{e}{e^2-1} \quad (4)$$

and the above equation for the focal length becomes:

$$F = \frac{a(1+2e-e^2)}{e} \quad (3a)$$

We also observe that:

$$\left(\frac{r^*}{F}\right) = \tan 4\alpha \quad (5)$$

where  $r^*$  is the radius at the intersection of the surfaces and  $\alpha$  is the grazing angle there, and, after lengthy algebra, we obtain:

$$(e-1) = \frac{4 \tan^2 \alpha}{1 - 3 \tan^2 \alpha} \quad (6)$$

The parameters of the mirror can now be calculated from equations 5, 6, 3a and 4 in that order. The results are (approximately):

Mirror Diameter  
(H-P Intersection,  
inches)

	$e - 1$	a (inches)	d (inches)
35.24	.0013443341	120.1614	.322857
33.29	.0011999766	120.1441	.288167
31.33	.0010630901	120.1276	.255277
29.37	.0009344476	120.1122	.224372
27.41	.0008157203	120.0979	.195853

The tolerances for the mirror can be divided into:

- a. Alignment tolerances between the individual mirrors of the nested set.
- b. Alignment tolerances between the elements of a single mirror; and
- c. Tolerances within an individual element (single hyperboloid or paraboloid).

We are assuming that the mirror supporting structures will be designed so that the position of each element can be adjusted or shimmed after its optical properties are determined. If this degree of freedom exists, then all necessary tolerances for categories a and b above have been met in existing mirrors. The group a and b tolerances, as will be shown below, are large compared to the wavelength of visible light and therefore conventional optical tests are adequate for their demonstration. There are now at least 10 grazing incidence mirrors (4 S-054, 6 S-056) which have optical resolution of one arc second or better, thus demonstrating that the tolerances of category b can be met with existing techniques. In addition, the two individual mirrors of each S-054 telescope are coaligned to an accuracy of better than 0.5 arc-second, thus satisfying the tolerances of category a. Each of these sets of tolerances will be discussed more completely below.

A. Alignment Tolerances Between Individual Mirrors of a Nested Set.

These tolerances are determined by the requirement that the focii of the different mirrors coincide. The translation tolerances perpendicular to the axis therefore are just the desired resolution in the focal plane, or about 0.0005 inch for 1/2 arc-second resolution. (The value achieved in the S-054 mirror alignment

is about 0.0001 inch.) The translational tolerance along the axis is the depth of field of the telescopes, or about  $\pm 0.004$  inch for these mirrors. The angular alignment tolerances are not critical because of the focusing properties of the telescope; errors of 10 arc-seconds correspond to mechanical tolerances of about 0.001 inch, whereas arc-minute errors would be acceptable in this parameter. All of the above tolerances correspond to good mechanical precision and are fairly routine in the optical industry. These tolerances were easily achieved in the fabrication of the S-054 mirrors.

Fortunately, it is not necessary to maintain coherence between x-rays reflected from different mirrors, or even widely separated parts of the same mirror; this would be necessary to obtain diffraction limited resolution which is several orders of magnitude better than expected here.

B. Alignment of the Individual Paraboloid and Hyperboloid Section.

These tolerances can be derived by considering displacements of the paraboloid only; displacements of the paraboloid and hyperboloid together have already been considered. We can consider a displacement error to modify the equations for the paraboloid by a quantity  $E(X, Y, Z)$  so that equation (1) becomes:

$$Y^2 + Z^2 = d [ 2 (X + F + 2ae) + d ] + E (X, Y, Z) .$$

If we now trace a ray through this system we find that the approximate effect of the error term is to introduce in angular change of magnitude:

$$\Delta \theta \approx \frac{1}{r^2} \left[ \frac{rdE}{dx} + \tan \alpha \left( E + Y \frac{dE}{dY} + \frac{ZdE}{dZ} \right) \right]$$

where  $\alpha$  is the grazing angle. That portion of the change in angle

which is common to all rays does not contribute to the loss of resolution since it can be compensated by realignment. Note that the effects of azimuthal errors are less than the axial errors by a factor of  $\tan \alpha$ . We can now consider the effects of various misalignment errors.

B-1. A relative axial translation by  $\delta$  is equivalent to the substitution  $X \rightarrow X + \delta$ , or  $E = 2\delta d$ ;

$$\text{and } \Delta\theta \approx \frac{2\delta}{r} \left(\frac{d}{r}\right) \tan \alpha \approx \frac{2\delta}{r} \tan^2 \alpha.$$

Therefore, for a blur circle diameter of  $1/2$  arc-second we obtain  $\delta \approx 0.1$  inch, which is not difficult.

B-2. A relative translation perpendicular to the axis in the Y direction equivalent to  $Y \rightarrow Y + \delta$ ;  $E = 2\delta Y + \delta^2$ ;

and  $\Delta\theta \approx 4 \left(\frac{\delta}{r}\right) \tan \alpha$ ; for a blur circle diameter of  $1/2$  arc-second we obtain  $\delta \approx 0.0005$  inch which requires careful machining but is fairly routine by optical standards.

B-3. A rotation of the paraboloid with respect to the hyperboloid is largely equivalent to introducing a flat mirror in front of the telescope, and ordinary optical tolerances result in a negligible loss of resolution.

The tolerances necessary to adequately align the two segments of an individual telescope are thus those of ordinary optical practice; this is largely the result of the grazing incidence optics. The achievement of these tolerances has been realized in at least ten existing mirrors.

### C. Tolerances Within an Individual Mirror Segment.

The above formula for the effects of error terms on the rays reflected from a paraboloid can be used to estimate the necessary tolerances on its fabrication provided that we do not consider

microscopic domains where diffraction effects are important. The tolerances on the hyperboloid are similar to those on the paraboloid but are more difficult to derive.

It is not necessary to apply the above tolerance conditions as a strict comparison between original design and the final product in some instances; for example, the final surface may be very nearly a paraboloid of slightly different focal length than the desired surface, and in this case the deviation in its manufacture may be offset by a translation of the actual surface along the telescope axis. The tolerance criteria here are thus to be applied to a "best fit" surface provided that the eventual "best fit" surface is adequate within the adjustment range of the support system, and does not result in an unacceptable change in the reflection angles. All tolerances on this large scale have also been met in at least ten existing grazing incidence mirrors.

Once a "best fit" surface is determined, the above formula may be used to determine the actual tolerances; in practice these tolerances must be stated in terms of the measurement technique. The principle error term is seen to be errors in slope along the telescope axis; these errors result in a displacement of the reflected ray by twice the value of the slope error. The azimuthal slope errors have smaller effects by a factor of the tangent of the grazing angle. In the past, the slope tolerances have not been specified because of difficulties in their measurement, and instead the deviation of the surface from a nominal curve has been somewhat over-specified in an attempt to control the slope errors. The actual allowed tolerances on the displacement of a surface without slope errors are essentially the alignment tolerances, which are quite large by normal optical standard as a consequence of the grazing incidence configuration.

In future mirrors it will be possible to specify and measure the gross contour to an accuracy of about one wavelength of visible light by means of hologram interferometry. This is quite adequate for displacement tolerances, but is not sufficiently sensitive for the detection of slope errors. (The sensitivity of this technique is limited to about one wavelength in the direction normal to the surface because of the grazing incidence optics.)

In previous mirrors the mechanical tolerances were written in a way which reflected the methods of measurement at that time and the necessary accuracy in the different dimensions. The following dimensions were usually specified:

1. Average radius at each end =  $\bar{R}_a, \bar{R}_b, \quad \overline{\Delta R} = \bar{R}_a - \bar{R}_b.$
2. Maximum out of roundness =  $\max | R(\phi) - \bar{R} |$
3. Maximum variation in  $\Delta R(\phi) = \max | \Delta R(\phi) - \overline{\Delta R} | =$   
 $\max | R_a(\phi) - R_b(\phi) - \overline{\Delta R} |$
4. Sagittal depth =  $\Delta S(x, \phi) =$  the deviation from a nominal curve running through the end points at which  $R_a(\phi)$  and  $R_b(\phi)$  are measured. In practice  $S(x)$  is measured by interferometric comparison of the mirror surface and a test plate, and the tolerances on this quantity are much smaller than the tolerance on the first three items above. Therefore, it is possible to measure the first three items only at the ends of the mirror segment, and then infer that the tolerances are met at other axial positions because of the tight tolerance in sagittal depth.

We will discuss the effects of these tolerances on the performance of the paraboloid; the tolerances on the hyperboloid are similar.

1. The principal effect of changing the radius of each end by

the same amount ( $\delta$ ) is to change the effective focal length of the parabola by  $(\delta/2 \alpha)$  where  $\alpha$  is the grazing angle. The tolerance on  $\delta$  was 0.0015 inch in the S-054 mirrors, and the value achieved was better than 0.001 inch in all cases. An error of 0.001 inch in  $\delta$  would necessitate a translation of about 0.035 inch for the smallest parabola being considered here. This would also introduce a negligible addition to the blur circle ( $\phi \sim 0.01$  arc-second).

2. The principal effect of changing the radius at each and by opposite amounts

$$(r_a \rightarrow r_a - \frac{\delta}{2}; r_b \rightarrow r_b + \frac{\delta}{2})$$

is also to change the focal length of the parabola by approximately  $\frac{F\delta}{L \tan \alpha}$ . The surface can then be put with a parabola that differs from the actual surface by less than  $1/4 (\tan \alpha) \frac{\delta}{r} \approx 0.004 \delta$  in this case. The slope error between the actual and best-fit surface is less than  $(\frac{\delta}{r}) \tan \alpha$ . In the S-054 mirror, the tolerance on  $\delta$  was  $< .00025$  inch, and the value achieved was 0.00007 inch which would result in a parabola focus shift of 0.06 inch with mirrors considered here. The resulting blur-circle contribution would be about 0.05 arc-second.

3. The variation in  $\Delta R(\phi)$  results in a direct contribution to the blur circle by an angle equal to  $2\Delta R(\phi)/L$ , where  $L$  is the length of the telescope. In the present mirrors a one arc-second diameter blur circle thus corresponds to  $\Delta R \approx 25.10^{-6}$  inches, or about one wavelength of visible light. This tolerance thus requires careful measurement by reasonably conventional optical techniques. It should be noted that this tolerance is applied to the "best-fit" surface rather than to the nominal



design surface. In the S-054 mirrors this tolerance is 0.0001 inch and somewhat better performance was actually achieved.

4. The effects of a roundness error depend upon the errors introduced in the azimuthal slope; for the simplest case of elliptical deformation the effect is to introduce the substitution  $Y^2 \rightarrow Y^2 (1 + \epsilon)$ ;  $Z^2 \rightarrow Z^2 (1 - \epsilon)$  in the equations for the parabola. This results in a maximum angular change of about  $3 \epsilon \tan \alpha$ . Thus, for the mirrors considered here, the total out of roundness must be less than 0.0005 inch to obtain a blur circle diameter contribution of less than one-half arc-second. In the S-054 mirror this was specified to be less than 0.0002 inch, and 0.00013 inch was achieved.

5. The maximum variation in  $\Delta S(X, \phi)$  has, as stated previously, been over stated in an attempt to control slope errors. The tolerance for the S-054 mirrors was 5 microinches, or about 1/4 wavelength of visible light. This corresponds to a slope error of 1/2 arc-second over a length of about 2 inches, and is necessary to improve this tolerance or its equivalent in order to be sensitive to slope errors with higher frequency spatial components.

It is thus seen that all tolerances on a macroscopic scale are within the present state-of-the-art of the optical industry, and have been achieved in several mirrors. The tolerances on a smaller scale, however, have not been sufficiently considered in the past and require further consideration.

The geometrical approach above is not valid when the scale becomes small enough so that diffraction effects become important. It is useful to divide the small scale mirror tolerances into surface finish requirements, which describe the microscopic roughness allowed by diffraction effects, and the intermediate horizontal

scale requirements which define the average slope of the surface over regions large compared to surface roughness criteria but small compared to the resolution of most conventional optical techniques.

The surface finish requirement is often calculated from the Rayleigh criterion which requires that surface irregularities introduce errors in the reflected wave front of less than  $\lambda/4$ . At a grazing angle  $\alpha$  the height variation  $h$  which leads to a  $\lambda/4$  wavelength error is  $h = \lambda/8\alpha$ . In the telescope system being discussed, the largest value of  $\alpha$  is 18.32 mr and the smallest wavelength reflected efficiently by this mirror is 3 Å; this results in a total allowable height variation of 20 Å; various other models of surface scatter yield, substantially the same result. This quality of surface finish is presently achieved in the better optical materials such as fused silica cervit, and certain semiconductor crystals. The polishing procedure for these large surfaces must be such that this surface finish is automatically achieved on at least a small scale.

The intermediate horizontal scale is defined by the horizontal distance required for a slope error to result in a vertical deviation equal to the surface roughness criteria of 20 Å. For discussion purposes, consider a tolerable slope error to be one that results in a one arc-second deviation of the ray; this deviation will result from a 1/2 arc-second axial slope error or a 25 (or greater depending on the mirror) arc-second error in the azimuthal slope. The horizontal distance required for the tolerable slope errors to result in a deviation equal to the surface finish requirement of 20 Å is then about 3 mm axially and about 60 μ azimuthally. These horizontal distances also happen to be those required for nominal angle changes of the above amounts in the design surfaces.

The telescopes may thus be considered flat over these dimensions which then define the horizontal scale. In summary, at the microscopic level the polishing process must result in surfaces which are smooth on a scale of  $20 \text{ \AA}$  and which are free of undulations on a spatial scale of about 1 mm in the axial direction and  $10 \mu$  in the azimuthal direction. The slope of the surface on this microscopic scale must be controlled to about  $1/2$  arc-second in the axial direction and 25 arc-seconds in the azimuthal direction; this is equivalent to a  $20 \text{ \AA}$  displacement over 3 mm axially or  $40 \mu$  azimuthally. We also note that adequate surfaces are presently achieved in flats or spheres of better optical materials. It is possible to remove material in steps of a few  $\text{\AA}$  over micron regions by ion bombardment; therefore, once the errors are determined and provided that the polishing process does not produce very high frequency errors, it will be possible to make the necessary corrections to the surfaces by ion bombardment and perhaps other techniques.

It should be possible to adopt existing measurement techniques to determine if these tolerances are being satisfied. The number of accurate measurements to be made is large, and as a practical matter, the measurement process must be reasonably automated.

The surface finish can be measured to sufficient accuracy with electron microscope techniques. Electron microscope studies of mirror surfaces are conventionally made by a replication process in which a replica of the surface is shadowed at a glancing angle by a heavier material; the electron transmission of the heavier material is then measured. The technique is thus insensitive to irregularities with slopes less than the grazing angle of the shadowing material. In present instruments this angle is limited to about  $1^\circ$  by the collimation of the shadowing

material; this is not a fundamental limit but simply represents the typical requirement for most applications. A shadowing angle of  $1^\circ$  is sufficient to detect slope errors which produce  $20 \text{ \AA}$  deviation in  $0.1 \mu$  or less.

The intermediate horizontal scale tolerances present the greatest measurement problem at the present time. The electron microscope is not capable of detecting small slope errors and a technique must be developed which has a vertical sensitivity of the order of the surface tolerance, or about  $20 \text{ \AA}$ , and a horizontal resolution adequate to detect an accumulation of small surface errors which constitute an error in the local average slope.

Multiple beam interferometers have achieved vertical resolution of less than  $10 \text{ \AA}$  with horizontal resolution of about one micron when measuring the difference between flat surfaces. It should be possible to extend this technique to a measurement of the difference between a test plate and the desired mirror surface. There is thus a gap between horizontal scales of  $0.1 \mu$  and  $1 \mu$  in the present measurement techniques; this gap could probably be filled by relatively minor modification to the electron microscope techniques.

A calculation of the effective area of the telescope as a function of wavelength for surfaces of nickel, fused silica, and platinum is shown in Figure 2-3. These values depend upon the real and imaginary parts of the index of refraction for each material. The real part was calculated from the Kramers-Kallmann-Marx expression which is adequate except for regions near absorption edges where the expression becomes singular because of certain approximations in its derivation. The imaginary part only depends upon the mass absorption coefficient and can be directly measured; unfortunately, the experimental data does not completely span

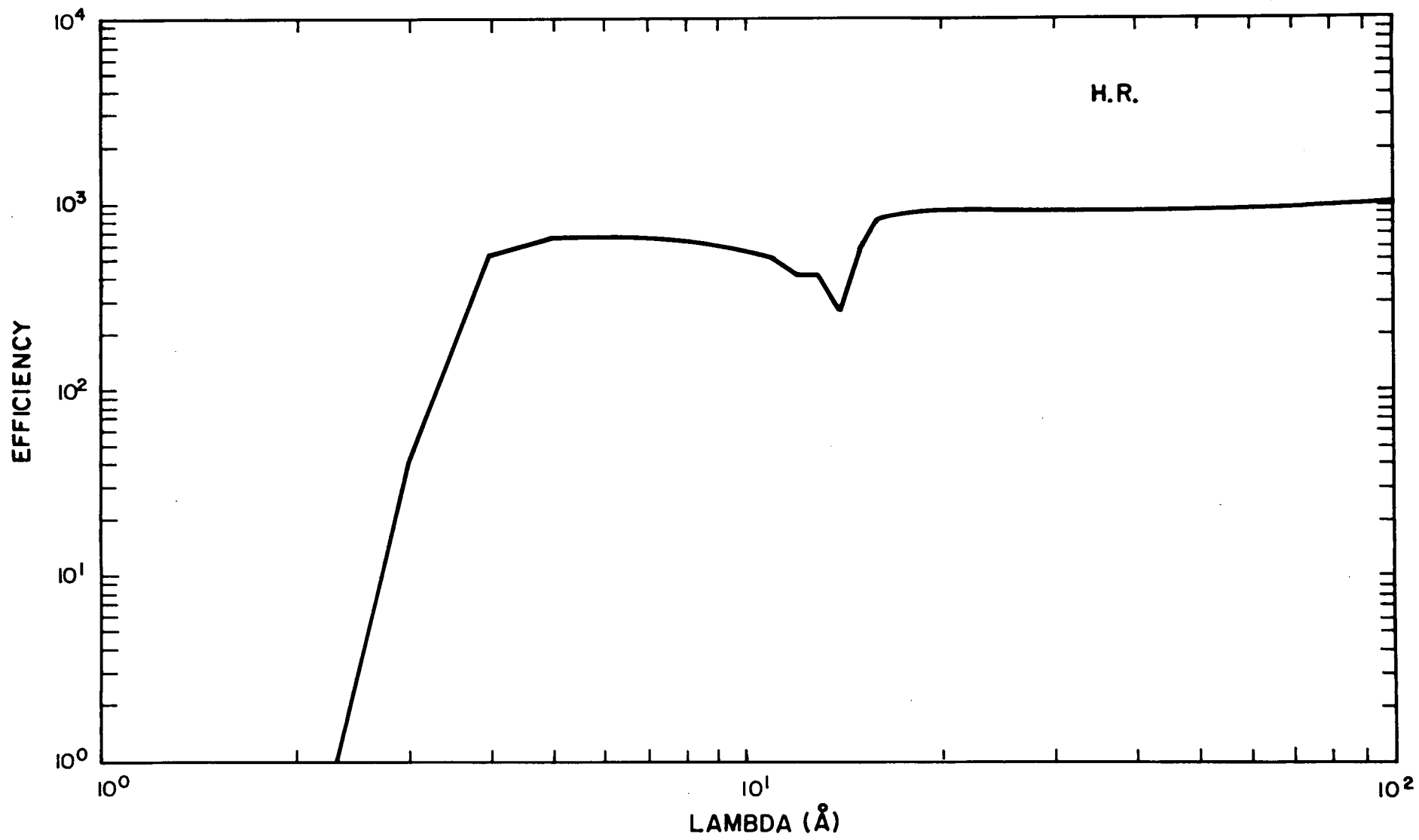


Figure 2-3  
High Resolution Telescope Effective Area

the wavelength interval of interest, and empirical models must be used. More accurate expressions for both parts of the index of refraction are available, and a better calculation should be made when the final configuration and material are chosen; the results, however, will not differ substantially from this calculation except for regions near absorption edges where the reflectivity will be greater than calculated here. In practice, the reflectivity will also depend upon the surface finish in a wavelength dependant fashion.

The nominal design wall thickness is 1/2 inch which results in a weight of 1500 pounds including mirror supports and assuming a glass material. The actual material will be selected after performing a laboratory evaluation, but in any event the mirror weight will not increase if Beryllium is substituted for the glass. Thin walls such as these have been shown to be practical in the S-054 mirrors. In the cylindrical shape of the mirrors, the deformation due to gravity is independant of the wall thickness to first order, and so thick walls are only necessary to support the material during the polishing process. With modern polishing techniques, these forces can be quite small. This approach is demonstrated by the one arc-second visible light resolution of the S-054 mirrors; deformations which are dependant upon wall thickness would affect the large scale contour and therefore the visible light resolution. The small scale irregularities would not depend upon wall thickness. The supporting structures for the mirror are shown in the Sketch F-SK-614-304 which is included. The support system holds the individual mirror segments in compression against a set of reference surfaces and can be adapted for either glass or metal wall mirrors. This sketch also shows the support system for the Detectors and the aspect system. The latter, which will be discussed in Section 5.1, is structurally an integral part

of the high resolution system in order to reduce the effects of structural deformations upon positional accuracy. The supporting structures and optical bench are estimated to weigh 700 lbs.

## 2.2 Large Area Mirror

The tentative design for the large area mirror incorporates the principle of a Baez device (Figure 2-4); the incident ray successively strikes two parabolas at approximately right angles to one another and at equal angles to the plane including their intersection and the focal point. The actual mirror would be composed of 16 identical modules (Figure 2-5); each module consists of a set of approximately parallel parabolic sheets followed by a similar set at right angles to the first. One of these modules is shown in Drawing F-SK-614-306. The Baez design has been chosen because of the possibility of semi-mass producing the individual segments at lower cost than the production of individually figured pieces; this design does, however, result in a longer focal length for the same collecting area and somewhat poorer resolution than the paraboloid-hyperboloid mirrors. In the present design, the radius of the blur circle will be approximately  $\frac{1}{22.5}$  times the distance off axis. There are also smaller correction terms, the largest being of order of 2 arc-seconds.

The effective area and weight of the mirror depend critically upon the thickness of the surface which is required to maintain the desired contour accuracy. The following results are obtained:

<u>Edge Thickness</u> (inches)	<u>Effective</u> <u>Area (cm<sup>2</sup>)</u>	<u>Volume of Wall</u> <u>Material (cubic inches)</u>
0.05	6,623	24,550
0.1	5,036	30,140

The worst case weight estimate, assuming fused silica mirror segments with 0.1 inch edges, is 3,000 pounds including an

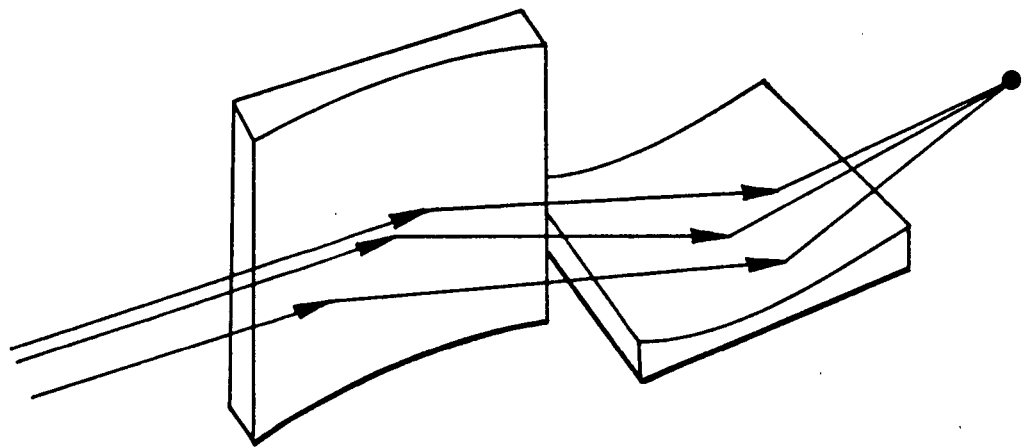


Figure 2-4. Baez Geometry for Large Area Telescope



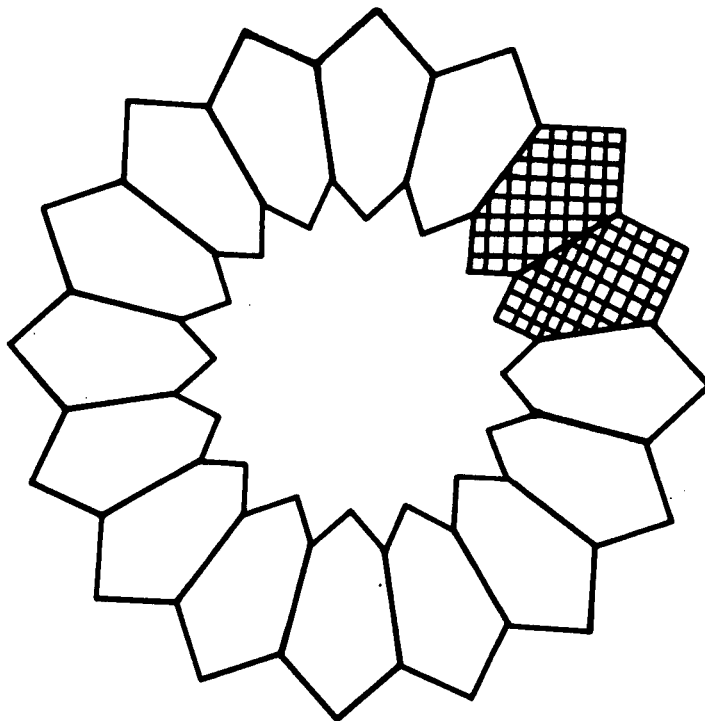


Figure 2-5. Large Area Telescope Modular Construction

estimated 600 pounds of structure. It may be possible to greatly increase the effective area by making the surfaces out of very thin, highly polished, coated silicon sheets; in this case, the structure would be larger in order to maintain the desired contours but the total weight should be reduced.

The focal length of the mirror is 45 feet and the grazing angles vary from 7.2 to 17.4 milliradians. The focal length is longer than the proposed launch vehicle and the detectors will have to be extended during the observations. The large area mirror and associated detector support structures are outlined in Drawing F-SK-614-308. The optical bench and other support structures will weight about 1600 pounds.

A calculation of the expected effective area as wavelength is given in Figure 2-6. This calculation is subject to the same difficulties as discussed previously in the High Resolution Telescope Section.

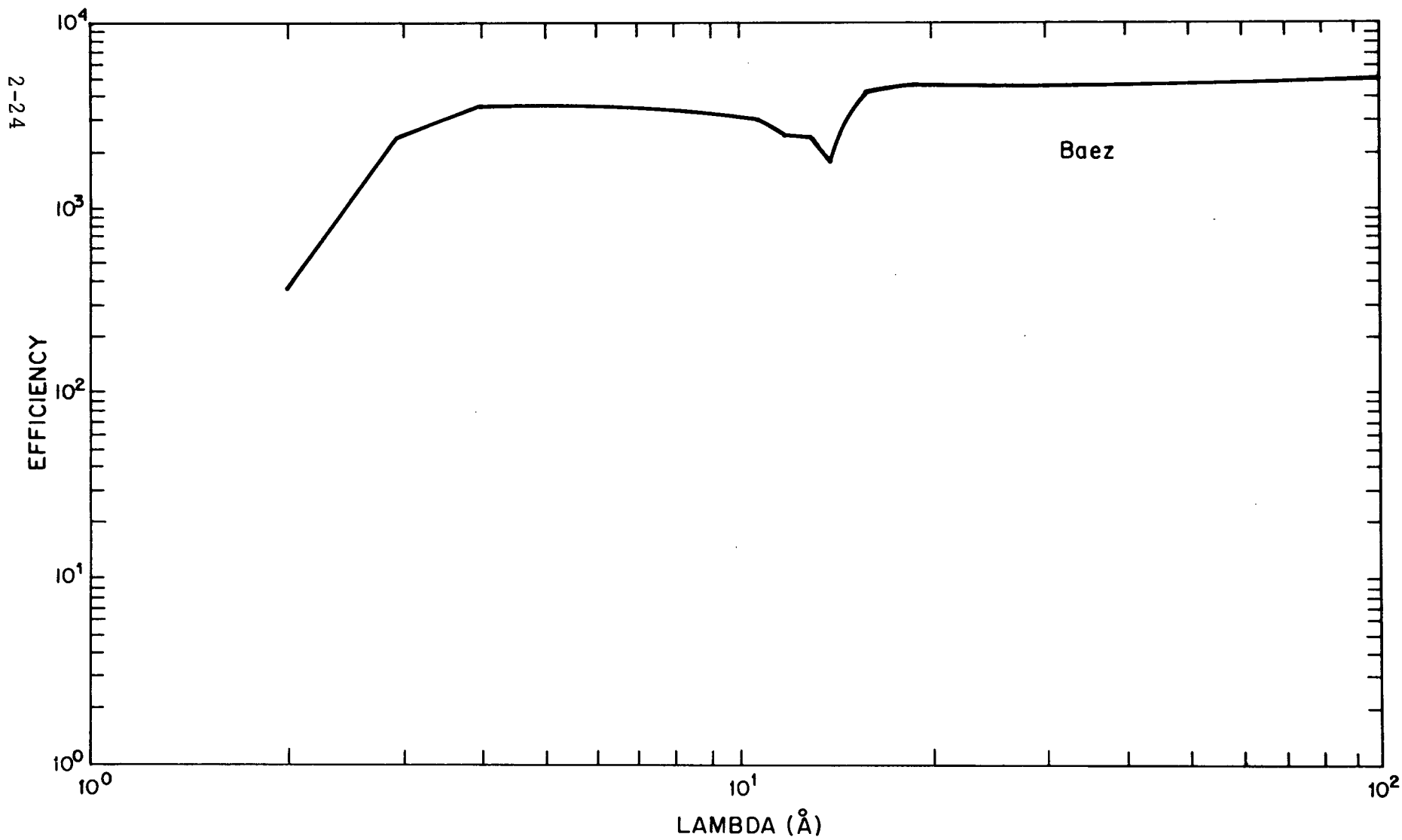


Figure 2-6  
Large Area Telescope Effective Area

### 3.0 PRIMARY EXPERIMENTS

#### 3.1 High Resolution Imagery

The AS&E experiment is designed to obtain high resolution images of x-ray sources from which accurate position, spatial structure, intensity and temporal variation measurements may be made. Low resolution spectral measurements will also be performed. A block diagram of the experiment is given in Figure 3-1.

The high resolution images are obtained by focusing the x-rays upon an x-ray sensitive multichannel plate image intensifier and recording the resulting visual image with a secondary emission current or other type of video tube. The present design provides four interchangeable image intensifiers for increased reliability and to allow the use of x-ray photocathodes with different spectral responses.

Low resolution spectral data are obtained by dispersing incident x-rays with a transmission grating located near the telescope mirror. Each point source in the field of view thus results in a point image and a line image in which the position along the line follows the normal grating function of wavelength. The spectral resolution is poorer than obtained with the crystal spectrometers to be discussed below, but as data are taken simultaneously over the entire spectral range, a higher data rate is obtained which enables the investigation of weaker sources and the temporal behavior of stronger sources. A six position filter wheel is included to obtain cruder spectral data from even weaker sources.

The experiment includes two principle calibration devices which may be inserted or removed upon command. The first, a radioactive source, allows a calibration of the detector efficiency. The second, a light sensitive photocathode, may be placed near

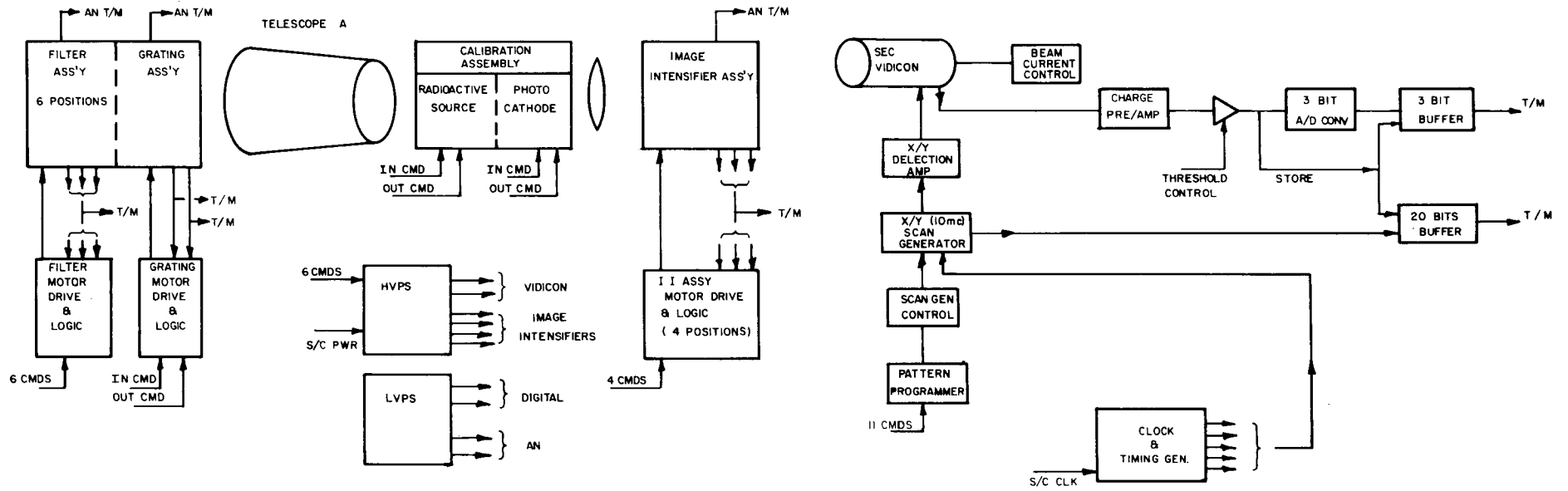


Figure 3-1

BLOCK DIAGRAM, AS&E HIGH RESOLUTION IMAGING EXPERIMENT

the image intensifier so that the detector will become sensitive to visual stars for in-flight measurements of the alignment offset between the telescope and aspect systems. The photocathode will be deposited upon a glass slide of proper thickness to compensate for small distance between the photocathode and the telescope focal plane. Fiducial marks may be obtained by focusing small electron or UV sources onto the image intensifier.

The SEC vidicon image field is divided into 1024 by 1024 one arc-second elements which results in a total field of view of 17 arc-minutes. It is not presently feasible to scan the entire field and maintain the one millisecond time resolution required for fast pulsar measurements; tentatively four scanning modes have been selected:

Mode	Field Size	Scan Rate (CPS)
A	1024 x 1024	16
B	128 x 128	1024
C	256 x 256	256
D	256 x 1024	64

All of these scan modes require approximately a 17 mc element scan rate. Mode A provides a scan of the entire field. Mode B provides the desired millisecond time accuracy for a field of approximately 2 arc-minutes. Mode C provides acceptable time resolution with a larger field of view and is included to allow a somewhat relaxed absolute pointing requirement. Mode D is included to obtain better time resolution during grating exposures; the long axis is oriented along the grating dispersion.

The combination of high resolution, high scan rate and variable field of view imposes severe restrictions upon the scanning electronics. A combination of digital and analog deflection

techniques will be used to provide a reversing linear deflection for the high speed horizontal deflection and a non-reversing digital deflection with blanked flyback for the lower speed vertical deflection. This approach minimizes the "dead time" associated with digital deflection rise times and yet maintains the flexibility required for variable field scanning.

The reversing linear deflection technique has the inherent problems of digital address synchronization and beam width error. Course address synchronization will be obtained by controlling the scan direction digitally and updating the digital address counter at the center scan crosspoint; fiducial marks may be used to compensate for drifts between the digital counter and the deflection circuitry. The beam width error results from the fact that an image scanned from left to right is first detected by the right edge of the beam, while an image scanned from right to left is first detected by the left edge. A first order correction is easily applied by subtracting the beam width from the digital address for right to left scans (assuming that left to right scans correspond to increasing address numbers). Dynamic focusing can then take care of the second order effect of beam width variation if that proves to be a problem.

At the beginning of each scan, a frame identification code and time will be stored and for each scan element in which the charge exceeds a preset threshold, twenty address bits and three amplitude bits will be stored. A maximum of 1,000 events/second is expected, and therefore the telemetry requirement will be approximately 25,000 bits/second including some housekeeping and the frame identification codes. The proposed data technique requires fewer bits than reading out the entire image of about  $10^6$  resolution elements, and it is unlikely that data compression

techniques exist which substantially reduce the data rate since most of the events are detector background and occur randomly over the field of view. There are indications that the detector noise rate may be less than stated here, but this cannot be assumed at the present time. The only source which will contribute a comparable number of events is Sco X-1, which can be observed with a smaller field of view and correspondingly smaller noise rate. The modes with smaller fields of view will require fewer address bits/event but more frame identifications will be necessary.

The power, weight, telemetry and command requirements are summarized in Table III-1.

TABLE III-1

<u>Weight Summary</u>		Relocatable Electronics
Detector Assembly	70 lbs	60 lbs
Grating Assembly	30	
Filter Assembly	<u>30</u>	
Total	130 lbs	

Telemetry - 25,000 bits/sec - (These will arrive asynchronously in 23 bit groups; the telemetry buffer will have to smooth the flow of data to the permanent storage system.

Command Bits

Filter Position	6
Grating	2
Power Supplies	10
Image Intensifier Selection	4
Calibration Sources	4
Program Generator	4



TABLE III-1--Continued

Gain Control	<u>2</u>
Total	32

Power (watts)

	<u>DC Requirements</u>		
	<u>Average</u>	<u>Peak</u>	<u>400 Hz</u>
Vidicon Deflection and Control Circuitry	9	9	
Data Processing Circuits	3	3	
Timing and Synchronization Circuits	.75	.75	
Motor Drives	<u>.75</u>	<u>.75</u>	
Total	13.5	13.5	
Low Voltage Power Supply Losses (70% Efficiency)	5.8	5.8	
High Voltage Power Supplies Losses	2.0	2.0	
Motors		18	
Vidicon Heater	—	—	<u>1.0</u> *
Total	21.3	39.3	1.0

---

\* This can be generated by a local oscillator if 400 Hz power is not available. Approximately 1.3 watts additional DC power would be required.

## 3.2 High Resolution Spectrometer

Crystals will reflect x-rays efficiently only when the incident angle is within a small angular interval about the Bragg angle defined by  $n\lambda = 2d \sin \theta_n$ . The MIT instrument utilizes the spectral selectivity to form a high resolution spectrometer. The device is similar to the conventional Johann geometry

(Figure 3.2) in which a cylindrical crystal of radius  $2R$  is tangent to the focusing circle of radius  $R$ . The focal plane image of a source is on the focusing circle, so all rays strike the crystal near the same angle, and therefore only a narrow range of wavelengths is reflected. All reflected rays are focused to a line on the focusing circle at the same distance from the crystal tangency point as the source, and conventionally a small detector is placed at this location. The fact that the angle of incidence is a (slow) function of the crystal location where the ray is reflected results in some loss of resolution when a single detector on the focal circle is used. This loss of information is avoided in the MIT instrument by placing an array of detectors near the crystal so that a reflected ray can be associated with a specific portion of the crystal and therefore with smaller intervals of incident angle and wavelength.

Normally, the instrument will be used to scan a portion of the spectrum; this is accomplished by simultaneously rotating the crystal, rotating the detector about the crystal through twice the angle of the crystal rotation and translating the crystal along the telescope axis. The instrument will scan back and forth between limits which can be set by commands; these limits may be narrow for studying an emission line, or broad for investigating an entire spectrum. Four Slewing rates will be required and up to six crystals will be available for different portions of the spectrum.

The following comments are intended to identify reasonable values for power, weight, and data rate requirements for the spectrometer system. The figures obtained are based upon typical parameters for the subsystems whose use is contemplated and upon our experience in implementing applicable electronics. These requirements as set forth are neither conservative nor optimistic,

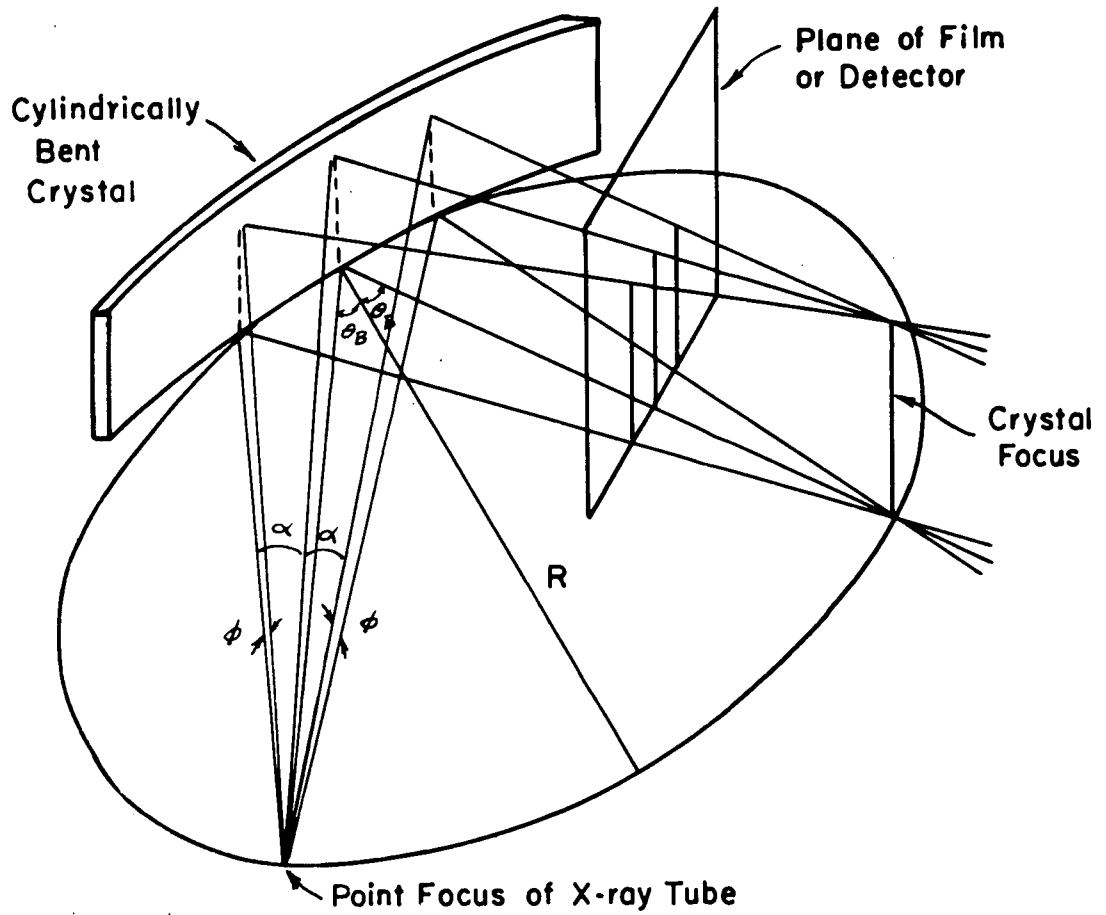


Figure 3-2 Focusing Circle Geometry

but are the "best reasonable estimate." Further refinement of these parameters will require a comparatively detailed design.

A spectrometer drive concept is shown in Figure 3-3. A command system is used to indicate forward and reverse stepping and the position to which the various subdrives are required to move. In addition, provision is made for automatically rotating the crystal at one of several preset rates by means of the step generator logic.

The motor to be used will probably be an incremental magnetic detent type stepping motor. A device having suitable characteristics which could probably be directly modified for space flight use is the SLO-SYN SS25. This device makes 200 steps per revolution. The steps are accurate to  $\pm .09^\circ$  nonaccumulative. The maximum "slewing" rate is 72 revolutions/minute. The shaft torque is 25 oz-in. The drive power is 5.6 watts, the weight is 1-1/4 lbs.

#### Maximum Slew Power

If it is assumed that the shaft is geared 4:1 to a worm of ten pitch and a motion of ten inches is required, the total number of revolution is:

$$N = 10 \times 10 \times 4 = 400 \text{ revolutions}$$

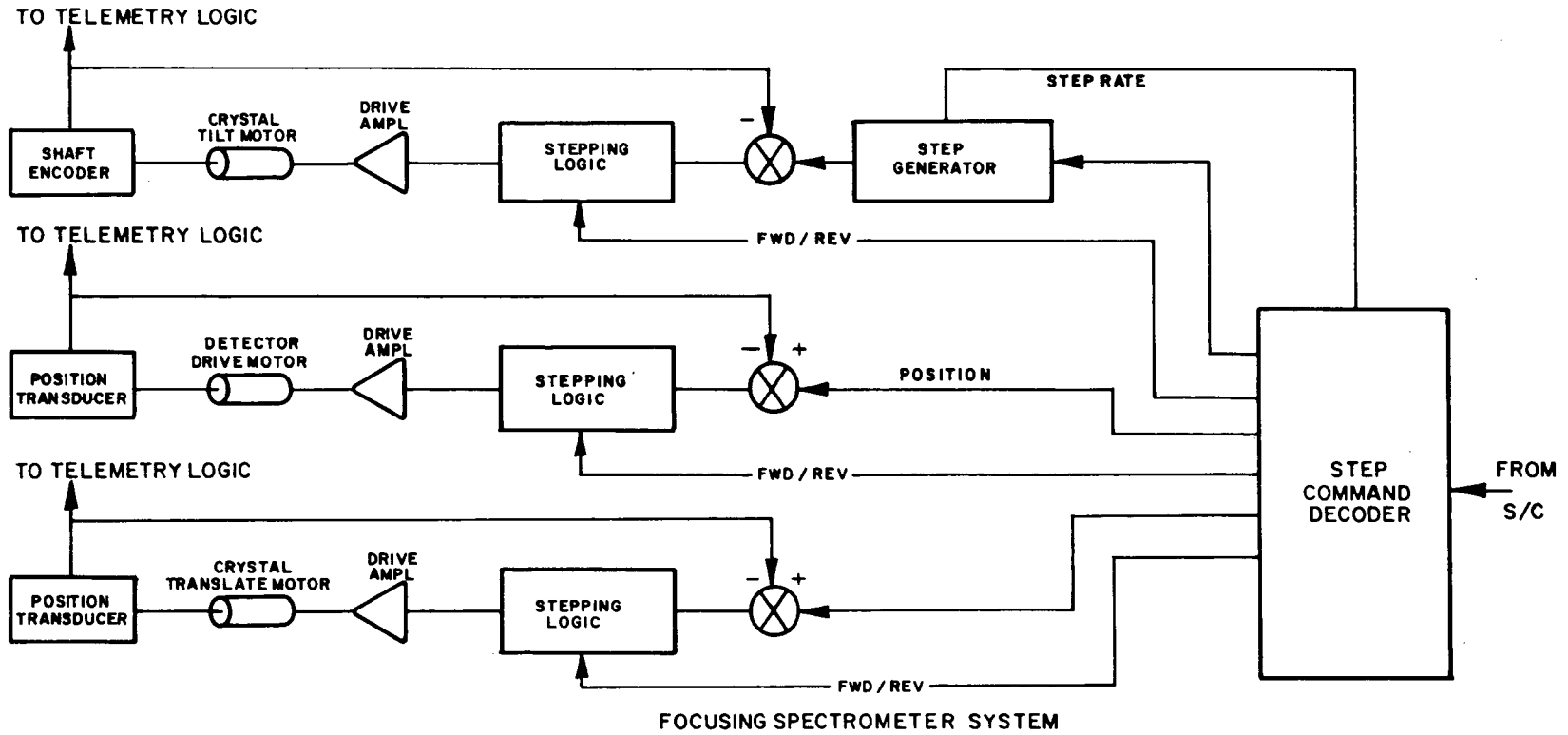
At 72 rpm, the minimum slewing time is:

$$T_{\max} = \frac{400/10}{72} = 5.56 \text{ minutes}$$

Assuming a complete slew once per 10 minutes at the fastest scan rate, the average power per motor during the fastest scanning rate is:

$$\bar{P}_{\text{slew}} = \frac{400/10}{72} \times 5.6 = 3.1 \text{ watts}$$

Since there are two "slewing" motors, the average maximum



FLAT CRYSTAL SPECTROMETER

Figure 3-3

SPECTROMETER DRIVE SYSTEM

power is 6.2 watts.

#### Crystal Tilt Drive Power

It is assumed that it is desired to rotate the crystal through  $65^{\circ}$  in 0.5' steps. This corresponds to 120 increments/degree or 43,200 increments per revolution. At 200 steps/revolution, this results in 216 revolutions or a gear ratio of 216:1. If a rotation through  $65^{\circ}$  is accomplished in ten minutes during the maximum scanning rate the motor speed is  $\frac{65 \times 120}{10 \times 200} = 3.9$  rpm = 13 steps/second. The power required is:  $P_{\text{tilt}} = \frac{3.9}{72} \times 5.6$  watts = 3 watts.

#### Drive Electronics

The drive electronics are estimated to consume about four watts. The logic requires about 1 watt and the drive amplifiers and transducers about three watts. This could be significantly reduced by pulse powering, but at the cost of a decrease in system reliability.

#### Weight

Weight for the spectrometer drive system is estimated at 11 pounds in addition to that of the mechanism and detector.

#### Spiraltron Array

It is assumed that an array of 100 x 100 spiraltron type detectors will be used. Each row and column will be subdivided into four alternating parts as shown in Figure 3-4. This subdivision will enhance the system reliability and simplify the amplifier-discriminator input. It can be seen from Figure 3-4 that each spiraltron is connected in parallel with 50 other units making a capacitive load of some magnitude in addition to the loading of the amplifiers.

Because of the relatively high gain of the spiraltron the expected charge per event is on the order of

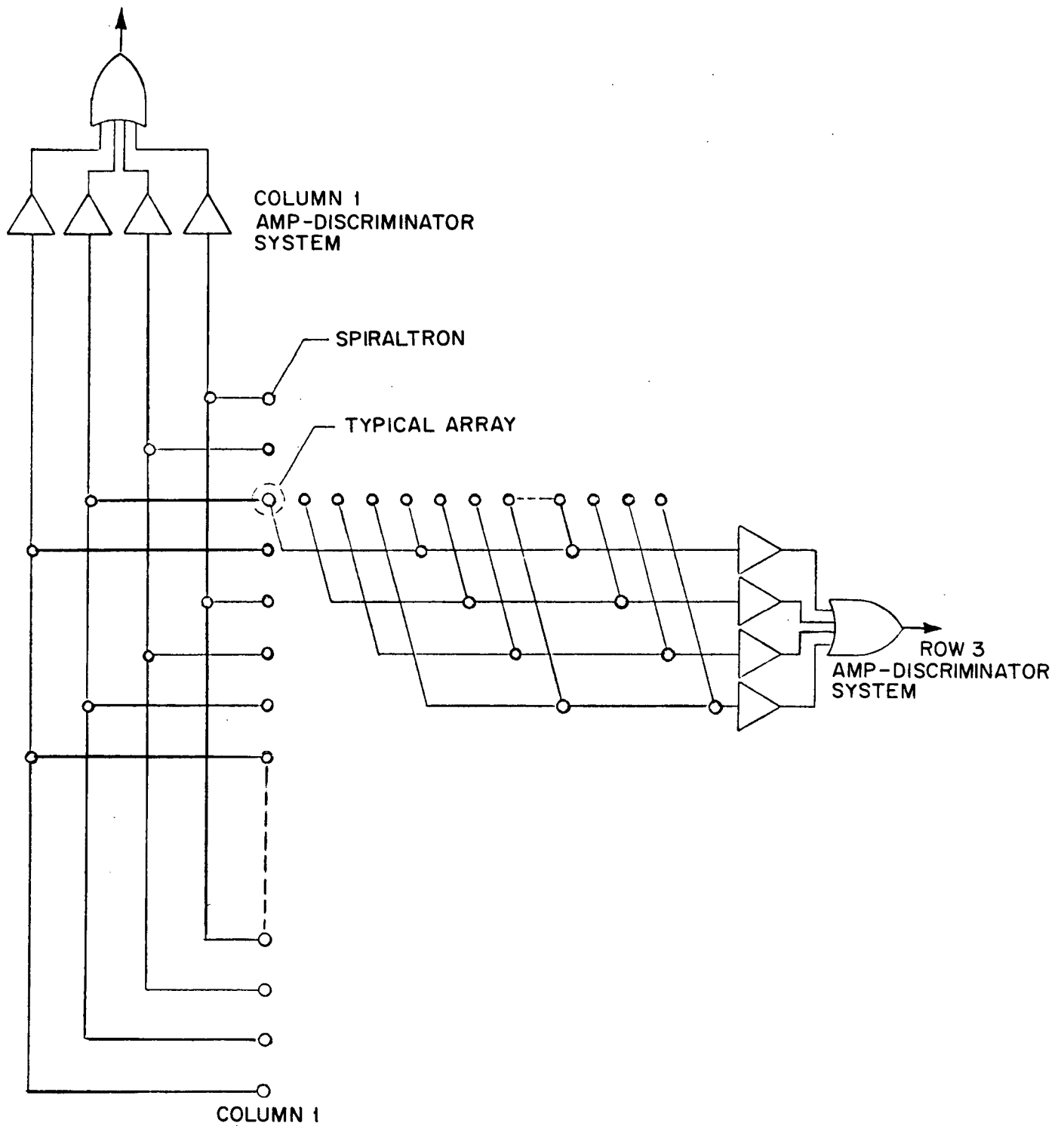


Figure 3 - 4.

SPIRALTRON ORGANIZATION

$$Q = 1.6 \times 10^{-19} \times 10^8 \text{ (gain)} = 1.6 \times 10^{-11} \text{ coulombs.}$$

If this is divided by 50, we obtain

$$Q^1 = \frac{1.6}{50} \times 10^{-11} = 3.2 \times 10^{-13} \text{ coulombs.}$$

If charge sensing is used, the voltage obtained from this charge on a 10 pf capacitor is:

$$V = \frac{Q}{C} = \frac{3.2 \times 10^{-13}}{10^{-11}} = 3.2 \times 10^{-2} = 32 \text{ millivolts}$$

This is an entirely satisfactory signal level and the option of charge sensing exists. This has the advantage of negating the array and amplifier input capacitance. We can provide a preamp-voltage amp-discriminator for approximately 8 mw per unit maximum. (This can be significantly reduced if voltage sensing can be used, but further study will be required to resolve that area.) Recognizing that there are 800 such systems, the total power for the array detectors is estimated at 6.4 watts maximum.

#### Address Identification and Formating

A detailed design is required for definitive estimating. A "worst-case" implementation without minimization would require 1400 gates (7 bits x 200 outputs) at 1 mw/gate which with periferal logic would require about 1.8 watts. (This can probably be reduced by at least a factor of two.)

#### Data Rate

If each event is represented by a 14-bit array location designation and a 6-bit time designation, the number of bits/event is 20. Taking the maximum event rate at 500/sec, the required data rate is:

$$R_{\text{data}} = 20 \times 500 = 10,000 \text{ bits/sec.}$$



Since time accuracies of the order of 1/2 millisecond are required, a time format word will be inserted approximately every 32 milliseconds so that 6 time bits will result in the desired accuracy, the total telemetry rate is about 11 kilobits/sec, which is less than the imaging experiment. Since these experiments cannot take data simultaneously, the same telemetry channels could be used. It is possible to implement an adaptive prescale so that the events which are tagged are identified in the following way:

<u>True Rate/sec</u>	<u>Telemetered Rate/sec</u>
0-50	0-50
50-100	Every other event (neglecting queing for short times)
100-500	Every 16th event

The prescale being used would be indicated in the format. This feature would reduce the data rate to 1000 bits/sec. It should be noted that a random access S/C storage would be more efficient since much of the time the event rate will be apparently less than 50/sec.

With respect to pulsar detection it is important to note that the time between samples at 1000 bits/sec is:

$$t = \frac{20 \text{ bits/sec}}{1000 \text{ bits}} = .020 \text{ seconds.}$$

However, the time flag will be appreciably more accurate, and as long as the "pulsing" is not synchronous with the data flow, an adequate trace can be put together.

Summary

<u>Power (watts)</u>	<u>DC Power</u>	
	<u>Average</u>	<u>Peak</u>
Drive Motors	6.2	11.2
Tilt Motors	.3	5.6
Drive Electronics	4.0	4.0
Array	6.4	6.4
Addressing & Format Logic	1.8	1.8
Housekeeping & Control Logic	0.5	0.5
Crystal Oscillator	3.0	3.0
High Voltage	<u>0.5</u>	<u>0.5</u>
Total	22.7	33.0
Power Supply Losses (70% efficiency)	<u>9.7</u>	<u>9.7</u>
Total	32.4	42.7

Weight (pounds)

Mechanism & Detector	26.0
Drive Systems	11.0
Oscillator	1.0
Power Converter	3.0
Electronics (at Detector)	<u>15.0</u>
Total Weight	56.0
Relocatable electronics	40.0

Telemetry                    11,000 bits/sec\*

\* (This includes clock updates and can be compressed to 1,000 bits/sec if necessary)

Command Bits

Set Scan Start	10
Set Scan End	10
Power Supplies	4
Calibration Source	2
Crystal Choice	6
Slewing Rate	4
Focal Plane Aperture	<u>4</u>
Total	40

### 3.3 Polarimeters

When soft x-rays are reflected through  $90^\circ$ , only the polarization component normal to the incident and reflected rays contributes effectively to the reflected power; the component of the incident ray which is polarized parallel to the reflected ray is reflected with extremely low efficiency. There are a variety of polarimeter designs based upon this fact; in the Columbia design the x-rays are reflected through  $90^\circ$  by a crystal with lattice planes oriented at  $45^\circ$  to the telescope symmetry axis as shown in Figure 3-5. The reflected ray is thus in the plane of the incident ray and the normal to the lattice planes at an angle of approximately  $90^\circ$  with the incident ray. A data proportional counter is placed in the desired direction and polarization is detected by rotating the entire assembly around the telescope axis and measuring the reflected power as a function of angle. A polarized x-ray source will result in a maximum in the counting rate when the azimuthal angle is such that the plane of the incident ray crystal normal, and reflected ray is perpendicular to the polarization of the incident ray.

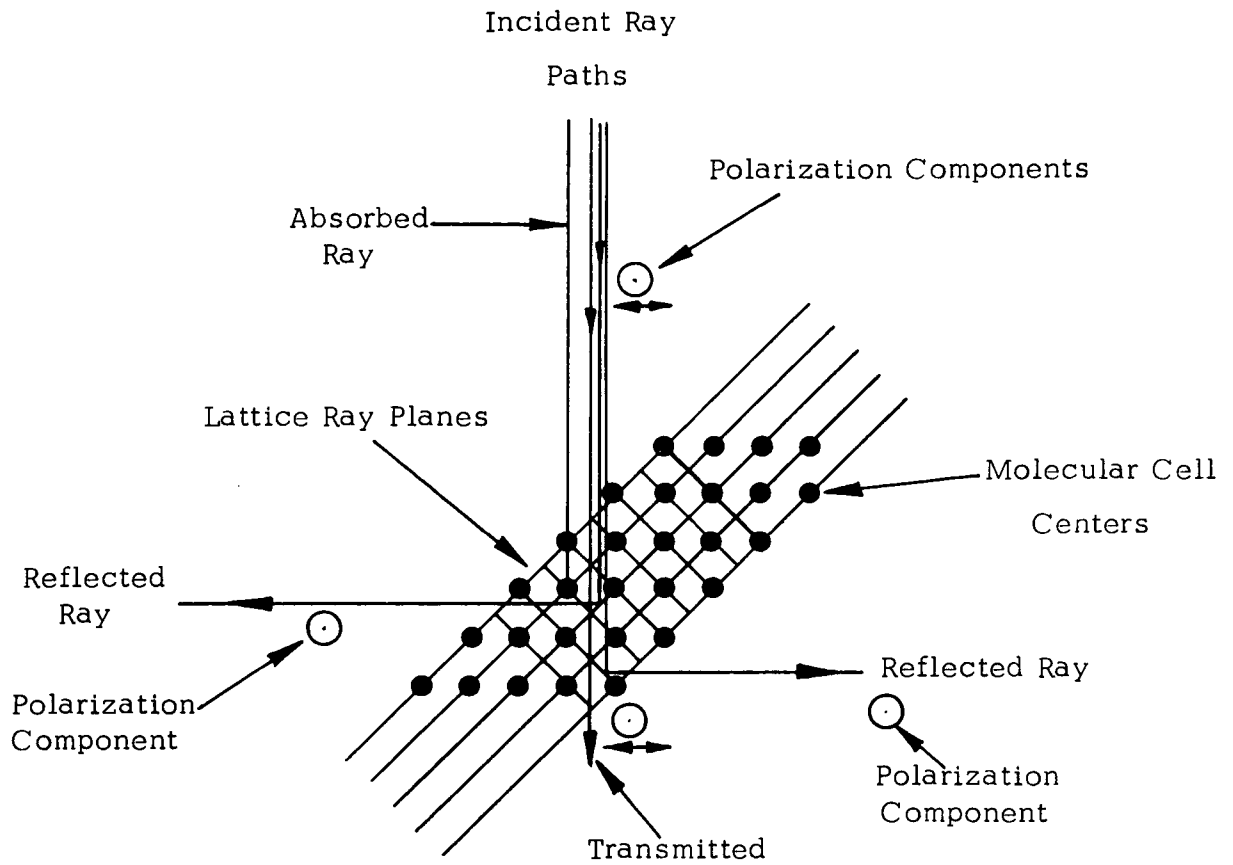


Figure 3-5. LiH Polarimeter Concept

Since the radiation must also satisfy Bragg's law for efficient reflection, only a narrow wavelength interval is efficiently reflected by a particular crystal. Tentatively two crystals, LiH and Graphite, have been chosen; These crystals reflect energy of 4.30 and 2.62 Kev respectively when the Bragg angle is  $45^{\circ}$ .

The LiH crystal has cubic symmetry as illustrated in Figure 3-5, and therefore, if the crystal is oriented so that radiation traveling in the axis direction is reflected in the +X direction, there will also be a set of lattice planes oriented so that radiation will be reflected into the -X direction. The same polarization component (the Z axis component) contributes to both directions of reflection and data counters are therefore included on both sides of the reflecting crystals. The graphite crystals do not have this symmetry and only one data counter can be used.

The crystals are purposely made quite thin so that the ray is unlikely to be absorbed after being reflected. Several crystals in series are thus required to reflect a significant portion of the incident radiation. A beam monitor counter is also placed after the crystals to measure the radiation passing through the crystals.

An electronics block diagram for the LiH polarimeter is shown in Figure 3-6.

Two proportional data counters, "A" and "B", as well as a Beam Monitor Counter are followed by typical proportional counter electronics including Pulse Shape Discriminators and Anti-Coincidence rejection circuits. The "A" and "B" data counter channels each terminate in 8 channel Pulse Height Analyzers. Each channel accommodates 10 bits or 1024 events; The Beam Monitor Counter electronics also terminates in an 8 channel Pulse Height Analyzer but with 13 bits or 8,192 events per

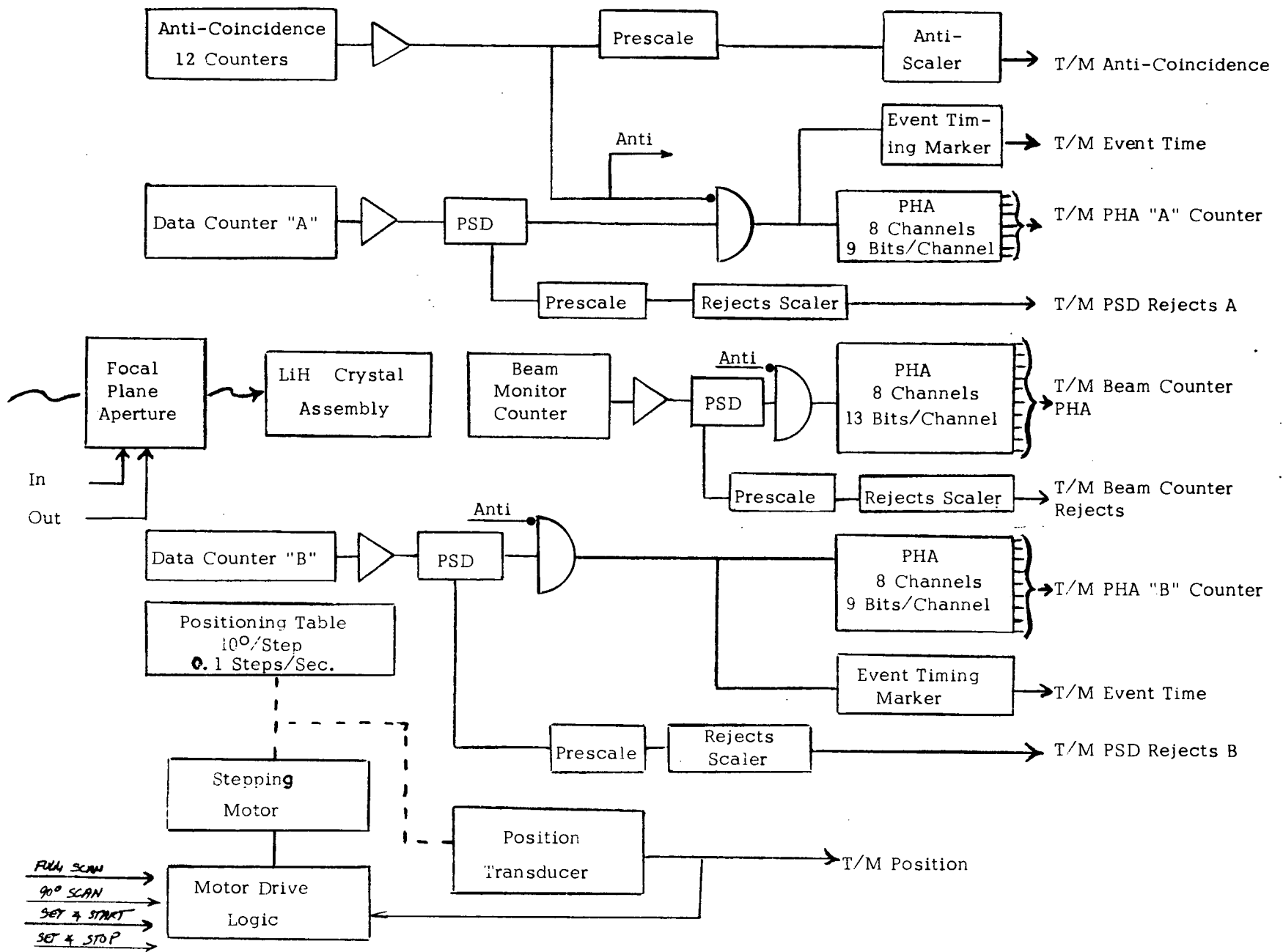


Figure 3-6  
LiH POLARIMETER

channel. The Data Counter "A" and "B" channels each provide "Pulsar" mode capability by means of the Event Timing Marker which indicates whether or not an event has occurred during the past one millisecond time slot.

The entire detector is mounted on a rotating table which is capable of being scanned in one of three possible modes: (1) a full scan of  $0^{\circ}$  through  $350^{\circ}$  and back again; (2) continuous scan between any two selected angles; and (3) alternating between any two points which are  $90^{\circ}$  apart. A 10 bit shaft encoder directly coupled to the rotating table will provide shaft position information.

Up-link data commands for control of table motion, insertion and removal of a fixed focal plane aperture and power supply control are required. The positioning system will utilize two codes interchangeably thereby deriving the advantages of simplicity and lack of ambiguity. The position encoder will be a Gray Code device which changes only one bit between adjacent positions thereby eliminating ambiguity at borderlines. The position will be commanded and processed in standard base two binary code which has the advantages of simple serial comparison techniques and relatively simple human interface. The conversion from Gray to binary code is easy when done serially starting with the most significant digit.

The Carbon Polarimeter is electrically similar to the LiH instrument except for the lesser number of anti-coincidence counters and the removal of the "B" data counter and its processing electronics. In all other respects, the instruments are electrically identical.

POWER ESTIMATES

<u>Graphite Power Estimates (watts)</u>	<u>DC Average</u>	<u>DC Peak</u>
Anti Coincidence Processor	. 52	. 52
Pulse Shape Processors (two)	1. 35	1. 35
Pulse Height Analyzer (data)	2. 88	2. 88
Pulse Height Analyzer (beam center)	3. 36	3. 36
Table Position Monitor	1. 05	1. 05
Scan Programmer	. 45	. 45
Timing & Synchronization Circuitry	. 45	. 45
Motor Drives	<u>. 30</u>	<u>. 30</u>
Total Elecronics	10. 36	10. 36
Low Voltage Power Supply @ 70%	4. 44	4. 44
High Voltage Power Supply	1. 50	1. 50
Motors	<u>9. 00</u>	<u>12. 00</u>
Total RQD	25. 30	28. 30

---

<u>LiH Polarimeter (watts)</u>	<u>DC Average</u>	<u>DC Peak</u>
Anti-Coincidence Processor	. 52	. 52
Pulse Shape Processors (three)	2. 02	2. 02
Pulse Height Analyzers (two data)	5. 76	5. 76
Pulse Height Analyzer (beam center)	3. 36	3. 36
Table Position Monitor	1. 05	1. 05
Scan Programmer	. 45	. 45
Timing & Synchronization Circuitry	. 45	. 45
Motor Drives	<u>. 30</u>	<u>. 30</u>
Total Electronics	13. 91	13. 91
Low Voltage Power Supply @ 70%	5. 96	5. 96
High Voltage Power Supplies	2. 00	2. 00
Motors	<u>9. 00</u>	<u>12. 00</u>
Total RQD	30. 87	33. 87



## TELEMETRY REQUIREMENTS

### Graphite Polarimeter

<u>Parameter</u>	<u>Maximum Count Rate</u>	<u>Bits/ Sample</u>	<u>Sample Rate</u> SPS	<u>Bits/Sec</u>
Anti-Coincidence	128	7	1	7
PSD Rejects	128	7	1	7
Event Time		1	1000	1000
PHA		80	1	80
PHA Beam Monitor		104	1	104
Table Position		8	0.1	1
Housekeeping Subcom				<u>6</u>
				1205

---

### LiH Polarimeter

<u>Parameter</u>	<u>Maximum Count Rate</u>	<u>Bits/ Sample</u>	<u>Sample Rate</u>	<u>Bits/Sec</u>
Anticoincidence	128	7	1	7
PSD Rejects A	128	7	1	7
PSD Rejects B	128	7	1	7
Event Time A		1	1000	1000
Event Time B		1	1000	1000
PHA "A"		80	1	80
PHA "B"		80	1	80
PHA Beam Monitor		104	1	104
Table Position		8	0.1	~1
Housekeeping Subcom				<u>6</u>
				2292

## COMMAND BIT REQUIREMENTS (EITHER POLARIMETER)

Scan Mode	2
Focal Plane Aperture	2
Start Scans	6
Stop Scans	6
Power Supplies	<u>4</u>
	20

### Weight Estimate (pounds)

LiH Polarimeter	38
Graphite Polarimeter	34
Relocatable Electronics	50

### 3.4 Non-Dispersive Spectroscopy and Stellar Identification

Solid state detectors have the best presently obtainable detector spectral resolution and efficiency using direct photoelectric interactions. The Goddard Space Flight Center's solid state detector experiment is primarily designed for realizing the full sensitivity capability of a grazing incidence x-ray telescope and providing spectroscopy with resolution sufficient for measuring line intensities. The experiment utilizes a cooled Si(Li) detector with an x-ray-transparent front window to extend the high efficiency to soft x-rays ( $\sim 10 \text{ \AA}$ ). The principal detector is surrounded by anti-coincidence solid state detectors to minimize the background arising from charged particles and Compton scattered photons.

The present state-of-the-art Si(Li) technology allows the achievement of an energy resolution of 125 eV FWHM (noise-limited, almost independent of energy). This will not improve very much in the next few years, since at 3 eV/ion-pair the system resolution is converging on that resolution allowed by electron

statistics. The present technology also allows for entrance windows of  $< 0.1$  micron of dead silicon, which would be virtually transparent to celestial x-rays were it not for the  $40 \mu\text{g}/\text{cm}^2$  of gold used for the creation of the p-contact. This amount of gold reduces the transparency of the window to only  $\sim 20\%$  at 1 Kev, but a like amount of nickel substituted for the gold, for example, could be used interchangeably with the gold (electrically), and would make the window considerably more transparent. We are presently instigating the development of such devices.

It is instructive to demonstrate the sensitivity of this detector with some realistic numbers. We note, first, that the well-known geometry of this type of device allows us to do a truly meaningful background estimation. We consider a bare crystal (no anti-coincidence) of area  $\approx 1 \text{ cm}^2$  and depth  $\approx 1 \text{ mm}$ , and distinguish between two separate background regimes:

- (1) True diffuse sky x-ray background which gets focused by the telescope.
- (2) "Internal" detector background due to charged particles and Compton interactions of higher energy photons in the crystal. The sky background component is just:

$$N \text{ (counts)} = S \frac{\epsilon A t}{L^2} I$$

where  $S$  is the detector area,  $A$  the gross mirror collecting area,  $\epsilon$  the net reflectivity, and  $L$  the focal length of the telescope. The  $N$  counts occur in a time  $t$  for a sky background intensity  $I$ . For the parameters:

$$\begin{aligned} S &\approx 1 \text{ cm}^2 & \epsilon &\approx 0.1 \\ A &\approx 10^3 \text{ cm}^2 & t &\approx 10^3 \text{ sec} \end{aligned}$$

$$L \approx 20 \text{ ft}$$

$$\frac{dI}{dE} \approx \frac{20}{E^2} \text{ cm}^{-2} \text{ sec}^{-1} \text{ sr}^{-1} \text{ Kev}^{-1}$$

we get  $N = 7$  counts in  $10^3$  sec in the energy range .5-5 Kev. This number is just proportional to the area of the detector, and can be made smaller if this area is made smaller. We note, however, that the diffuse background contamination of a 100% efficient device in the focal plane of the above telescope is only about  $3 \times 10^{-4}$  cts/ $\widehat{\text{min}}^2$ -sec. In the absence of any other background contamination, then, with the restriction of a  $10^3$  sec exposure, a detector need not be smaller than  $3 \widehat{\text{min}}^2$  (3 mm diameter) to have an average background rate of one count per total exposure.

With regard to charged particle rejection, it is obvious that active anti-coincidence is required for extremely low background. Almost all charged particles which pass through the device will identify themselves by the deposition of more than a few Kev of energy, but the very few which cut the corners of the crystal must be anti-coincided if we desire maximum detector sensitivity to weak sources.

A meaningful estimate of background contamination from Compton interactions in the raw device described above can easily be made because we know the geometry so well (i. e. we know the location and extent of the dead material). The contribution from this source has been estimated on the basis of no collimation or attenuation of the diffuse background above 10 Kev (clearly much worse than the actual case). The total contribution is best broken down into three energy ranges for the incident Compton scattered photons, and for an exposure of  $10^3$  sec with the above raw  $1 \text{ cm}^2$  detector we obtain:

$$N (E < 50 \text{ Kev}) = 5.8 \text{ cts}/10^3 \text{ sec}$$

$$N (50 < E < 100 \text{ Kev}) = 1.9 \text{ cts}/10^3 \text{ sec}$$

$$N (E > 100 \text{ Kev}) = 0.07 \text{ cts}/10^3 \text{ sec}$$

We see, immediately, that the detector volume is such that photons with energy  $> 100 \text{ Kev}$  will not be a problem, but that lower energy photons will create a .5-5 Kev background which is equal to the true .5-5 Kev sky background through the telescope. It is only necessary, therefore, to have an efficient (for  $E < 100 \text{ Kev}$ ), thin dead layer anti-coincidence detector to eliminate this component with respect to the .5-5 Kev sky background through the telescope. We could use a scintillator like CsI, for example, but we would then have the serious problem of enclosing the dead cold-finger contact to the Si(Li) within the anti-coincidence volume. It is much more reasonable to contain the anti-coincidence within the cold contact. It is possible to segment the device, as shown in Figure 3-7 taking separate outputs from the A and B portions of the central crystal. The anti-coincidence volumes C and D are tentatively chosen to be Ge(Li), since 1 cm of Ge(Li) is a virtual backstop for  $E < 100 \text{ Kev}$  (while the same thickness of Si(Li) is still transparent). The detector is then operated in the mode ABCD, with a background for discrete sources limited by the sky background focused by the telescope of  $3 \times 10^{-4} \text{ cts}/\text{sec-min}^2$ . This corresponds to a sensitivity to discrete x-ray sources of about  $10^{-4} \text{ photons}/\text{cm}^2\text{-sec}$  in a  $10^3$  second exposure.

A unique system for correlating the x-ray source with optical images has been devised to complement the x-ray observations. The front surface of the solid-state detector reflects visible light while transmitting the x-ray photons to the sensitive portion of the detector. The visible light reflected from the solid state detector is then imaged by a mirror and lens system and detected.

As shown in Figure 3-8, the Si(Li) detector is placed below the focal plane. Just above this plane, at a 50-degree inclination, there is a flat mirror whose central region is appropriately cut out to serve as an entrance port for the incident light cone. Images of x-ray and/or optical sources are formed in the focal plane. Beyond this focal plane, the diverging light rays are reflected by the polished surface of the Si(Li) detector and subsequently by the inclined mirror. They are finally focused by a lens onto a sensitive image detector such as a channel plate multiplier.

The location of an x-ray source and the correlation with optical data is accomplished by means of beam choppers (wires) located in the focal plane and sequentially scanning the field of view in a stepwise motion. The limiting resolution of better than 10 arc seconds expected for the telescope, and an anticipated jitter of about 1 arc sec/sec, allow the efficient use of 10 arc sec resolution elements in a 10 second exposure. We may note, however, that if we locate a point x-ray source to an accuracy of 10 arc seconds we will, in most cases, be in a position of identifying it with an optical counterpart of 21st magnitude or brighter. The expected sensitivity of this optical system for direct stellar identification is for 18th magnitude or brighter (for 10 second exposure).

The present plan is to have the beam choppers controlled by a programmable stepping motor so that the dwell times at any position will be  $\sim 10$  seconds and that the steps of each chopper will be matched to its occultation width. In this manner, the total occultation time for a point source will be less than 10% of the overall exposure, in accordance with the pursuit of a maximum sensitivity experiment.

An electronics block diagram is shown in Figure 3-9. In addition to the indicated telemetry, there will be some synchronization and housekeeping telemetry requirements. The total will be far less than with other operational modes of the telescope. The weight and power estimates for this detector are dominated by the refrigeration system which unfortunately cannot be defined well until the vehicle thermal system is understood. We have chosen to make very conservative weight and power estimates until better information becomes available. It is assumed that the refrigerator will be operated for extensive periods when the rest of the experiment is inactive.

An alternative to an actively refrigerated detector is a passively cooled device. Infrared detectors flown on Nimbus satellites have been kept at  $\sim 70^{\circ}\text{C}$  with the use of "cooling cones" to dissipate power generated in the detector. Such "cooling cones" are nothing more than high reflectance "cones" with the detector at the apex and the base pointing to cold space, allowing the easy rejection of several milliwatts of detector bias power. If the system can be configured such that the "cooling cone" base never points sunward, it should be possible to take advantage of the technology developed for the Nimbus detectors to passively cool this experiment. In so doing, the power requirements can be decreased by an order of magnitude.

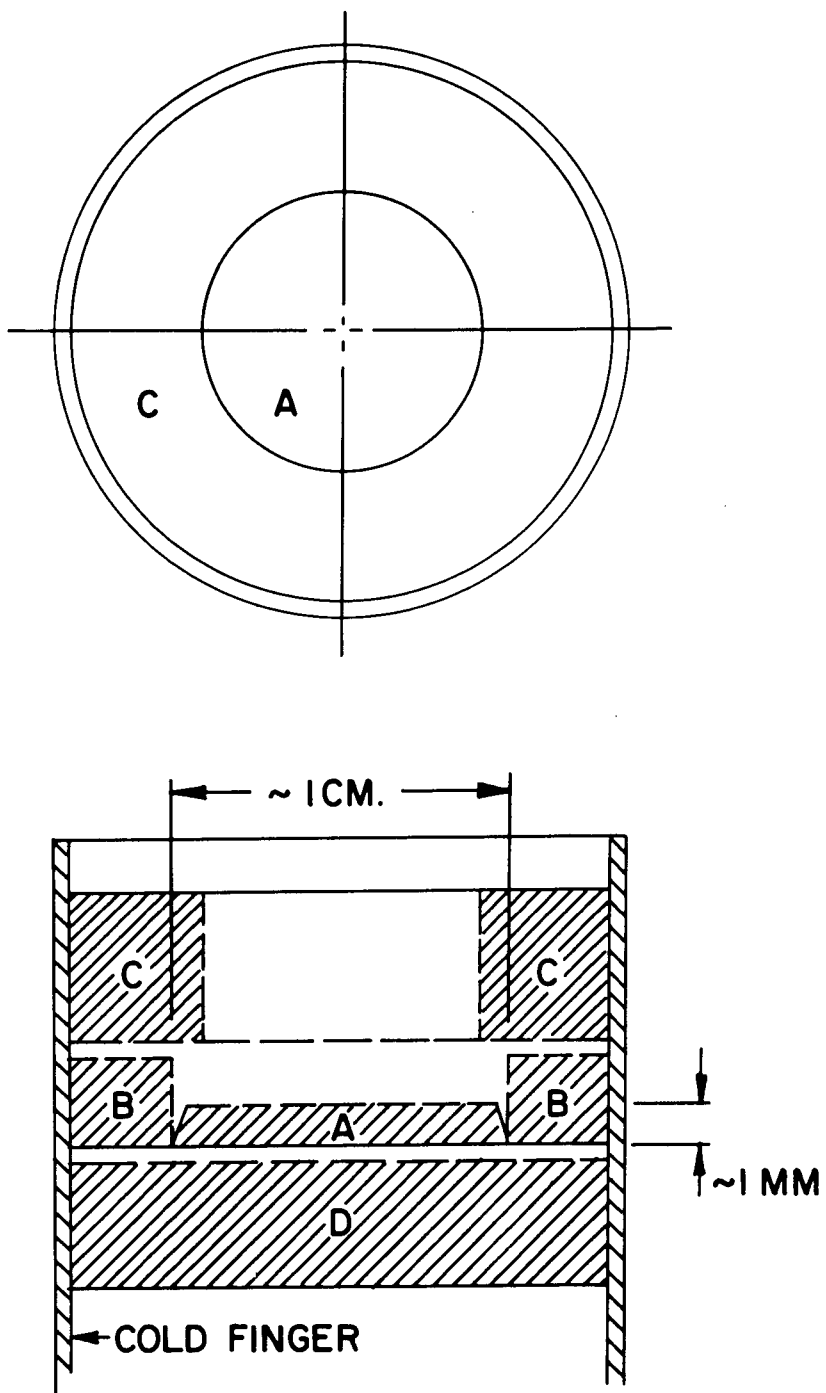


Figure 3-7 Composite Si(Li) Detector



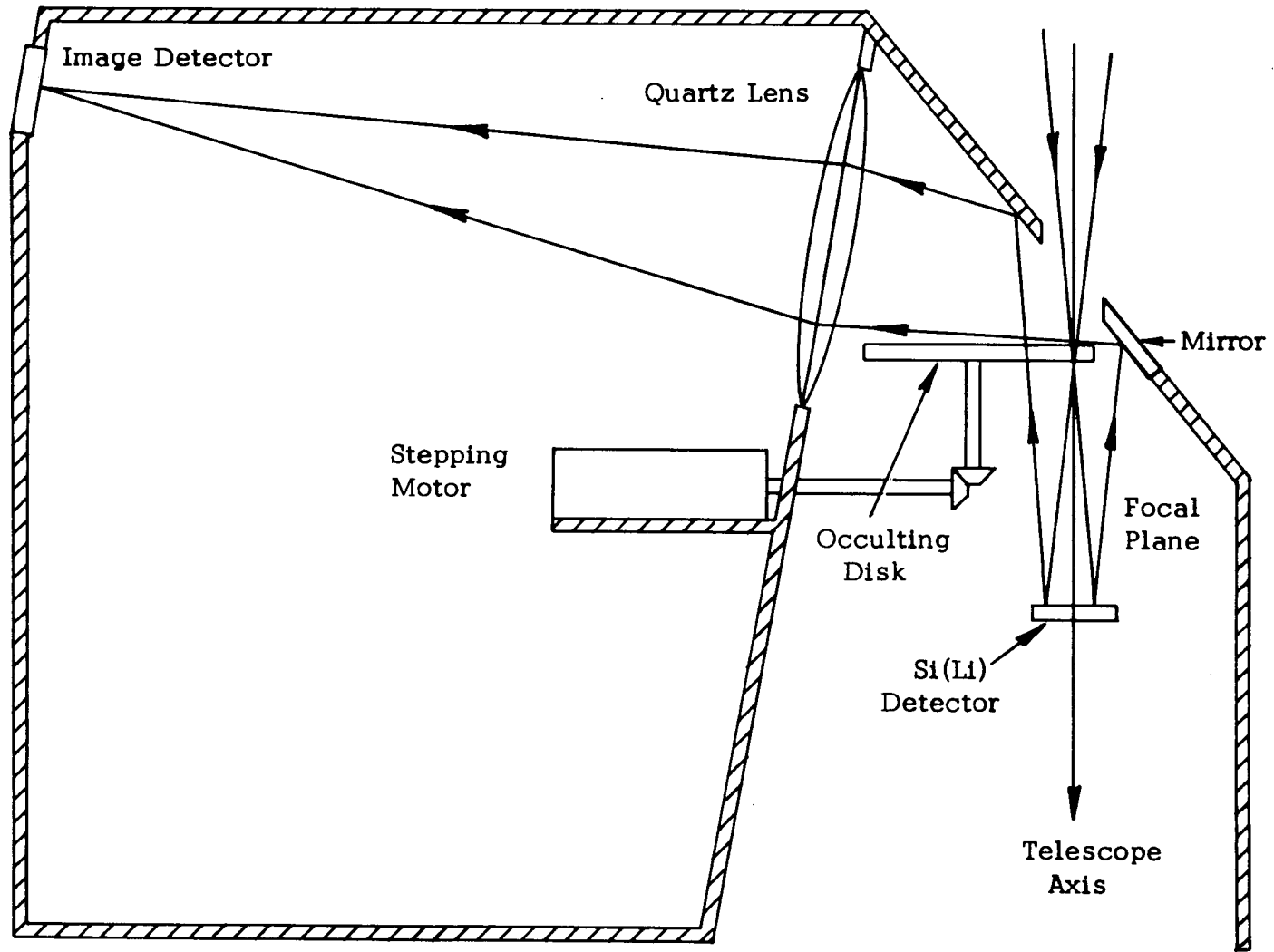


Figure 3-8

GSFC OPTICAL CORRELATOR

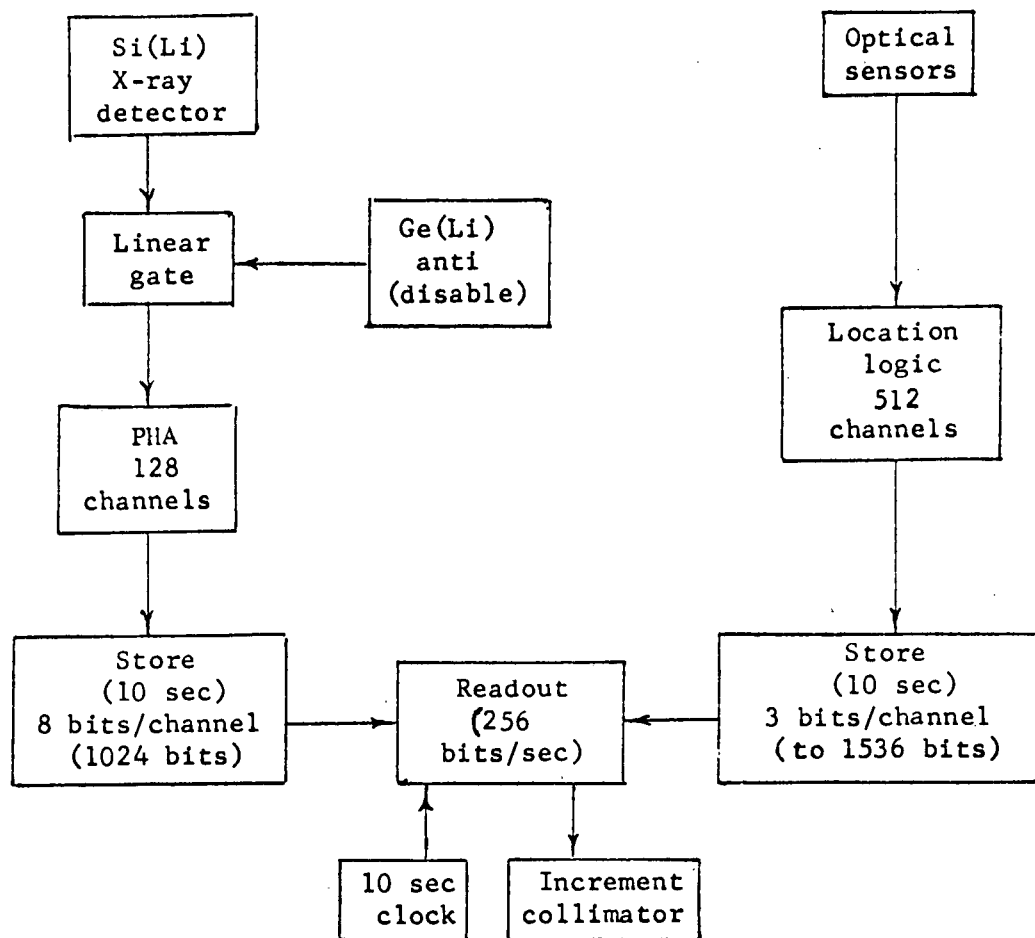


Figure 3-9

BLOCK DIAGRAM FOR GSFC EXPERIMENT

## 4.0 SUPPORT AND SUBSIDIARY EXPERIMENTS

These experiments have been included to support the primary experiments or to extend the capabilities of the observatory for certain important data which is not obtainable with the primary experiments.

### 4.1 Proportional Counter

Many of the x-ray objects have a substantial flux in the 1 to 10 Kev x-ray range which makes possible their observation with conventional proportional counters. The performance of such counters is well understood. They can be constructed to be stable over long periods of time and can be properly calibrated over their range of energy sensitivity. Several important applications can be recognized of an array of counters looking along the same axis as telescopes. In contrast with the proportional counters, it may not be possible to guaranty the stability of many of the other instruments in this facility; thus, the proportional counters provide a cross-calibration when viewing common targets. This is particularly important since many of the x-ray sources are known to vary and cannot themselves serve for the purposes of calibration. Also, in looking for time variability, particularly for stronger sources, such an array can have very high counting rates and thus be more sensitive to small changes in intensity than the telescope instruments. Thus proportional counter system has been included for this purpose. The collecting area will be approximately  $2500 \text{ cm}^2$ , and the collimator acceptance angle will be about  $1^\circ$  FWM. The mechanical arrangement is shown in Drawing F-SK-614-305.

The proportional counter detectors, as well as the anti-coincidence counters, are divided into two independent portions each of

which has its own power supplies and processing electronics.

The processing electronics (Figure 4-1) which is reasonably conventional, utilizes anti-coincidence, as well as pulse shape discrimination rejection techniques. The rejected events due to PSD and anti-coincidence are accumulated respectively in separate scalers. Prescalers assure a reasonable telemetry rate for these quantities.

An Event Time Marker provides a pulsar mode and identifies whether or not an event has occurred within the immediately preceding one millisecond time window. Periodically, a code word and time will be inserted in place of the data.

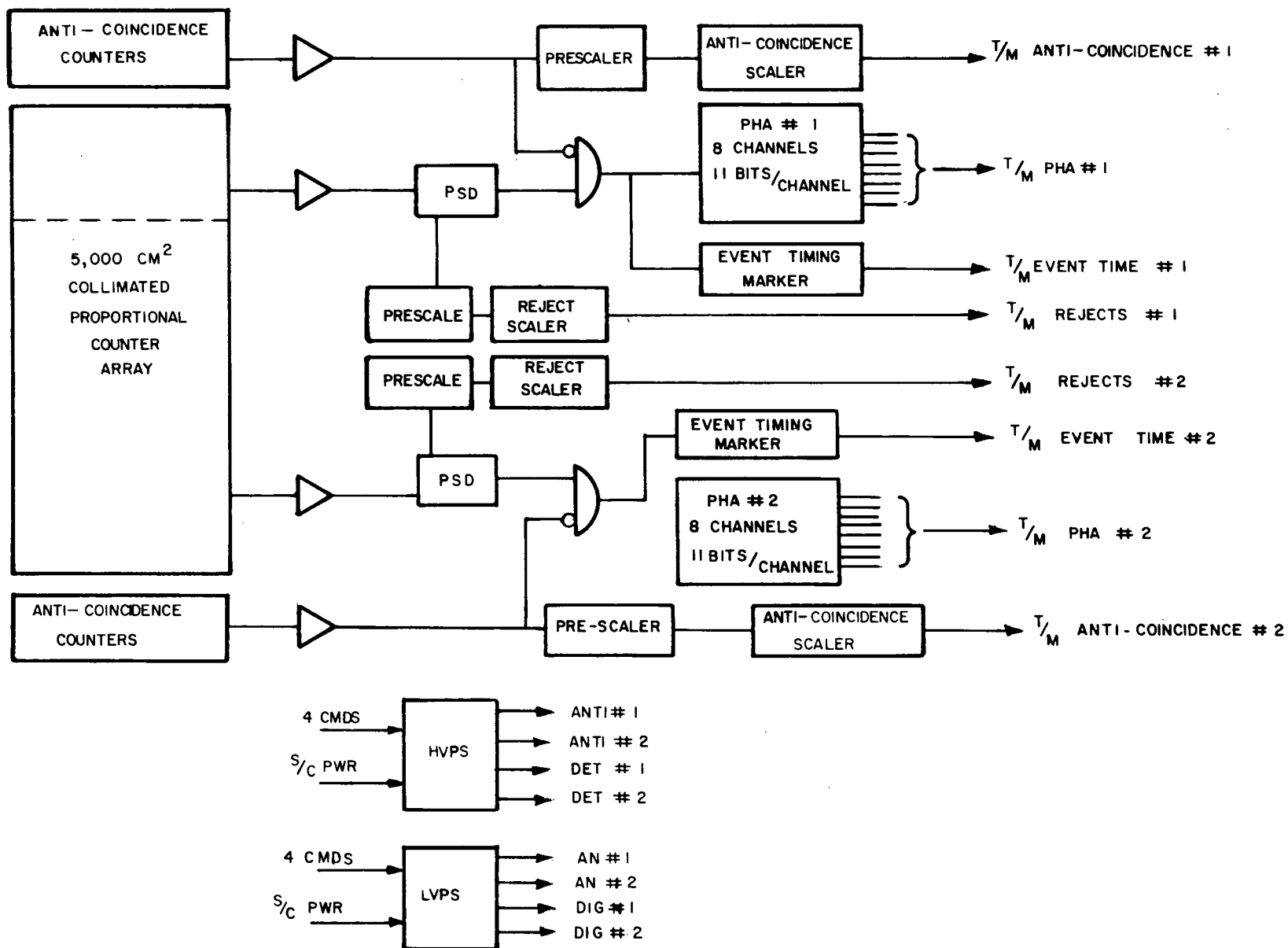


Figure 4-1  
PROPORTIONAL COUNTER

SUMMARY

Telemetry

	<u>Sample Rate/sec</u>	<u>Bits/ Sample</u>	<u>Bit Rate BPS</u>	<u>Max. Count Rate/Sec.</u>
PHA #1	1	11x8	88	2,048/channel
PHA #2	1	11x8	88	2,048/channel
Anti-Coincidence #1	1	7	7	128
Anti-Coincidence #2	1	7	7	128
PSD Rejects #1	1	7	7	128
PSD Rejects #2	1	7	7	128
Event Time Marker #1	1,000	1	1,000	1,000
Event Time Marker #2	1,000	1	1,000	1,000
Housekeeping (sub-com)	1	6	<u>6</u>	
			2,210	
			BPS	

Command Bits

Power Supplies 8

Weight (pounds)

Counters and Pre Amps	81
Collimator	30
Structure	50
Electronics	<u>5</u>
Total Weight	166
Relocatable Electronics	30

Power (watts)

	<u>Average</u>
Anti-coincidence Processor	.53
Pulse Shape Processors	6.25
Pulse Height Analyzer	3.12

<u>Power (watts)</u>	<u>Average</u>
Pulse Location Analyzer	4.86
Pulse Location Analyzer	3.75
Timing & Synchronization Circuitry	<u>.60</u>
Total Electronics	19.11
Low Voltage Power Supply @ 70%	8.19
High Voltage Power Supplies	<u>2.0</u>
Total RQD	29.30

#### 4.2 Flat Crystal Spectrometer

A collimated flat crystal spectrometer has been included to study the astronomically important emission lines such as  $\text{Fe}^{24}$  and  $\text{Fe}^{25}$  which are beyond the high energy cutoff of the telescopes. The system consists of a collimator ( $\sim 500 \text{ cm}^2$ , 36' FWHM acceptance), flat crystal and proportional counter detector. The proportional counter is surrounded by anti-coincidence counters to reduce the charged particle background. The device concept is shown in Figure 4-2. Additional mechanical details are given in Drawing F-SK-614-307.

A lithium fluoride crystal would be used because of its high peak reflectivity ( $> 40\%$ ) and a rocking curve somewhat broader than the natural line widths of the lines to be observed. Because of these properties it is highly efficient for observations of high energy x-ray lines. The  $4.026 \text{ \AA}$  2d spacing of LiF and its high second order reflectivity allows the 3-18 Kev region to be observed. The highly ionized calcium and iron lines are believed to be the only strong lines in this region, but this instrument will be the first to be able to investigate this energy region. Also, because of the high sensitivity of this instrument and because it will observe the source continuously, very weak lines from

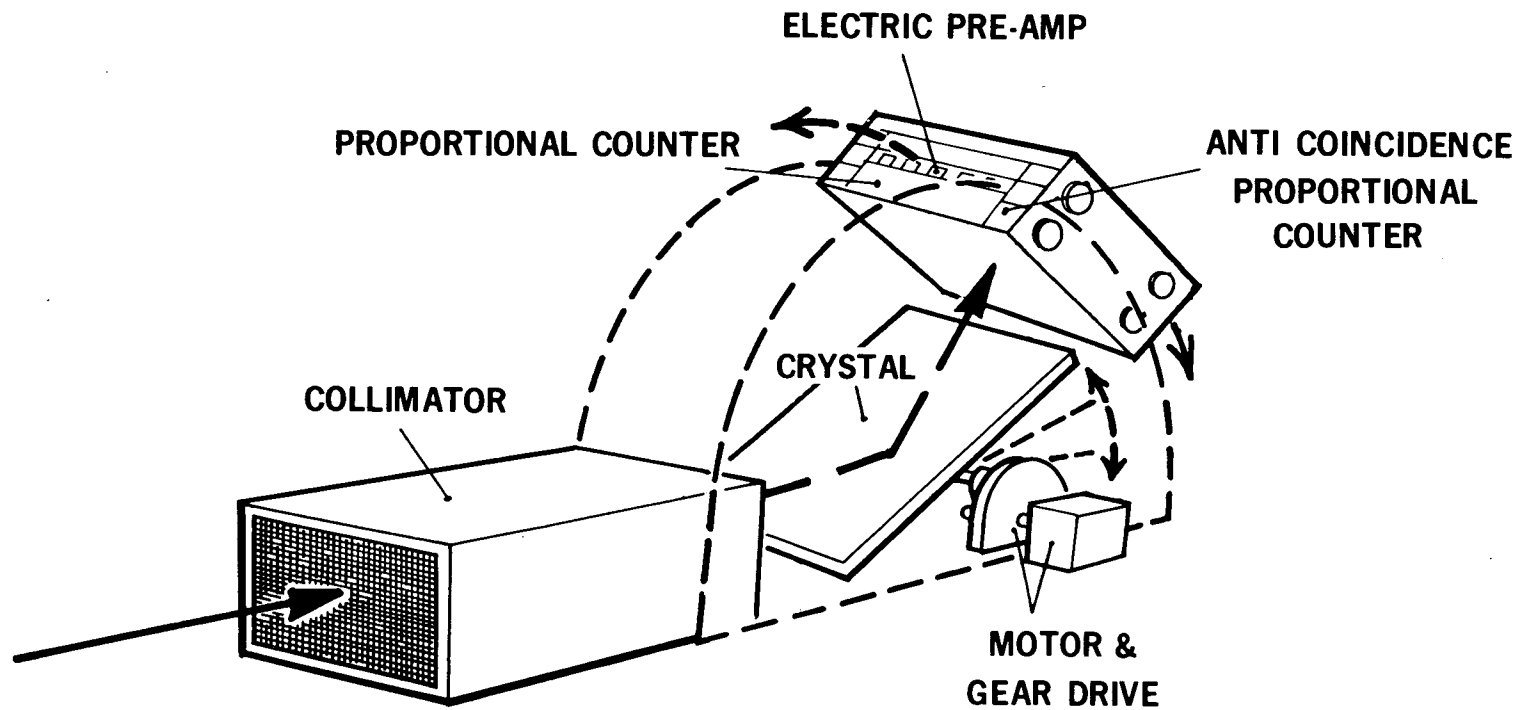


Figure 4-2

CRYSTAL SPECTROGRAPH 500 Cm<sup>2</sup>



the stronger sources could be observed, giving important information on the composition of strong x-ray sources and the production of heavy elements.

Doppler shifts and broadening of about 1 part in  $10^4$  can be observed, thereby allowing source temperatures and velocities to be obtained. Temperatures and information on production mechanisms can also be obtained from the relative strengths of different ionization states.

The flat crystal spectrometer will complement well the high resolution spectrometer. Comparisons of temperatures, velocities, line strengths and relative abundances obtained from the two spectrometers will be important in understanding x-ray production mechanisms and the nature and evolution of these sources. X-ray line emission is important in the 1-60 $\text{\AA}$  region. Because grazing incidence telescopes do not work in the lower wavelength and of this region, the flat crystal spectrometer was proposed in order to complete the program spectroscopical investigations of x-ray sources.

The spectrograph crystal and proportional counter detector are mounted on a mechanical drive system which maintains the proper relative orientation of both crystal and detector during the range of scanning angles. The drive for this mechanism is a magnetic detent gear head stepping motor providing a crystal rotation of 1 arc-sec/step. The total scan will require 12.5 minutes. A 15 bit shaft encoder mechanically coupled to the crystal will monitor its angular displacement with a resolution of 5 arc-sec.

A scan programmer permits selection via up-link data commands of the crystal scan start and stop angles. A "Scan Ident" output will provide data for establishing event time.

The detector, a collimated proportional counter, will utilize pulse shape discrimination and anti-coincidence techniques to filter undesired events. The occurrence of an event will enable the shaft encoder reading to be stored and subsequently telemetered. Figure 4-3 contains a block diagram of the electronics.

During a small portion of the crystal scan, the proportional counter detector will be illuminated by a radioactive source. This will allow for calibration as well as verification of gross spectrograph operation.

#### SUMMARY

##### Telemetry Requirement:

<u>Parameter</u>	<u>Sample Rate/Scan</u>	<u>Bits/Sample</u>	<u>Bit Rate BPS</u>	<u>Max. Count Rate/Sec</u>
Anti-Coincidence	1	6	6	64
PSD Rejects	1	6	6	
Events	240	15	3,600	240
Scan Ident	1	8	8	
Housekeeping Sub-com			<u>7</u>	
			3,627 BPS	

A more detailed design could reduce the 3600 BPS events requirement by a factor of about two.

##### Power (watts)

Anti-Coincidence Processor	.53
Pulse Shape Processor	.60
Crystal Position Monitor	1.20
Scan Programmer	.60
Timing & Synchronization Circuitry	.45

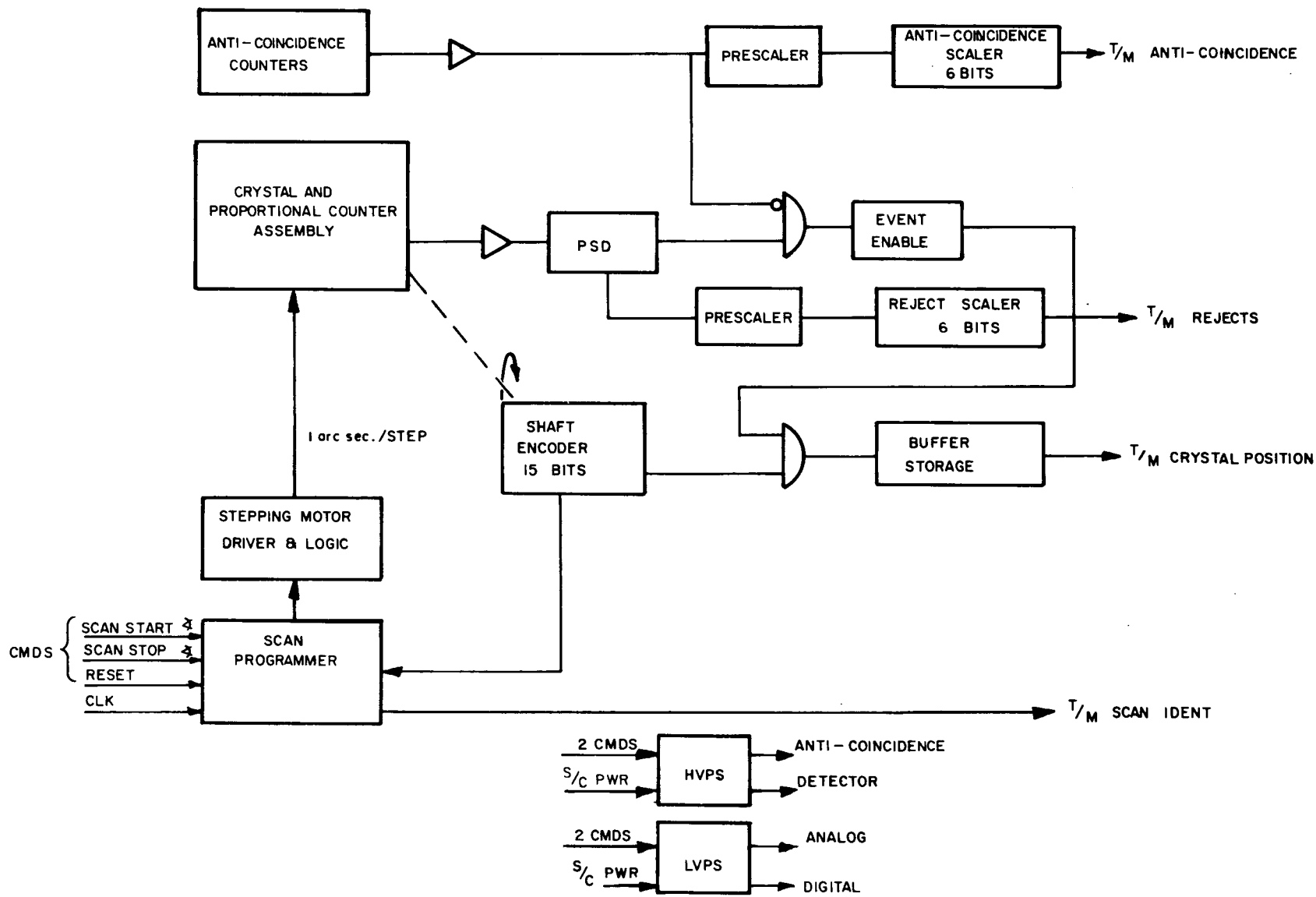


Figure 4-3  
SPECTROGRAPH

Motor Drive	<u>.15</u>
Total Electronics	3.53
Low Voltage Power Supply @ 70%	1.51
High Voltage Power Supplies	1.00
Motor	<u>6.00</u>
Total RQD	12.04

Command Bits

Start Angle	10
Stop Angle	10
Power Supplies	<u>4</u>
Total	24

Weight (pounds)

Collimator	18
Crystal Drive Assembly	37
Structure	40
Detector Assembly	<u>22</u>
Total Weight	117
Relocatable Electronics	20

4.3 Large Area Telescope Imaging System

An imaging detector sensitive at low energies has been included for measuring the structure in the diffuse background and the soft coronal emission of nearby typical stars. The detector is a multianode proportional counter in which the anodes are constructed of a resistive material such as one mil nichrome (20 ohms/cm). The coordinate along the wire is measured by comparing the charge collected at the two ends by low input impedance charge sensitive preamplifiers. The orthogonal coordinate is determined by the anode wire collecting the charge. In the present design there are 32 anode wires spaced at 1 arc-minute intervals. In an alternative design being considered,

the spacing of the center ten channels would be reduced to 1/3 arc-minute to take advantage of the improved detector resolution in the center of the field of view. In order to maintain symmetry, each of the outer 22 channels would consist of 3 anodes wired in parallel so that all anodes will have the same spacing and therefore the same electrical characteristics.

A block diagram of the electronics is shown in Figure 4-4. If individual preamplifiers were used at the end of each wire, a total of 64 would be required; the actual design requires only 16; the anodes are divided into two groups of 16, each of which is arranged into a 4 by 4 matrix as follows:

		Left Preamplifier					
		1	2	3	4		
	1	1	2	3	4	}	
Right	2	5	6	7	8		Anode number
Pre-	3	9	10	11	12		
Ampli- fier	4	13	14	15	16		

Thus, for example, an event on the 7th anode will result in charge being collected by the second right and third left preamplifier. If the collected charge exceeds a certain threshold the information may be used to form an event address.

The charges collected by all preamplifiers on the left and right sides are then summed to form the signal  $Q_R$  and  $Q_L$ . The position along the wire is given by:

$$\frac{d}{l} = \frac{Q_R}{Q_R + Q_L}$$

where  $d$  is the distance from the left edge and  $l$  is the total

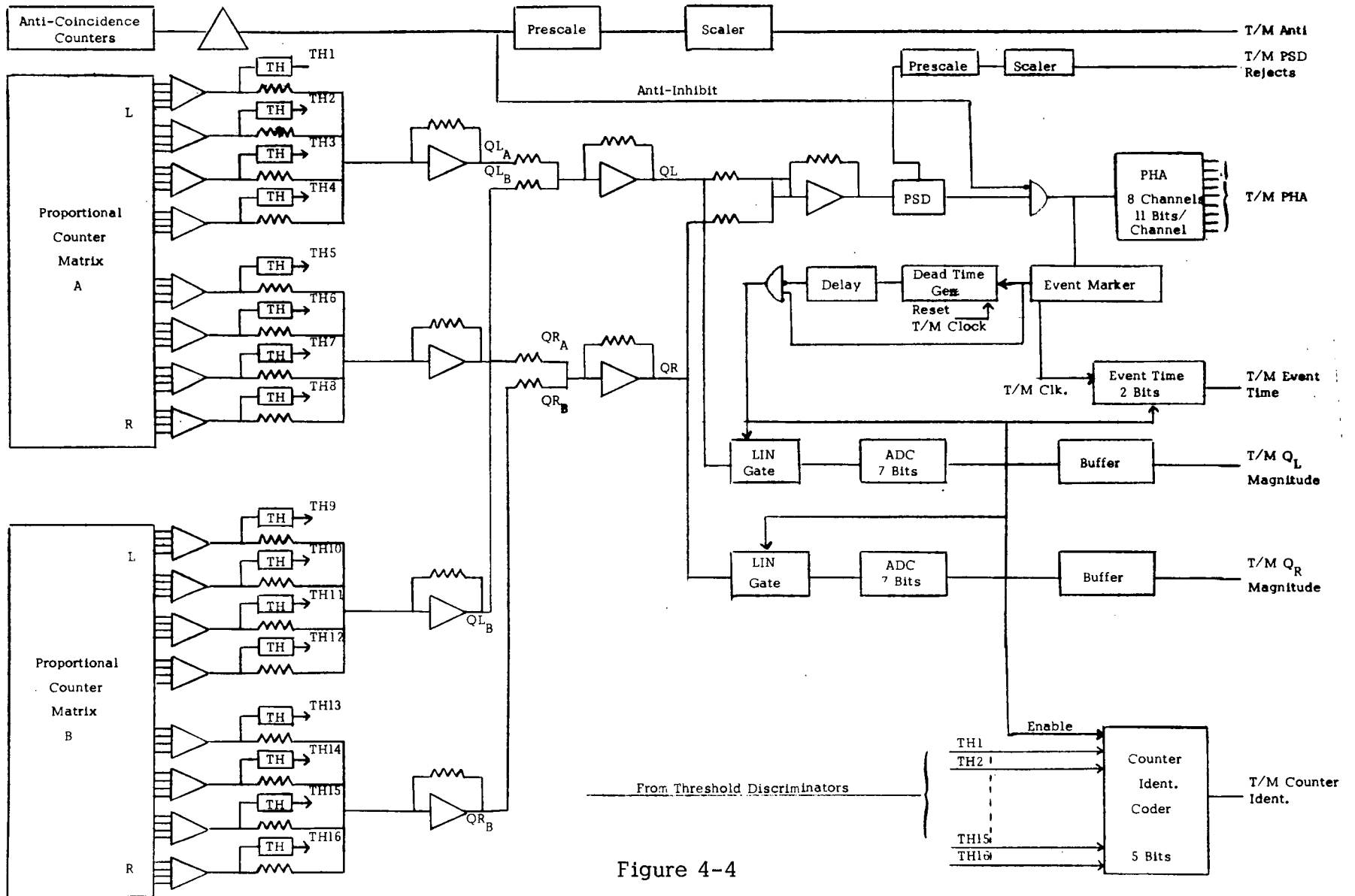


Figure 4-4

MULTI-CELLED PROPORTIONAL COUNTER ARRAY

length of wire. This division could be performed on the spacecraft and only the result telemetered, but we prefer to telemeter both quantities  $Q_R$  and  $Q_L$  and perform the division on the ground. The 7 bit digitizing of these quantities will result in one part in 16 maximum position error at the edge and one part in 32 error at the center of the field of view for an event with 1/8 of the total charge range. The positioning error for more energetic events will be less.

$Q_L$  and  $Q_R$  are also summed to form the total charge  $Q$ . This signal is subjected to pulse shape and anti-coincidence discrimination, and, if acceptable, produces an event marker and the total charge signal is processed by an 8 channel pulse height analyzer. The pulse height analyzer which has a capacity of 2048 events/channel and is read out once per second, provides the total counting rate and pulse height distribution in the event of a very high counting rate source. In addition, the position coordinates and a more accurate event time for up to 250 events per second are also telemetered to ground. The event marker associated with the first acceptable pulse in each 4 msec time frame results in the following processes:

1. Linear Gates present  $Q_L$  and  $Q_R$  to 7 bit analog to digital converters which produce and store in a buffer the 14 event position data bits.
2. The Event Time generator indicates in which 1 msec time window the event occurred within the 4 msec frame (2 bits).
3. The Counter Ident Coder identifies which proportional counter contained the event.
4. A register is set which prevents subsequent events being analyzed during that 4 msec frame.

SUMMARY

Telemetry Requirement:

<u>Parameter</u>	<u>Max. Count Rate/Sec</u>	<u>Bits/ Sample</u>	<u>Sample Rate SPS</u>	<u>Bits/Sec</u>
Anti-coincidence	128	7	1	7
PSD Rejects	128	7	1	7
PHA	2000	88	1	88
Event Time	250	2	250	500
Q <sub>L</sub> Magnitude	250	7	250	1750
Q <sub>R</sub> Magnitude	250	7	250	1750
Counter Ident	250	5	250	1250
Housekeeping (sub-com)				<u>8</u>
				5360

Power Estimates (watts)

<u>Proportional Counter</u>	<u>Average</u>
Anti-coincidence Processors (two)	1.05
Pulse Shape Processor (two)	1.35
Pulse Height Analyzers (two)	6.24
Timing & Synchronization Circuitry	<u>.30</u>
Total Electronics	8.94
Low Voltage Power Supply @ 70%	3.83
High Voltage Power Supplies	<u>2.00</u>
Total RQD	14.77



Weight (pounds)

Detector Assembly 15

Relocatable Electronics 60

Command Bits

Power Supplies 8

4.4 Large Area Telescope Mosaic Crystal Spectrometer

Mosaic crystals, which can be thought of as many thin layers of slightly misaligned perfect crystals, have large effective reflectivities at higher energies because an x-ray photon will penetrate the mosaic crystal with comparatively small absorption until it strikes a subcrystal having the proper Bragg angle; it will then have a high probability of being reflected. The Columbia objective crystal spectrometer consists of a crystal placed in front of the large area telescope. Unidirectional x-rays from a point source strike the crystal and are reflected at angles corresponding to their wavelengths. The reflected x-rays are then focused by the large area mirror and detected with the AS&E position sensitive proportional counter. It is not necessary to know the crystal angle with great accuracy since the wavelength is determined by the angle between the incident and reflected ray; it is necessary to know the source and telescope axis directions accurately, and the vehicle axis must be offset from the source as if the source were being observed with a mirror.

The present design has two crystals, LiH and graphite, on either side of a large flat rotating table. The mirror angle with the telescope axis varies from  $30^\circ$  to  $60^\circ$  in  $1/4^\circ$  steps during observation periods; this corresponds to a vehicle motion of  $60^\circ$  to  $120^\circ$  in  $1/2^\circ$  steps. The actual observing program will concentrate upon weak sources and the steps will occur at approximately orbit intervals.

The crystal would be deployed after launch and would be stored to the side of the large area telescope when not in use. The crystal dimension results in about 10% loss of effective area at the  $30^\circ$  angle, and about 20% obscuring of the high resolution telescope at the  $60^\circ$  angle. The latter effect is not important as it is unlikely that the high resolution telescope would have a source to observe at the vehicle offset angle required by the objective crystal spectrometer.

The electronics for the objective crystal consists of a system to drive the crystal to a preset angle in  $1/4^\circ$  increments and a 15 bit (3 arc-second in  $30^\circ$ ) shaft encoder. There is also a deployment and storage requirement. A redundant reset system will be provided.

The LiH crystal will consist of square modules, 2 inches by 2 inches by 1 cm thick, which must be sealed to avoid water contamination. The graphite crystals will be made in 2 inch hexagons  $1/16$  inch thick. The total crystal dimension is 98 x 53 inches; this will be supported by a stiffened honeycomb structure.

Alternately, the mosaic may be placed at the focus of the large area telescope. A Johansson spectrometer with a spherically bent crystal with a radius of 20" would be placed at the focus of the large telescope. Two crystals, a compacted graphite crystal for the 2 to 4 Kev region, and an SHA (sorbitol hexaacetate) crystal for the 1 to 2 Kev region, will be used.

This spectrometer will have lower resolution (500-1000) than the high resolution spectrometer, but its high efficiency combined with the high efficiency and large area of the Baez telescope will allow very weak lines to be detected. For brighter sources, a short scan would give a spectrum that could be used to determine

the lines to be investigated by the high resolution spectrometer.

The compacted graphite can be thought of as composed of many slightly misaligned small perfect crystals. Neglecting absorption, x-rays penetrate the mosaic crystal until they strike a small crystalite oriented at the proper Bragg angle. Therefore, a spectrum within approximately  $\pm 1/3^\circ$  of the Bragg angle setting of the crystal is dispersed on the focusing circle. A multi-wire proportional counter  $1/2$ " wide x  $3/4$ " high with wire spacings of  $.015$ " to  $.030$ " placed at the focus will detect this dispersed spectrum. The wavelength range from 3 to  $6\text{\AA}$  will be scanned by rotating the crystal in  $1/4^\circ$  steps.

The 6 to  $13\text{\AA}$  range will be scanned with an SHA crystal, or a crystal with a similar 2d spacing, with a high peak reflectivity and a broad rocking curve (3 arc min or larger at  $45^\circ$  Bragg angle). The broad rocking curve insures that the entire line is reflected from the crystal even if it is Doppler broadened by high temperatures or high radial velocities. Because this crystal is not mosaic, only one or two wires in the proportional counter will be used to detect the reflected x-rays at the crystal focus. Because of the narrower rocking curve of this crystal, it will be scanned in 1 arc min steps.

SUMMARY

Command Bits

Crystal Choice	2
Deploy - Reset	2
Redundant Reset	1
Power Supply Cable	2
Set Angle	<u>6</u>
Total	13

<u>Telemetry</u>	<u>Bits</u>	<u>Samples/Sec.</u>	<u>Bits/Sec</u>
Shaft Position	15	1/10	1.5
Crystal Choice (Redundant)	1	1/10	.2
Deploy - Reset Monitors (Redundant)	3	1/10	<u>.3</u>
			2.0

Power (watts)

<u>Objective Spectrometer</u>	<u>Average</u>
Crystal Position Monitor	.8
Scan Programmer	.4
Motor Drive	<u>.2</u>
Total Electronics	1.4
Low Voltage Power Supply @ 70%	<u>.6</u>
	2.0
Motor	<u>15.0</u>
Total	17.0

<u>Weight (pounds)</u>	
LiH Crystals	62
Graphite	26
Crystal Frames (sealed) (2548 units)	120
Structures	183
Honeycomb	26
Skin	32
Motors, Shift, Encoders, Bearings, Deployment Mechanism, Electronics, etc.	<u>200</u>
Total	649

#### 4.5 Scintillation Counter Assembly

The scintillation counter assembly is included to extend the energy acceptance of the system, for it is often found that measurements over a small portion of the spectrum are consistent with a variety of spectral forms if each form has a few adjustable parameters.

The proposed detector is quite conventional. Nine standard 100 cm NaI crystal - phototube assemblies are contained in an anticoincidence counter and passive shield. A passive collimator ( $5^\circ$  FWHM) precedes each crystal. The electronic system will allow up to 125 events per second, each event being coded with 3 amplitude and 3 time bits. In addition, all acceptable events are stored in an 8-channel (256 events/channel) pulse height analyzer which is readout once per second. The anti-coincidence counter rate is also read once per second.

SUMMARY

Weight (lbs)

9 Modules

Collimator 6.5

Crystal 1.3

Phototube & Pre Amps 4.0

11.8 (X9) 106.2

Anti-coincidence Shield

Scintillator 30

Metal 120

Phototubes & Pre Amps 20

Power Supplies 10

Total 286.2

Relocatable Electronics 30.0

Telemetry

Item	Bits/Sample	Sample/sec	Total
------	-------------	------------	-------

Events	6	125	750
--------	---	-----	-----

8 Ch PHA	64	1	64
----------	----	---	----

Anti-coincidence Rate	8	1	8
-----------------------	---	---	---

Miscellaneous House-			<u>8</u>
----------------------	--	--	----------

keeping (sub-com)			830 BPS
-------------------	--	--	---------

Command bits

Power Supplies	8
----------------	---

Power

Average and Peak Watts

Pre Amps	1.2
----------	-----

Anti-coincidence Processor	.53
----------------------------	-----

Pulse height Analyzer	3.12
-----------------------	------

Timing Circuits	<u>.60</u>
-----------------	------------

5.45

Low Voltage Power Supply Losses	2.34
High Voltage Power Supplies	<u>3.0</u>
Total	10.79

#### 4.6 An All-Sky Detector for Transient X-Ray Phenomena

There is presently considerable evidence to the effect that extra-solar x-ray emission of transient nature may be frequent, be it the appearance in the sky of a new source (i.e., nova outburst), a large flare in a nearby stellar object, or temporal variations of existing x-ray sources. It is mandatory that provision is made for the early detection of such possible flareups for the benefit of the more elaborate experiments at the focus of the telescope(s). The requirements for a detection system may be stated as follows:

1. All-sky coverage at all times.
2. Spatial resolution as needed to guide the pointing of other instruments and for obtaining high sensitivity.
3. Low internal detector background, also required for achieving high sensitivity.

A multi-anode proportional counter, similar to the one used in the imaging scheme described earlier, is suited for this application. Appropriate collimation must be provided so that a point x-ray source within the field of view appears roughly on only one of the counter's resolution elements. This may be accomplished in a manner which parallels the concept of the pinhole camera as illustrated in Figure 4-5. The field of view is within a 60 degree cone and is subdivided by means of the multiple anode construction and by differential information obtained through charge collection from both ends of the resistive anodes. The proposed construction calls for each resolution element to correspond to about 15



square degrees near the center of the field of view. The number of such elements per counter are about  $10^3$ .

The sensitivity attained by this detector will depend on its response to the diffuse x-ray radiation and on the intrinsic background (vis., not subject to collimation). Considering the former, let  $a$  be the area per resolution element (and for the "pinhole") and  $h$  the distance from the surface of the counter to the "pinhole". The maximum geometric factor per element is given by

$$F \simeq \frac{a^2}{h^2} \quad (1)$$

For a field of view as shown in Figure 1 we have  $h = d/2 \tan 60$  where  $d$  is the linear dimension of the counter. If  $n$  is the number of anode wires in the first layer, we have approximately

$$d \simeq n \sqrt{a}$$

Substituting in (1) we get

$$F \simeq 12 a/n^2 \quad (2)$$

The above equation shows the effect of spatial resolution on the sensitivity of the counter (through the reduction of its background rate).

We may examine the counter response in a 1 keV bin near 3 keV, a region where gas counter efficiency is usually at its maximum. The spectrum of the diffuse x-radiation may be represented by (Boldt et al., Nature, in press)

$$\left( \frac{dN}{dE} \right)_{\text{diff}} = 10.3 E^{-1.35} \quad \text{cm}^{-2} \text{sec}^{-1} \text{kev}^{-1} \text{ster}^{-1}$$

For the 1 keV bin we have

$$(F)(N_b) = 28a/n^2 \text{sec}^{-1} \text{element}^{-1} \quad (3)$$

with  $a \approx 1 \text{ cm}^2$  and  $n = 32$ , (3) gives the rate  $.027 \text{ sec}^{-1} \text{ element}^{-1}$ .

Present indications are that the intrinsic detector background of multi-anode proportional counters at rocket altitudes is rather flat and of the order of  $10^{-3} \text{ cm}^{-2} \text{ sec}^{-1} \text{ keV}^{-1}$ . This is more than 1 order of magnitude smaller than the contribution of the diffuse radiation. Thus it is the latter which will most likely limit the sensitivity of the proposed detector unless it becomes possible to increase the number of anodes considerably. For the present discussion we will neglect intrinsic detector background when estimating sensitivity to a point x-ray source.

If we accumulate data during the time interval  $T$ , the counts in an energy bin  $\Delta E$  at  $E$  attributed to a source in the field of view are

$$N \approx \left( \frac{dN}{dE} \right) s a T \Delta E \text{ element}^{-1}$$

The statistical significance of  $N_s$  in terms of number of  $\sigma$  above the corresponding background counts, in the same counter element and accumulated during an equal time interval, is given by

$$n_\sigma = N_s / \sqrt{N_b}$$

Combining this expression with (3) and setting  $\Delta E = 1 \text{ keV}$ , we have

$$n_\sigma = \left( \frac{dN}{dE} \right) s n \sqrt{\frac{aT}{28}} \quad (4)$$

setting  $n_\sigma = 5$  and  $T = 10^3 \text{ sec.}$ , Equation (4) then gives

$$\left( \frac{dN}{dE} \right) = .026 \text{ cm}^{-2} \text{ sec}^{-1} \text{ keV}^{-1}$$

For a source having spectral shape similar to that of Sco X-1 the above intensity is 300 - 400 below the corresponding Sco X-1 intensity. The

threshold intensity for Crab-like x-ray spectra is about 20 times below Tau XR-1. This sensitivity may be increased by taking a wider energy bin and by accumulating data for longer periods of time.

A few construction details are outlined in Figure 4-5. Each detector is (tentatively) comprised of 2 back-to-back layers of 32 anodes each and the corresponding ground wires. All anodes of the second layer are tied in parallel and used in anticoincidence with the anodes of the first layer. Anode grouping will be used to reduce the number of pre-amplifiers needed per counter.

Gas pressure is maintained by means of x-ray transmission windows supported by circular collimator ribs. The latter are designed for maximum transmission at the corresponding angles of incidence.

In Figure 4-6 we show schematically an arrangement of four such detectors placed concentrically inside a single gas volume for  $2\pi$  coverage with considerable overlap. All-sky coverage can only be achieved with 2 such systems with a total of 8 counters and about  $8 \times 10^3$  resolution elements. If we consider 8 bit onboard storage per element, the total memory capacity required is  $6.4 \times 10^4$  bits. Readout after  $10^2$  sec accumulation necessitates about 640 bits/sec from the telemetry.

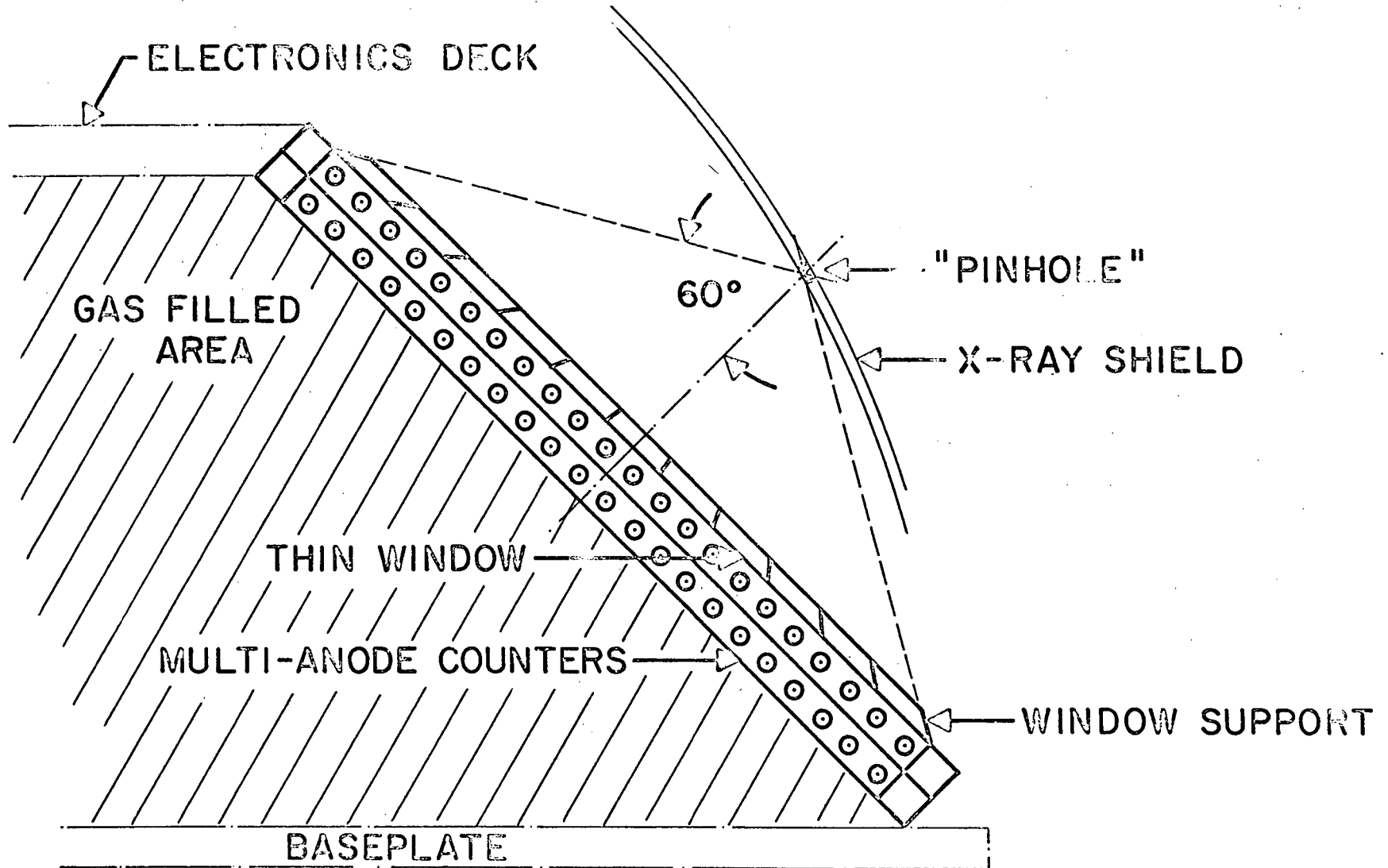
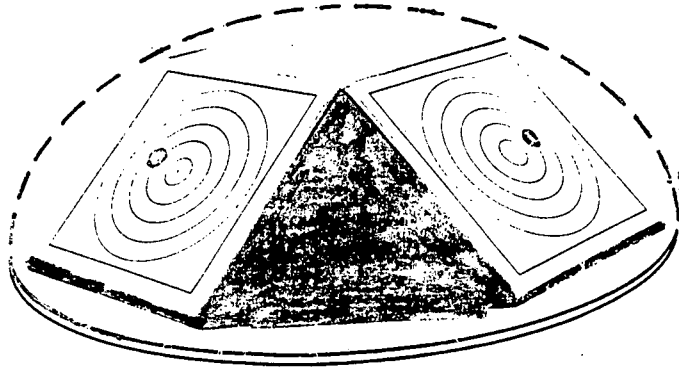


Figure 4-5. X-Ray Transient Detector Element



Reproduced from  
best available copy.

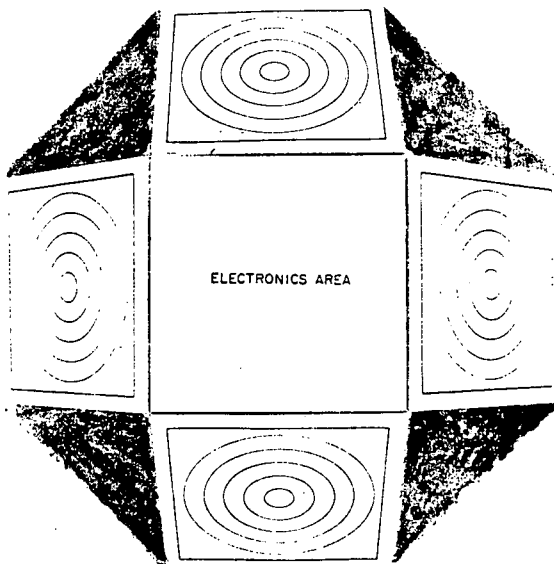


Figure 4-6. X-Y Transient Detection System

## 5.0 ESSENTIAL SCIENTIFIC SUPPORT SYSTEMS

### 5.1 Aspect System

Although as a support system the aspect system is physically a part of the high resolution imagery experiment (Section 3.1).

The primary function of the aspect system is to record the history of the telescope pointing; it may provide other functions such as providing error signals for stabilization purposes or even, as an experiment, to observe ultraviolet emission from selected stars.

The requirement for aspect is most intimate to the high resolution imaging experiment which is attempting to record position of x-ray sources to one arc second. In order to do so it is necessary to record individual stellar positions continuously with a precision of about 10 arc seconds. The proposed system consists of a long focal length lens or mirror and a high sensitivity visible light image tube. Given an image tube with 1000 line resolution, a field of view of 7.5 square degrees results. In order to obtain an average of 5 stars in such a field, the device must be sensitive to 8th mag. stars, which is quite feasible for a system with a six inch diameter lens and a one second integration time.

The aspect lens is mechanically an integral part of the high resolution x-ray mirror, and the aspect readout system is supported by the same frame which supports the high resolution telescope, as previously discussed. A sun sensor controlling a sun shade prevents overdriving the image intensifier/SEC transducer.

The star field data will be accumulated, and the data telemetered at a rate of one frame/second. The vidicon will be scanned using a 1024 by 1024 element raster requiring an element sweep rate of somewhat greater than 1 msec. Figure 5-1 is a block

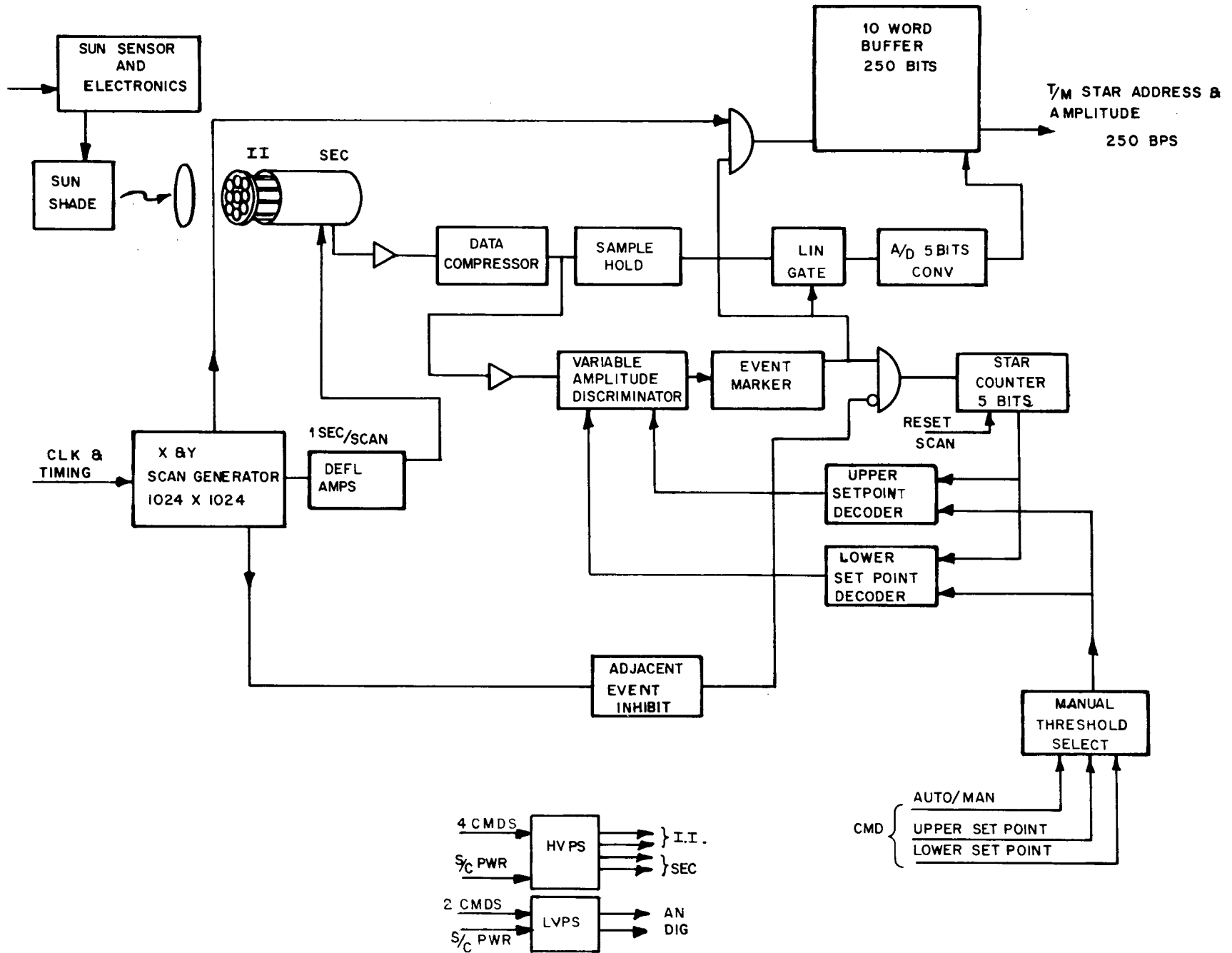


Figure 5-1 ASPECT SENSOR

diagram of the electronic system. A pseudo-automatic threshold control will limit the number of telemetered data points to about 10 of the brightest stars in the frame. The automatic threshold system counts the number of stars which exceed a baseline amplitude threshold. If the number exceeds the maximum upper limit, the thresholds of the discriminator are raised by a proportionate value. If the number is less than the minimum acceptable limit, the thresholds of the discriminator are lowered. The dead band provided by the upper and lower set points will minimize system hunting. Provisions for establishing upper and lower set point thresholds via up link telemetry are included. The adjacent element inhibit excludes the scattered light near bright stars and extended objects from the automatic threshold system. The video data is compressed prior to being digitized because the dynamic range of the signals may be as large as 6 orders of magnitude. An event marker permits the star amplitude to be digitized and stored in the buffer memory along with its X and Y address.

It may be necessary to use a second coarser aspect system to provide intermediate precision aspect data. Such a system can be similar to the high precision system except for the use of a shorter focal lens and a larger field of view.



SUMMARY

Telemetry Requirements:

	<u>Sample Rate/Sec</u>	<u>Bits/Sample</u>	<u>Bit Rate</u> BPS
Star Data	1	250	250
Housekeeping	1	15	<u>15</u>
			265 BPS

<u>Power</u>	<u>Average DC</u>	<u>Peak DC</u>	<u>400 Hz</u>
Vidicon Deflection & Control Circuitry	5.95	5.95	
Data Processing Circuitry	2.96	2.96	
10 Word Buffer	1.50	1.50	
Sun Sensor Electronics & Motor Drive	0.20	0.20	
Timing & Synchronization Circuitry	<u>0.50</u>	<u>0.50</u>	
Total Electronics	11.11	11.11	
Low Voltage Power Supply @ 70% off	4.75	4.75	
High Voltage Power Supplies	<u>1.50</u>	1.50	
Motors		<u>3.00</u>	
Vidicon Heater			<u>1.00</u>
Total RQD	17.36	20.06	1.00

Weight

Lens and Sun Shade	35
Detector	25
Electronics at Detector	5
Structure	<u>40</u>
Total Weight (fixed)	105
Relocatable Electronics	35

## Command Bits

Power Supplies 6

### 5.2 Vehicle Pointing System

It is necessary to be able to point the vehicle to any location in the sky with an absolute accuracy of within one arc-minute and a motion of less than one arc-second/second. It would be useful but not essential to refine this pointing capability to a few arc-seconds after in-flight alignment measurements determine the offset between the pointing system and the experiments. It should be possible to slew the vehicle from one target to another in a small fraction of an orbit. Although no explicit pointing system has been considered, it should be noted that there are large volume elements which could be used for wheels or other guidance components.

### 5.3 Detector Interchange System

Two systems are required for interchanging detectors at focii of the two telescopes. Monitors must also be provided.

## SUMMARY

	<u>High Resolution</u>	<u>Large Area</u>
Telemetry (Redundant) bits/sec	0.2	0.8
Command bits (Redundant)	4	8
Power (DC)	.1 watts	.2 watts
Power (Peak)	15 watts	15 watts
Weight	60 pounds	100 pounds

### 5.4 Telemetry Buffer and Storage

In general, data will tend to arrive asynchronously whereas an even flow of data to the telemetry storage will probably be necessary. A possible technique is to construct parallel

shift registers and fill one register asynchronously as events occur while reading the other shift register into storage synchronously.

The maximum experiment average data rate will be about 37,500 bits/sec and a tape recorder or similar storage system with a capacity of 100 minutes or  $2.25 \times 10^8$  bits will be required. It should be possible to read out this data in 5 minutes, or at a rate of  $7.5 \cdot 10^5$  bits/sec. Space qualified recorders are available which meet these requirements. For example, Leech makes a recorder which stores  $1.5 \cdot 10^9$  bits and can read in or out at speeds of  $10^6$  bits/second.

#### 5.5 Command System

The experiments require a total of 227 command bits. A system for storing up to 5 sets of commands per orbit to allow a series of observations is required. The command system must also store the necessary instructions for pointing the vehicle. It should be possible to choose a starting time for each set of observations. In many cases, the result of the command bit will be to provide power to one or another system.

#### 5.6 Common Electronics

The spacecraft will have to provide a variety of clock signals which must be accurate to about 0.1 millisecond/day for pulsar observations. Many other functions of the experiments are similar, and the possibility of combining these functions into a central set of electronics or a small programmable computer should be investigated.

#### 5.7 Thermal Control System

A change in focal length of  $\pm 0.004$  inches ( $\frac{\Delta f}{f} = 17 \cdot 10^{-6}$ ) results in a blur circle diameter of  $1/2$  arc second in the high

resolution telescope. This implies either a thermal control system with an accuracy of about  $\pm 2^{\circ}\text{C}$  depending upon the structural materials, or an active system to control the focal length. The large area telescope requirement is much looser. A 5 arc second blur circle corresponds to  $\frac{\Delta f}{f} = 245 \cdot 10^{-6}$ , and the thermal control system must maintain an accuracy of  $\pm 10^{\circ}\text{C}$ . This suggests that the vehicle should provide a control system of intermediate accuracy but at least within  $\pm 10^{\circ}$  and a more accurate thermal control or active focal length adjustment system be provided for the high resolution telescope and aspect system. The active control system would consume less power but probably would be less reliable.

The thermal gradients must also be controlled. The high resolution mirror temperature must stay within  $2^{\circ}\text{C}$  of the average temperature of the optical bench, and local longitudinal gradients in the mirror must be less than about  $.5^{\circ}\text{C}/\text{inch}$ ; these local gradients must not be allowed to accumulate over the mirror so as to result in a change anyplace in the mirror of more than  $2^{\circ}\text{C}$ . The azimuthal gradients must be controlled to a similar tolerance. The final values of these tolerances requires a detailed analysis of the mirror system, but the above values may be used for planning purposes.

The solid state detector refrigerator power requirements will be substantially lower if the spacecraft environment is cooler. A low temperature heat sink for this system would also decrease the power consumption. Finally, all of the detectors will be less noisy at a lower temperature. For these reasons we suggest that the spacecraft temperature be kept at  $0 \pm 10^{\circ}\text{C}$  and the high resolution telescope and aspect system be kept at  $15 \pm 2^{\circ}\text{C}$  or else provided with an active focal length control. A thermal control system for a telescope of this size may be expected to require 100 watts or less with moderate attention given to thermal insulation from the rest of the system.

## 6.0 SUMMARY OF VEHICLE REQUIREMENTS

### 6.1 Vehicle Experiment Package Dimensions

Diameter = 102" (useful)

Length = 30 feet

### 6.2 Pointing Requirements

6.1 Absolute accuracy (after in-flight base sighting) 1 arc minute radius of error

6.2 Stability; during one second of time the telescope axis shall be confined within an error circle of less than one arc second in diameter.

### 6.3 Thermal Control

The vehicle temperature shall have an allowable tolerance of  $\pm 10^{\circ}\text{C}$  about a nominal temperature, a low ( $\sim 0^{\circ}\text{C}$ ) nominal temperature is preferred. An independent thermal control system or active focal length control system will be provided for the high resolution mirrors.

### 6.4 Experiment Telemetry Requirements

<u>Experiment</u>	<u>Operating Requirement</u>	<u>Contribution to Max. Rate</u>
High Resolution Telescope		
Imaging (AS&E)	25,000	25,000
Spectrometer (MIT)	11,000	-----
Large Area Telescope		
LiH Polarimeter (Col)	2,292	
C Polarimeter (Col)	1,205	
Solid State Detector (GSFC)	300	
Imaging	5,360	5,360
Objective Spectrometer	2	
Proportional Counter	2,210	2,210
Flat Crystal Spectrometer	3,627	3,627
Scintillation Counter	830	830

<u>Experiment</u>	<u>Operating Requirement</u>	<u>Contribution to Max. Rate</u>
Aspect System	265	265
MISCL Housekeeping (Sub-com)	20	<u>20</u>
Total (Worst case)		37,312
Total Storage (100 minutes)		$2.2 \cdot 10^8$
Playback rate (20:1)		$7.5 \cdot 10^5$

#### 6.5 Experiment Command Bits

<u>Experiment</u>	<u>Requirement</u>
High Resolution Telescope	
Imaging (AS&E)	32
Spectrometer (MIT)	40
Large Area Telescope	
LiH Polarimeter (Col)	20
C Polarimeter (Col)	20
Solid State Detector (GSFC)	10
Imaging	8
Objective Spectrometer	13
Proportional Counter	8
Flat Crystal Spectrometer	24
Scintillation Counter	8
Aspect System	6
MISCL Functions, Detector Motions	20
Pointing Angles (1' c 3 axis)	<u>18</u>
	227*

---

\* This number may be reduced by sharing commands among non-simultaneous experiments.

C.S

6-3

6.6 Experiment Power Requirements

Experiment	Operating		Standby		Contribution to Max. Requirement	
	Ave.	Peak	Ave.	Peak	Ave.	Peak
High Resolution Telescope						
Imaging (AS&E)	21.3	39.3				
Spectrometer (MIT)	32.4	49.2			32.4	49.2
Exp. Interchange App.	.1	15				
Large Area Telescope						
LiH Polarimeter (Col)	30.87	33.87			30.87	33.87
C Polarimeter (Col)	25.30	28.30				
Solid State Detector (GSFC)	200	200	190	190	190	190
Imaging (AS&E)	14.77	14.77				
Objective Spectrometer (Col)	2	17				
Exp. Interchange App	.2	15				
Proportional Counter	29.30	29.3			29.3	29.3
Flat Crystal Spectrometer	12.04	12.04			12.04	12.04
Scintillation Counter	10.79	10.79			10.79	10.79
Aspect System*	17.36	20.06			17.36	20.06
High Resolution Telescope Thermal Control System	100	150			100	150

---

\* This experiment also requires 1 watt of 400 Hz power. If this is not available, an additional 1.3 watts DC will be required.

## 6.6--Continued

Experiment	Operating		Standby		Contribution to Max. Requirement	
	Ave.	Peak	Ave.	Peak	Ave.	Peak
Telemetry Buffer and Electronic Systems (not including Data Storage and Transmission Devices or Command System, Pointing Control Systems, etc.)	30	30			30	30
Total					<u>452.76</u>	<u>525.26</u>



6.7 Experiment Weights (See Figure 6-1 for the weight distribution)

Experiment	Weight (lbs)	
	Fixed Position	Relocatable Electronics
High Resolution Telescope		
Mirror	1500	
Optical Bench	700	
Imaging Detector Assembly	70	60
Spectrometer Detector Assembly	56	40
Aspect Lens	35	
Aspect Detector Assembly Structure	70	35
Experiment Interchange Apparatus	60	
Filter Wheel	30	
Grating Assembly	30	
Large Area Telescope		
Mirror	3000	
Optical Bench and Boom	1600	
Experiment Interchange Apparatus	100	
LiH Polarimeter	38	50
C Polarimeter	34	
Solid State Detector	50	15
Imaging Detector	15	60
Objective Crystal	650	
Proportional Counter Assembly	166	30
Flat Crystal Assembly	117	20
Scintillation Counter	286	30
Telemetry Buffer and Common Electronic Systems, (not including Data Storage and Transmission Devices, Command System, Pointing Control Systems, etc.)		
Totals	8607	440

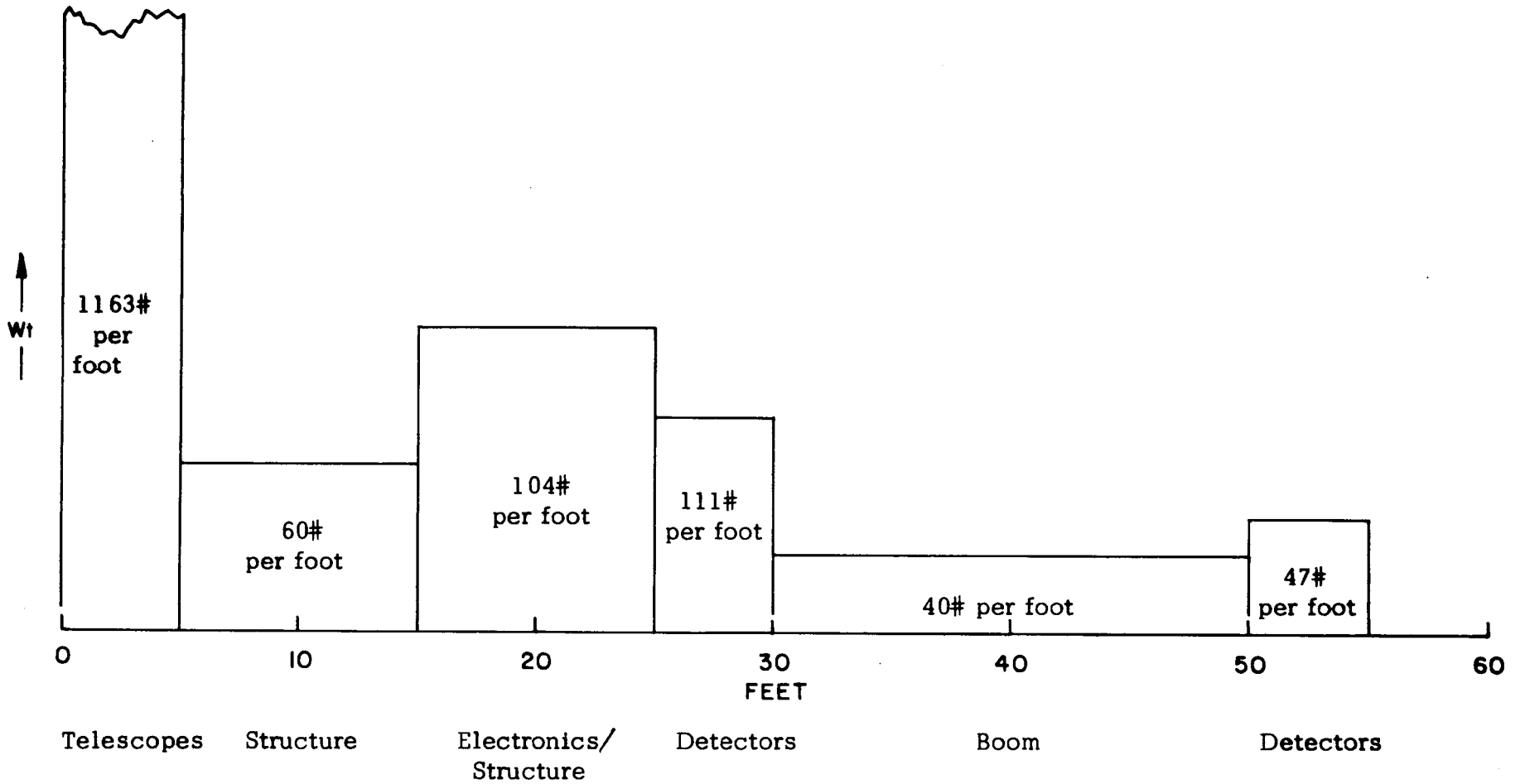


Figure 6 - 1.

WEIGHT DISTRIBUTION (BOOM EXTENDED)

## 7.0 SUPPORTING PROGRAMS

### 7.1 350-Sounding Rockets

The sounding rocket program has traditionally been a means to support advanced experiments and techniques and the x-ray telescope mission requires similar support. Normally, individual experimenters are fully responsible for developing their own scientific payload; however, we believe that the facility concept can be extended to sounding rocket payloads. In particular, we would urge the implementation of a program which comprised the development of two payloads for use by a number of experimenters; one, utilizing a high resolution mirror similar in construction to the  $1000 \text{ cm}^2$ , 1 arc second mirror recommended for the facility; and the other, a large area collector, similar to the Baez collector described earlier.

Individual experimenters would incorporate their own instruments into these payloads at the focal plane of the appropriate telescope. The several payloads, flown two or three times per year, would allow each group one or more sounding rocket flights per year. The following desirable objectives could be met by such a program.

1. Development and testing of essential flight hardware; particularly, the telescopes, aspect system, individual experimenters hardware.
2. Performance of selected observations on the x-ray sources. Such observations would not only provide important scientific information regarding the sources, but would allow the determination of certain key parameters needed for time-lining the facility observational program.

### 3. Development of means of data processing

The Aerobee 350 allows use of substantially larger payloads than the 150. A 16" aperture telescope could be incorporated into such a payload. This would provide about  $250 \text{ cm}^2$  geometric area of high-resolution mirror and about twice this for the moderate resolution Baez collector. A possible configuration is shown in drawing RSK-614-318. A volume of cylindrical shape of about 20" long and 16" in diameter is available for focal plane instruments. Of this, 10" is behind the focal plane.

#### 7.2 One-mile X-ray Test Facility

Nearly-parallel beams of x-rays are now in operation or being installed at various institutions for this purpose; but these are inadequate for the optics described here. By nearly-parallel we mean a divergence across the aperture of telescope which is small compared to the average grazing angle of the front mirror. For a facility one mile long and a 36 inch aperture telescope, the divergence would be 2 arc minutes, which is acceptable (for a 300 foot facility, the divergence would be about 30 arc minutes which is comparable to the grazing angle). Such a long facility could be utilized to test and align the entire payload since the apparent "direction" of the x-ray source located at the far end would be shifted (by parallax) by no more than a few arc minutes between instruments.

Clearly such a facility is beyond the means of any one group, but is appropriate for a NASA center. One end would need to be large enough to accommodate the entire payload; the other end need only accommodate a modest sized x-ray source. The evacuated tube between the two ends need only be maintained at rough vacuum.

### 7.3 Orbital Operations and Data Retrieval

During orbital operation the facility will be returning the order of  $3 \times 10^9$  bits of data per day. In addition commands will be transmitted to the spacecraft numerous times per day for the purposes of controlling the operations. These figures should not represent an unusual burden on the ground tracking facilities. However, to be consistent with the notion of a facility and considering that many of the planned observations will represent qualitative improvements over anything performed previously, it is mandatory that a significant fraction of the data be distributed to experimenters, processed and analyzed in near-real-time and the results used to update the observational program of the facility. By near-real-time, we mean the order of 24 hours.

### 7.4 Coordinated Ground-based Observations

The correlation of the x-ray sources with visible and radio objects is one of the primary objectives of x-ray astronomy. Such correlation can take two forms:

1. Study of the optical and radio characteristics of the x-ray source.
2. Simultaneous observations of the variations of intensity over a very broad range of wavelengths including x-rays.

Such studies make the availability of ground facilities mandatory. At the present time, astronomers are having difficulty satisfying their requirements for conventional programs of observations, the requirements for the support of x-ray astronomers for the facility and other programs will no doubt overtax existing facilities. We strongly urge that NASA consider the possibility of providing ground-optical facilities, devoted primarily to x-ray correlated studies to supplement existing facilities.

APPENDIX E  
ASE-2978

Effect of Varying Microchannel Plate and  
Phosphor Voltage on X-ray Image Quality

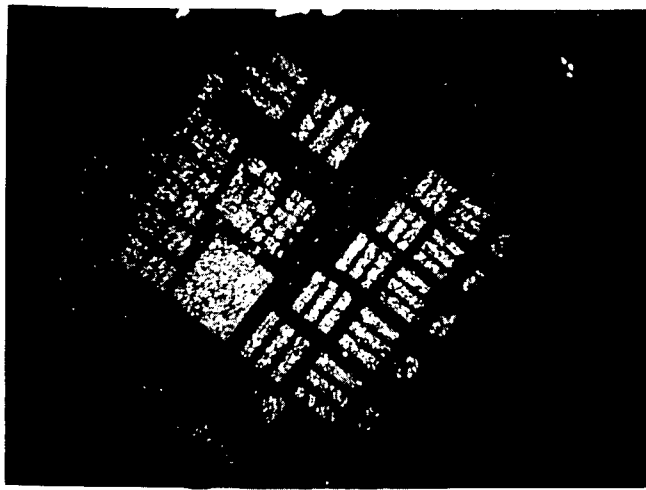
## EFFECT OF VARYING MICROCHANNEL PLATE AND PHOSPHOR VOLTAGE ON X-RAY IMAGE QUALITY

The effect of microchannel plate voltage and phosphor voltage on X-ray image quality were studied photographically by viewing the fiber optic output of an image intensifier with a camera containing Kodak 2485 film. The image intensifier was irradiated by an  $^{55}\text{Fe}$  source (5.9 keV/2.1 Å) and an etched copper resolution grid was placed in front of the microchannel plate. Some of the resulting images for various combinations of voltages are shown in Figures E-1 and E-2. The results are summarized in Figure E-3 which shows the relative photographic efficiency as the voltages are varied. Up to a point increasing the gain increases the number of counts because a larger fraction of the X-rays are producing enough light in the phosphor to be recorded. A plateau is eventually reached, indicating that essentially all X-rays converting at the photocathode are resulting in spots on the film. Examination of the original negatives show that there is a limit to useful gains; beyond this point the spots become larger because of halation in the film. The voltage at which this degradation in spatial resolution sets in depends on the method of readout and also on the X-ray wavelength. There does seem to be a range of voltages which provides maximum efficiency without degrading the resolution, although this point deserves further study. With the voltages in this operating range and no X-rays present, the observed noise rate was less than 0.5 per square centimeter per second.

Difficulty was experienced in measuring the resolution conventionally because the fine areas of the resolution mask do not afford high contrast to X-rays. The spot size, about 60 microns, corresponds to about 8 line pairs per millimeter. It is possible,

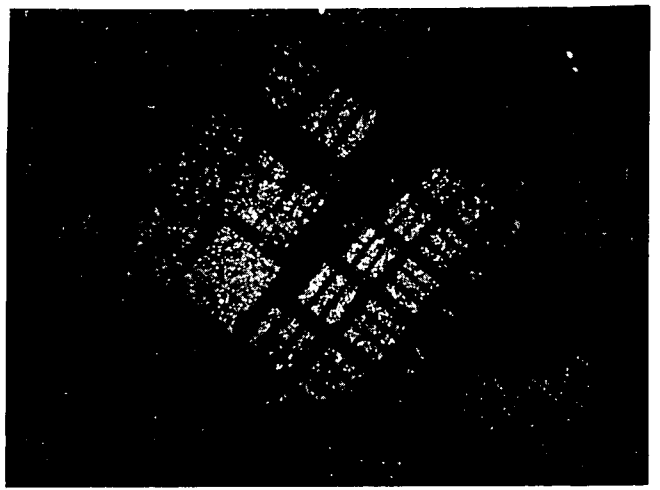
of course, to locate spot centers to considerably better accuracy when the device is operated so that individual spots are resolved.





12-23

(a) 1.0 - 4.0



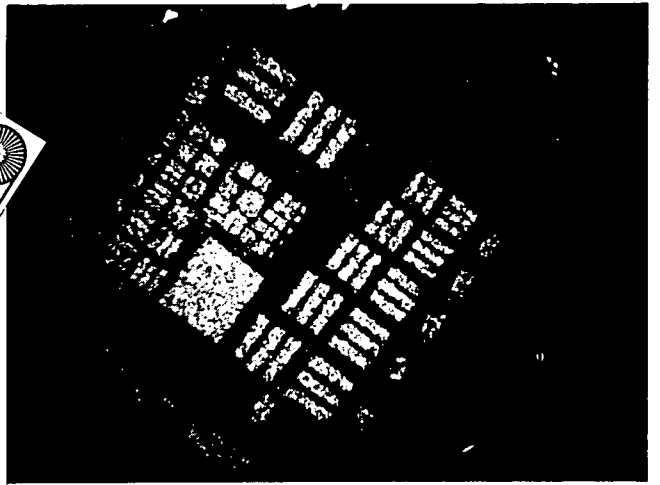
12-17

(d) 1.0 - 5.0



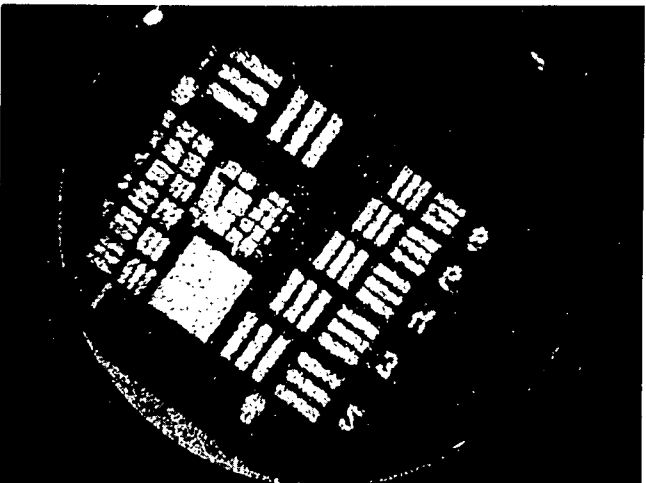
12-19

(b) 1.1 - 4.0



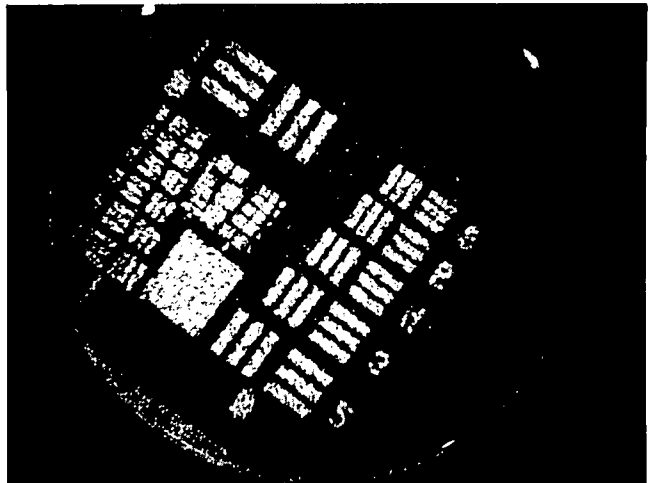
12-29

(e) 1.1 - 5.0



12-31

(c) 1.2 - 4.0

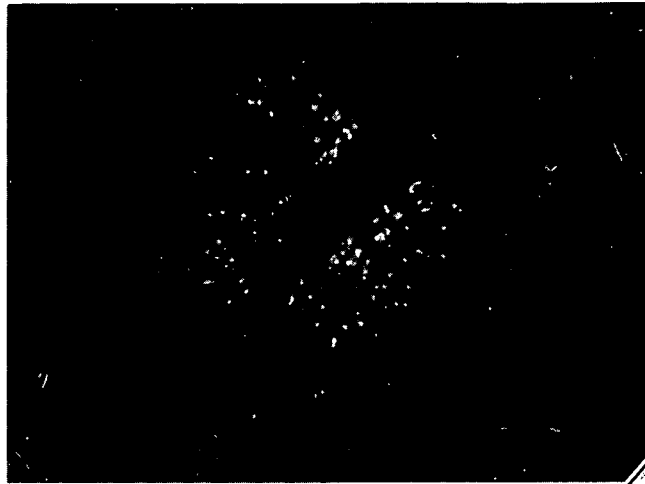


12-25

(f) 1.2 - 5.0

Reproduced from  
best available copy.

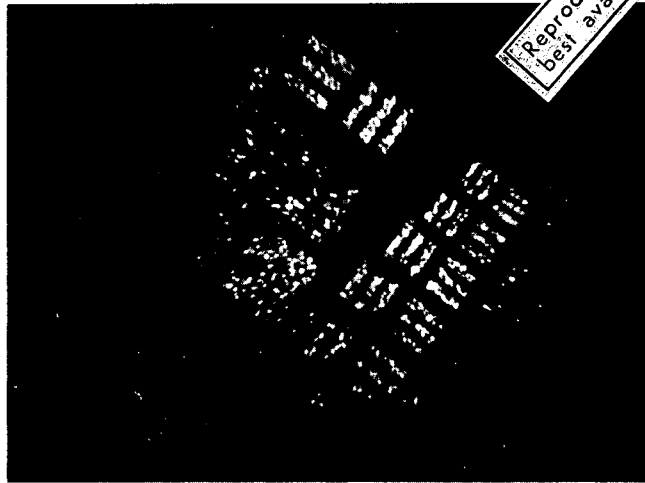
Figure E-1 Pictures of the image intensifier phosphor taken with Kodak 2485 film. The voltages across the MCP and the potential at the phosphor, both in kilovolts, are shown in that order.  $\text{Fe}^{55}$  x-rays were incident upon the MCP.



13-18

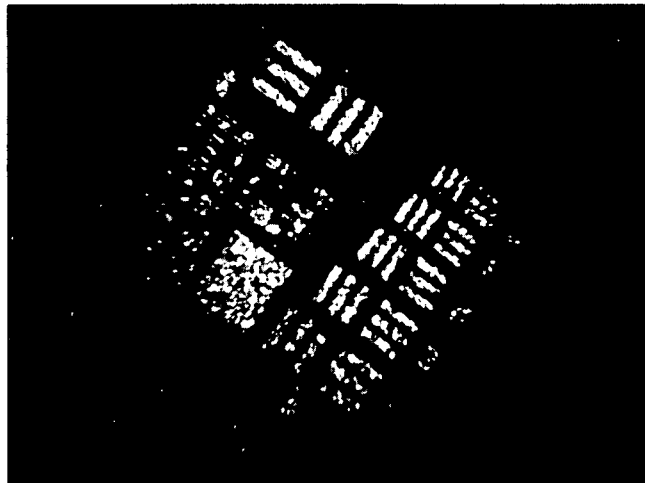
(a) 1.0 - 5

Reproduced from  
best available copy.



13-24

(b) 1.1 - 5



13-30

(c) 1.2 - 5

Figure E-2 Photographs under similar conditions taken with Kodak Tri-X film.

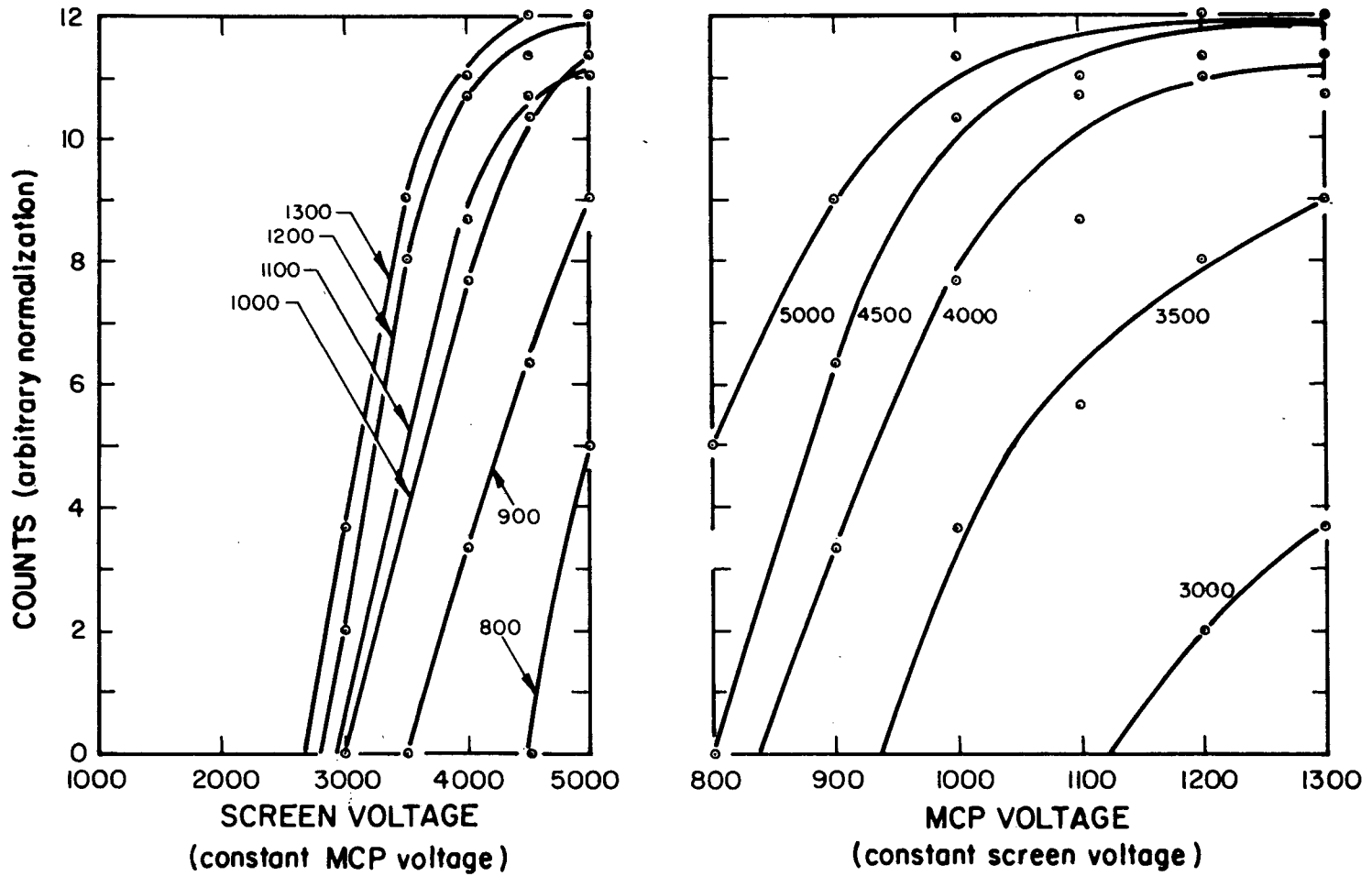


Figure E-3. Relative Quantum Efficiency as a Function of MCP Voltage, and of Phosphor Voltage.